



Direct observation of air gap formation during solidification.

MARTINEZ-FUEYO, Adolfo Jose.

Available from the Sheffield Hallam University Research Archive (SHURA) at:

<http://shura.shu.ac.uk/20021/>

A Sheffield Hallam University thesis

This thesis is protected by copyright which belongs to the author.

The content must not be changed in any way or sold commercially in any format or medium without the formal permission of the author.

When referring to this work, full bibliographic details including the author, title, awarding institution and date of the thesis must be given.

Please visit <http://shura.shu.ac.uk/20021/> and <http://shura.shu.ac.uk/information.html> for further details about copyright and re-use permissions.

POND STREET
SHEFFIELD S1 1WB

6868

BAR CODE

101 381 282 4

**Sheffield City Polytechnic
Eric Mensforth Library**

REFERENCE ONLY

This book must not be taken from the Library

PL/26

R5193

ProQuest Number: 10697328

All rights reserved

INFORMATION TO ALL USERS

The quality of this reproduction is dependent upon the quality of the copy submitted.

In the unlikely event that the author did not send a complete manuscript and there are missing pages, these will be noted. Also, if material had to be removed, a note will indicate the deletion.



ProQuest 10697328

Published by ProQuest LLC (2017). Copyright of the Dissertation is held by the Author.

All rights reserved.

This work is protected against unauthorized copying under Title 17, United States Code
Microform Edition © ProQuest LLC.

ProQuest LLC.
789 East Eisenhower Parkway
P.O. Box 1346
Ann Arbor, MI 48106 – 1346

DIRECT OBSERVATION OF AIR GAP FORMATION
DURING SOLIDIFICATION

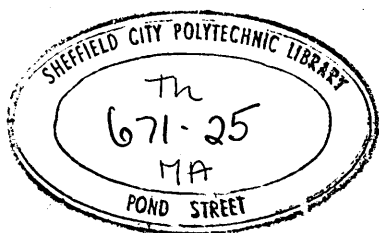
by

Adolfo José Martínez-Fueyo
Lic. Phys. (Universidad Central de Venezuela)

A thesis submitted in partial fulfillment
of the requirements of the Degree of
Master of Philosophy of the Council for
National Academic Awards

DEPARTMENT OF METALLURGY
SHEFFIELD CITY POLYTECHNIC

July 1978



79-16805-01

ABSTRACT

In order to determine the way in which an air gap forms at the mould/casting interface a mould with one transparent glass wall and three metal walls with integral cooling channels has been developed in which metals can be melted and solidified.

Using a variety of cooling rates at the glass face and in the metal walls this apparatus has been used to study visually air gap formation during the solidification of pure tin and 50% lead-tin alloy at some 20° and 50°C above the solidus arrests respectively.

Hills' solidification algorithm has been used to classify the solidification experiments in a way that correlates qualitatively the solidification modes with the appearance of an air gap.

It has been concluded from the experimental results that the air gap starts to form at the corners of the cast ingot when it is cooled uniformly.

Theoretical analyses of heat flow were made and compared with published data in order to ascertain the influence of air gap formation on heat removal rates. This comparison showed that the formation of ^{an} air gap has a somewhat smaller

effect on heat removal rates in both continuous and static castings than has been attributed by many previous authors.

P R E F A C E

This dissertation is submitted for the degree of Master of Philosophy of the Council for National Academic Awards.

The research was carried out in the period October 1976 to July 1978 in the Department of Metallurgy, Sheffield City Polytechnic. During the period spent at the Polytechnic the author has attended post-graduate lecture courses on the following topics:

1. Process Metallurgy
2. Solidification
3. Continuous Casting
4. Arc Steelmaking
5. Quality Control
6. Metals and Competitive Materials
7. High Strength Alloys
8. Thermodynamics
9. Mechanical Metallurgy
10. Heat treatment

The author would like to express his appreciation to Universidad de Carabobo (Venezuela) for the provision of financial support, and to the Collaborating Establishment - British Steel Corporation, Swinden Laboratories.

Grateful thanks are expressed to Dr. A. W. D. Hills, Mr. G. Butterworth and to J. Dixon of British Steel Corporation for their interest, guidance and constant encouragement throughout the course of the work. Also, grateful acknowledgements are expressed to technicians of the Department of Metallurgy, Sheffield City Polytechnic.

The results obtained are to the best of my knowledge, original except where reference is made to the work of others. No part of this dissertation has been submitted for a degree at any other University or College.

Department of Metallurgy
Sheffield City Polytechnic

Adolfo José Martínez-Fueyo
July 1978

ABSTRACT	
PREFACE	
I INTRODUCTION	
II PREVIOUS WORK	
II.1 Experimental methods for studying air gap formation	3
II.1.1 Electrical methods	3
II.1.2 Thermal analysis methods	5
II.1.2.1 The variation of $\partial\theta/\partial x$ at the mould/metal interface	6
II.1.2.2 Heat/flux analysis	9
II.2 Theoretical models for air gap formation	12
II.2.1 Elastic models	12
II.2.2 Elasto-perfectly plastic model	14
II.2.3 Viscoelastic model	15
II.2.4 Coupled thermoelastic model	16
II.2.5 Solid contraction model	18
II.3 Influence of cooling rate on solidification	20
III EXPERIMENTAL APPARATUS	22
III.1 Moulds	22
III.1.1 Beakers	22
III.1.2 Mould A	22
III.1.3 Mould B	23
III.2 Cooling System	24
III.3 Temperature Measurement	26
III.4 Heating	27
III.5 Equipment for air gap widths measurement	27
III.5.1 Interferometer	27
III.5.2 Laser	28
III.6 Metals and alloys used	28

	PAGE
IV EXPERIMENTAL PROCEDURE	30
IV.1 Experiments in beakers	30
IV.2 Experiments in mould A	31
IV.3 Preliminary experiments in mould B	33
IV.3.1 Use of the interferometer	33
IV.3.2 Use of the laser beam	34
IV.3.3 Preliminary experiments using the thermal analysis method and visual observations	35
IV.4 Final Assembly	37
IV.4.1 Experimental procedure	37
IV.4.2 Thermocouple calibration and temperature corrections	37
IV.4.2.1 Thermocouple calibration	37
IV.4.2.2 Temperature correction	38
V RESULTS	39
V.1 Air gap formation studies	39
V.2 Thermal analysis results	39
V.3 Photographic Records	40
V.4 Visual Observations	40
VI DISCUSSION	41
VI.1 Thermal analysis	41
VI.1.1 Combined effect of superheat and cooling conditions	41
VI.1.2 Effect of undercooling	43
VI.1.3 Solidus arrest	44
VI.1.4 Study of the cooling curves after the solidus arrest	45
VI.2 Visual observations	45
VI.3 Estimate values of heat transfer coefficients	49
VI.3.1 Natural convection	49
VI.3.2 Forced convection	50
VI.3.3 Film water cooling	52
VI.3.4 Heat transfer coefficient from the mould to the cooling water passages	53
VI.4 Estimation of solidification times	55

VI.5	Theoretical calculations for comparison with published heat flow data during solidification to ascertain the influence of the air gap on the heat transfer	58
VI.5.1	Comparison for metal moulds	58
VI.5.2	Comparison with continuous casting	60
VI.6	Laser defocusing	64
VII	CONCLUSIONS	65
	REFERENCES	67
	LIST OF SYMBOLS	
	LIST OF FIGURES	
	LIST OF TABLES	

I INTRODUCTION

The heat transfer conditions that apply between a freezing ingot and its mould constitute one of the most important elements in the analysis of both static and continuous casting. In continuous casting, these conditions determine the thickness of the initial shell that forms and it is the strength of this shell that controls the speed at which continuous casting is possible. For both static and continuous casting the quality of the initial shell is determined very largely by the heat transfer conditions that apply, and this determines the quality of the surface finish, as well as the subsequent development of microstructure.

The influence on heat transfer rates made by the mechanism of formation, and the magnitude of the air gap between the mould and the ingot surface in industrial casting processes have been the subject of much speculation. In the majority of the experimental investigations, the air gap has been detected indirectly by means of thermal analysis rather than by direct visual observation or measurement.

It is generally assumed that the liquid metal and the inner surface of the mould are initially in very close contact, giving conditions for very high heat removal rates. These conditions, if maintained, would give heat removal

rates far in excess of those obtained in practice. It is further assumed that the solidified shell bows inwards towards the liquid core once the thermal stresses developed in the shell are sufficient to overcome the metallostatic pressure.

In the work described here, the formation of the air gap at a glass wall in a static mould has been investigated experimentally during the solidification of 50% lead-tin alloy and pure tin. The metal side walls of the mould as well as the glass wall have been subjected to different cooling conditions. During the course of some of the experiments the evolution of the air gap has been recorded on film and thermal analysis measurements have been made on the solidifying metal.

A study of the previous work on air gap formation is presented in the next chapter, the experimental apparatus and procedures in chapters III and IV and the experimental results in chapter V. The results obtained in this work are discussed together with those of previous workers in chapter VI and the conclusions are presented in chapter VII.

II PREVIOUS WORK

II.1 Experimental methods for studying air gap formation.

II.1.1 Electrical methods

The electrical method, for the determination of air gap formation, is based on the assumption of a perfect electrical contact between the mould and the ingot. When the liquid metal is poured into the mould there is a perfect electrical contact between liquid metal and the mould but when a solid shell forms and an air gap appears the electrical contact is broken between the solidified shell and the mould. In a review carried out by Linacre⁽¹⁾ on the process of gap formation the experiments of Mikura⁽²⁾ and Matuschka⁽³⁾ who have dealt with the electrical contact method, are summarised.

Mikura⁽²⁾ used, in his experiments, a small insulated probe the end of which was flush with the inner surface of a 38mm inner diameter water-cooled mould. The probe was connected in series with a battery and a lamp, and then to the mould, so that the lamp was alight as long as there was contact between the steel and the probe and other points of the mould. When separation occurred, at the end of the probe, the lamp became disconnected instantaneously. Four such probes were fitted at the same height in the mould, and the time periods the four lamps

TABLE I

SEPARATION TIMES IN MYKURA'S EXPERIMENTS

Experiment	Separation Times of Four Probes (seconds)			
1	11	14	--	--
2	6	6	12	--
3	3	15	--	--

TABLE II

RESULTS OF MATUSCHKA'S EXPERIMENTS

Experiment	%Composition of Ingot			Separation (2 probes) in seconds	
	C	Cr	Other		
1	0.65	--	--	85	37
2	0.20	--	1.5 Ni	56	18
3	0.4	1.0	3.5 Ni	100	90
4				77	
5	0.8			270	169
6				284	
7	0.7	4.0	18.0 W	178	179
8	0.2	12.0		170	120

were alight, during each of three experiments, are given in table I. Matuschka used a similar apparatus with only two probes on each of two adjacent walls of a 0.3 ton cylindrical ingot mould 1275mm high, 250mm diameter and with 80mm thick walls, i.e. a diameter to height ratio of 0.20 and a thickness to diameter ratio of 0.32. The probes were located at 250mm from the top, i.e. a height ratio of 0.20. The times taken for air gap formation, after teeming, are given in table II.

As can be seen from tables I and II, there is natural scatter in the results both when the type of steel is constant and when different steels are used. The values for different classes of steel varying from 284s to 18s and up to 60s difference for the same steel in Matuschka's work and, from 3s to 15s in Mikura's work.

Taylor⁽⁴⁾ in a review on continuous casting has quoted the works of two authors (Rudoi⁽⁵⁾, Gordienko et al⁽⁶⁾) who have dealt with air gap formation during the continuous casting processes. Rudoi⁽⁵⁾ placed a network of contact sensors in a 175 x 420mm mould, 58 contacts on each broad face and 30 on each narrow one. Each sensor was connected to a light bulb which was lit when contact was made and photographs of light banks were taken.

Rudoi concluded that no true air gap really existed, but that the steel shell continuously made and broke contact with the mould wall and therefore, heat was extracted in pulses rather than continuously. Gordienko et al⁽⁶⁾ made contact measurements versus time at two levels on a curved mould machine, of billet cross-section 130 x 145mm. When percentage contact times were compared simultaneously for opposite faces no evidence of an inverse relationship was found. That is, if one face has a low percentage of contact, the opposite face does not necessarily have a high percentage: thus the slab faces appears to act somewhat independently.

II.1.2 Thermal analysis methods.

In these methods a number of thermocouples are placed within the mould and mould cavity with their hot junctions at predetermined positions and cooling curves are obtained for each thermocouple. From the cooling curves obtained from thermocouples placed inside the mould at the mould/metal interface, air gap formation times can be determined. In addition, air gap formation times can be determined from analysis of the heat flux crossing the metal/mould interface as determined from heat balances

either on the solidifying metal, or on the cooling medium. Various authors (7,8,9-10,11,12) have used the above methods as described below.

II.1.2.1 The variation of $\partial\theta/\partial t$ at the mould/metal interface

This method consists of recording the thermal history at the mould/metal interface. This recording is made by positioning thermocouples in the mould near to the inner surface. The temperatures recorded are plotted versus time, obtaining in this way cooling curves for the particular region where the thermocouples have been positioned. These curves show a perceptible variation in the cooling rate, $\partial\theta/\partial t$. This variation appears on the curves as an inflection which has been explained either as the separation of the solidified metal shell from the mould or vice versa. The time at which this inflection takes place is taken as the air gap formation time. Mackenzie and Donald⁽⁷⁾ made temperature measurements during the casting of three ton ingots in duodecagonal moulds 1372mm high, 560mm inner diameter and with 132mm thick walls, i.e. a diameter to height ratio of 0.41, and a mould thickness to diameter ratio of 0.24. The experiments were carried out on low and plain carbon steels poured into the mould at 1530°C. The data were represented on plots of temperature versus time. The plotted curves of temperature versus time for thermocouples located at

1070mm from the bottom of the ingot, i.e. at 0.78 height ratio, and the mould-ingot interface curve showed the inflection about 240s after teeming.

Bishop et al⁽⁸⁾ carried out experiments on the solidification of ingots in square section moulds where the thermal history of both the ingot and mould were studied during the course of solidification. The moulds were uniform in wall thickness from top to bottom and ranged from 40 to 110mm. The ingots were tapered from 180mm at ^{the} top to 170mm at ^{the} bottom and were 510mm long, i.e. a width to height ratio of 0.33-0.35, a thickness to width ratio ranging from 0.22 to 0.65. For thermocouples positioned at mid-height they found that the inflection which occurred in the temperature versus time curves for both the mould and ingot sides was due to air gap formation. This was proved by the authors by pouring a similar ingot into a mould 50mm thick, i.e. a thickness to width ratio of 0.28, with a 45° tilt such that the bottom face remained in continuous contact with the mould, whilst the opposite face could shrink away to form an air gap. The mould-ingot interface temperature on the top side fell when the air gap formed at 85s after pouring but on the bottom side it climbed steadily throughout solidification. They claimed that the air gap forms earlier when using thin moulds as compared to using thick moulds. This effect was ascribed to the more rapid heating of the thin mould which then expands and pulls

away from the ingot.

Druzhimin and Mazun⁽⁹⁾ have obtained experimentally the changes in temperature of the copper walls of a continuous casting mould 1430mm in length. They have observed that the temperature of the copper wall decreases from the meniscus level of the cast metal downwards, with a significant drop in temperature in the zone 200-300mm below the liquid steel meniscus. Four thermocouples placed around the mould walls 245mm below the meniscus showed different temperature readings. The authors claimed that the differences in the thermocouple readings, for the couples placed 245mm, i.e. a length ratio of 0.17, were due to the formation of an air gap between the billet and the mould wall as a consequence of metal contraction and warping of the walls.

Veinik⁽¹⁰⁾ claimed that, with no coating at all on a chill mould, the curves of temperature versus time measured at different locations intersected. He interpreted this as indicating that considerable shrinkage of the metal occurred resulting from the great initial intensity of heat exchange, but corresponding to this was a smaller temperature drop in the cross-section of the casting. This reduction in the temperature drop was

accompanied by a redistribution of temperature, resulting in an increase in the temperature of the surface layers of the casting⁽¹⁰⁾.

II.1.2.2. Heat flux analysis

This method consists in calculating the heat flux through the metal-mould interface during the course of the solidification process. From the heat flux versus time curves it is possible to identify the air gap formation time and its influence on the heat transfer mechanism. Mackenzie and Donald⁽⁷⁾ calculated the rate of heat transfer for the solidification of ingots in the duodecagonal moulds described in (II.1.2.1). They calculated the heat flux from the temperature distribution in the mould which was being determined by them experimentally. They assumed the mould wall to be a cylinder. Calculations were then made to determine the heat content of wedge sections of these cylinders. These calculations were performed by plotting temperatures in the wedge against incremental volumes, each being proportional to the square of the radius. The plotted curves were for thermocouples located at 1070mm from the bottom of the mould, i.e. at 0.78 height ratio. The graphical integration of these curves allowed them to determine the energy stored in the wedge which they subsequently plotted against

time, the gradient of this curve gave the instantaneous rate of increase in heat content of the wedge. After the corrections for the heat dissipated from the mould surface were made, a heat flux versus time curve was obtained. This curve is illustrated in fig.1.

Mackenzie and Donald found that the rate of heat transfer per unit of area of the ingot surface was comparable in all their experiments. They explained the rapid fall in the rate of heat transfer to the mould, fig.1, as the separation of the ingot from the mould being caused by expansion of the mould, contraction of the ingot or by both of these factors.

Fowler and Savage⁽¹¹⁾ calculated the heat flux from the mid-height point of a steel ingot to the mould from the incremental heat losses over separate time intervals.

They considered the cross section of the ingot and mould as a rectangle and equated the surface ingot temperature to the average surface temperature, assuming a parabolic temperature distribution throughout the solidified shell. The values of heat fluxes for different times from the mid-height of an eight ton ingot cast at 1530°C are shown in fig.2. As can be seen, the heat flux 4 min. after the start of teeming was 600 kW/m^2 corresponding to a black body temperature of 1530°C , this being the temperature that was

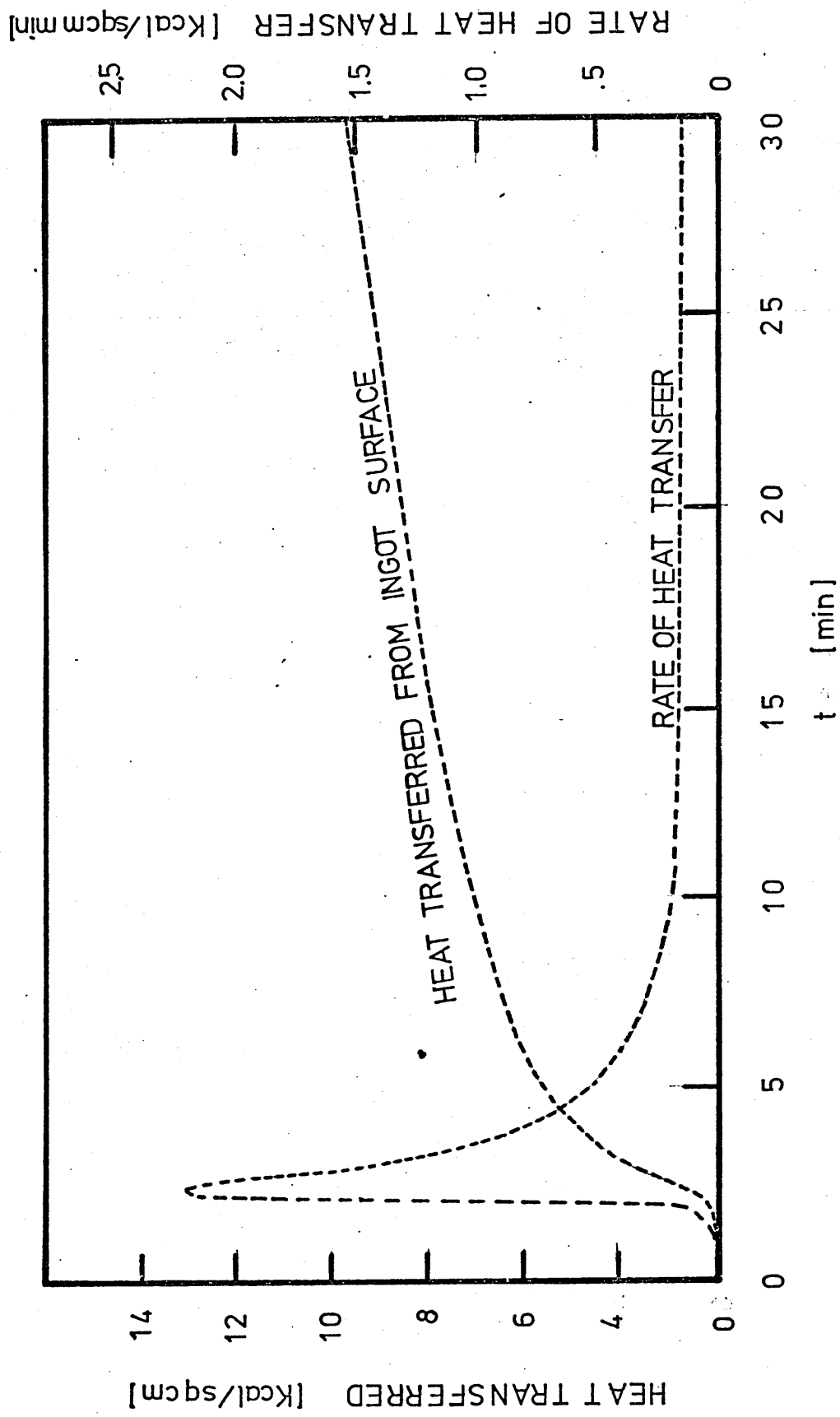


Figure. 1 Rate of heat transfer from ingot to mould 107 cm level. [After Mackenzie and

Donald (7)]

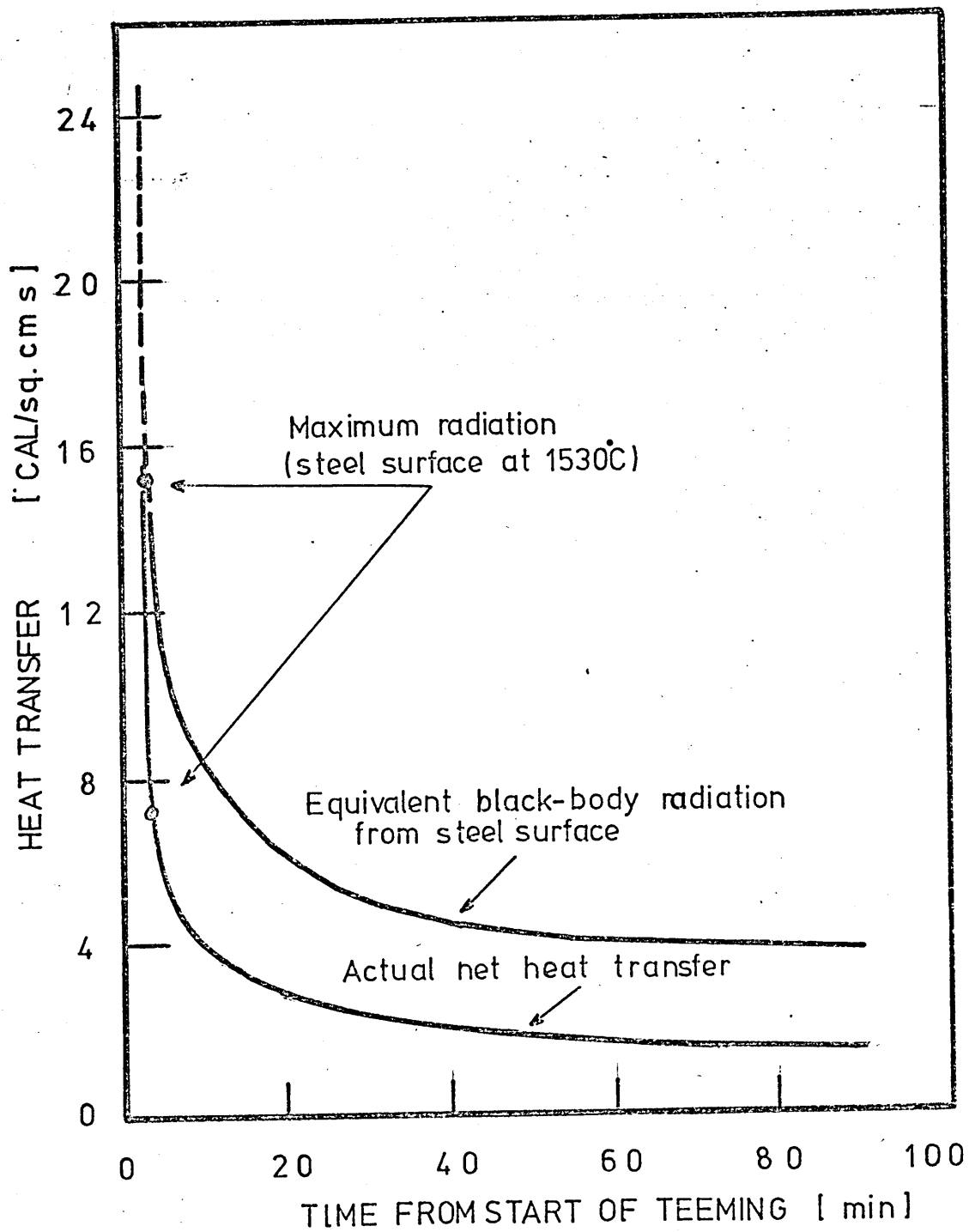


FIG. 2 Heat transfer between ingot and mould
(After Fowler and Savage (11))

measured at that time⁽¹¹⁾. They suggested that air gap formation times were less than four minutes and that the subsequent heat transfer from the ingot to the mould was entirely by radiation across the gap formed.

Volk and Wunnenberg⁽¹²⁾ carried out heat flux measurements in a continuous casting mould of 200 x 240mm cross section and 1%/m taper. One of the wide faces of the mould was sub-divided into eight equal horizontal cooling zones. Each zone was connected to independent water circuits, arranged to allow individual determinations of the quantity and temperature rise of the cooling water flowing through that section. They used oil, and low and high melting point powder fluxes as casting aids. The experiments were carried out with low alloy tube steels which were cast with superheats of 10° to 20°C in the tundish and, casting speeds ranging from 400 to 1200 mm/min. They obtained heat flux values for different depths in the mould. These values were averaged over the measuring period and throughout several heats. The final results were plotted against the distance from the top of the mould⁽¹²⁾ and are shown in fig.3.

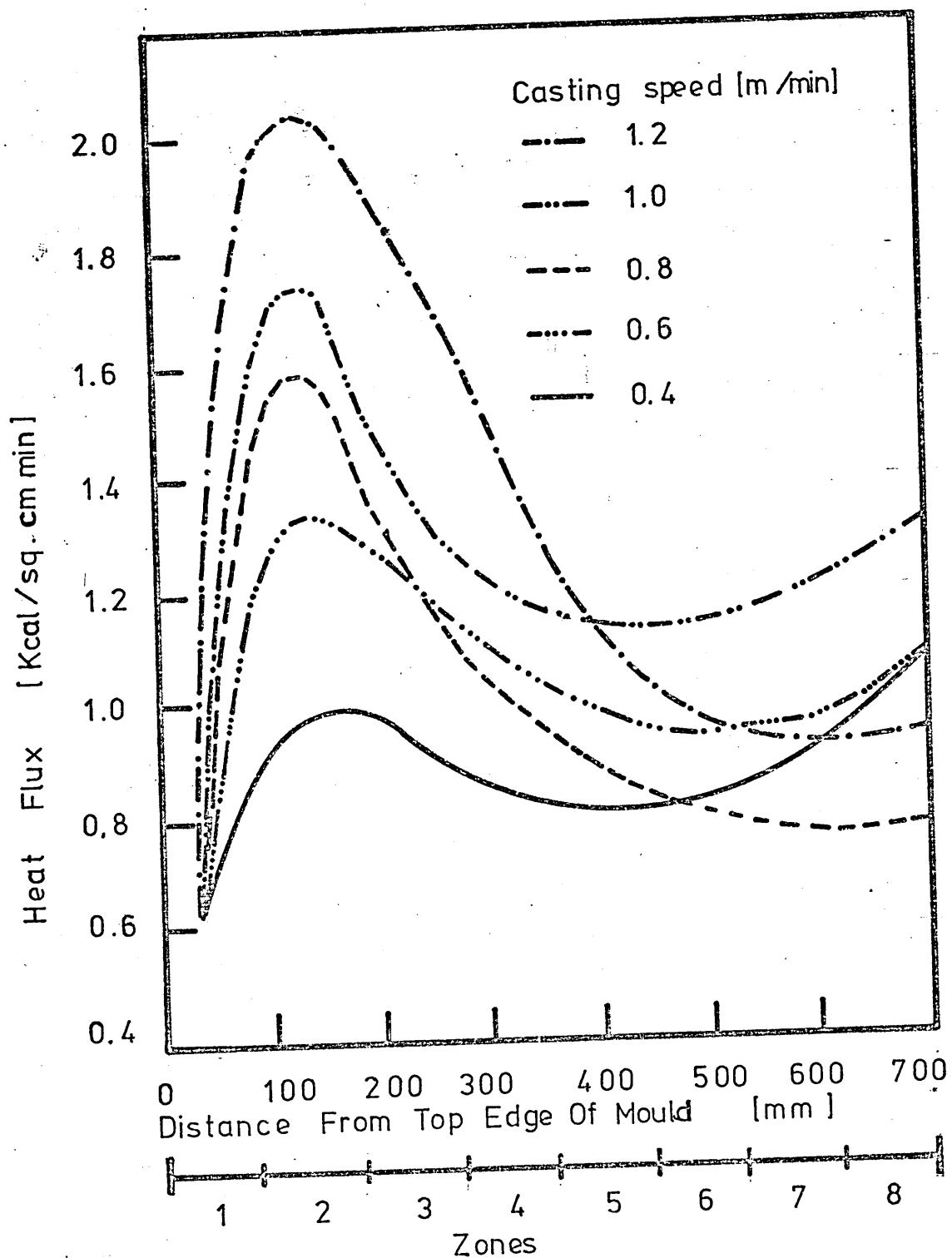


FIG. 3 Effect of strand speed and distance from the mould top on heat flux (After Volk and Wunnenberg (12))

II.2 Theoretical models for air gap formation

II.2.1 Elastic models

In all the elastic models developed to date, the main assumption has been to consider, the solidifying layer for a square or rectangular cross section mould, as an assembly of four separate beams. For each of these beams a purely elastic behaviour is assumed up to the melting point. The modulus of elasticity is assumed either dependent on or independent from temperature. Savage⁽¹³⁾ in his model for continuous casting of steel slabs considers the solidified layer as an assembly of four beams simply supported with a constant Young's modulus up to the melting point of steel. The beam tends to bow concavely towards the liquid core by the action of the thermal stresses originating from the thermal gradient throughout the shell. This latter effect is obliterated until the ferrostatic pressure is overcome by the thermal stresses in the solidified shell. The time at which the ferrostatic pressure is overcome by the thermal stresses was taken by Savage⁽¹³⁾ as the time of air gap formation.

Tien and Koump⁽¹⁴⁾ went a step further than Savage⁽¹³⁾. They have considered in their model a linear temperature-dependent Young's modulus which is nil at the melting point of the material. By assuming the solidified skin

to be an assembly of four separate beams, each behaving elastically, they calculated the stress distribution and distortion of the solidified shell. The calculations were carried out for an exponential decrease of the beam surface temperature and for different thicknesses of the beam. They considered two cases: a simply supported beam and a built-in beam. They found for both cases a time dependent displacement. For a simply supported beam, the displacement changed from a positive to a negative value and remained negative thereafter, i.e. the beam changed from a convex to a concave shape as solidification proceeded. For a built-in beam the displacement was always positive, i.e. the shape of the beam was convex towards the liquid core as solidification proceeded. The final shape of the simply supported beam determined in Tieu and Koump's model agrees with that from Savage's model.

Oeters and Sadermann⁽¹⁵⁾ have also employed the assumption of the shell behaving as an elastic beam, fixed at the ends, to analyse the air gap formation. They calculated the deformation of the solidified shell both due to the thermal contraction and the ferrostatic pressure. In addition they considered the deformation of the mould both due to (i) thermal expansion and (ii) the action of the temperature gradient through it. Adding

the respective contributions of the deformation of both mould and shell, they calculated the air gap evolution.

II.2.2. Elasto-perfectly plastic model

In idealised plastic theory it is assumed that the yield condition is independent of the plastic strain. When this requirement is fulfilled, the idealised solid is termed perfectly plastic. If the elastic portion of the strain is included in the analysis, the solid is said to be elastic-perfectly-plastic. Based in the above theory, Weiner and Boley⁽¹⁶⁾ developed an elasto-perfectly plastic model for the prediction of thermal stresses during solidification of a metal in square moulds. Similar assumptions to those made in the elastic models are made in this one. Firstly, the solidified shell is considered as an assembly of four separate beams, each beam being constrained against bending but otherwise unconstrained. Secondly, the yield stress of the material is assumed to decrease linearly to reach zero at its melting point. With these assumptions Weiner and Boley reached the conclusion that the stress at the cooling surface was compressive, this being reverse of the predictions made when plastic flow is omitted.

II.2.3 Viscoelastic model

This model takes into account the inelastic behaviour shown by solid materials at temperatures near to their melting points. When the material is subjected to a constant force and its temperature is raised to a high level, the elongation of the material will be observed to increase continuously with the passage of time. This mode of inelastic behaviour is known as creep. The phenomenon of creep is referred to as viscoelastic behaviour of the material. A particular solid may behave elastically or exhibit one or both types of behaviour in a process, viscoelastic and plastic, depending upon the duration of the process and the stress and temperature levels obtained. Weiner and Boley⁽¹⁷⁾ have identified this behaviour in a schematic diagram which is illustrated in fig. 4.

Lightfoot⁽¹⁸⁾ and Feltham⁽¹⁹⁾ applied the viscoelastic model to study the air gap formation times during solidification of steel ingots in cylindrical moulds. Due to the number of simplifying assumptions made by these authors, in order to solve their mathematical problems, their results are not reliable.

Richmond and Tien⁽²⁰⁾ applied the viscoelastic model to the solidification problem of a metal in a rectangular mould. Due to the assumptions made the problem was transformed from

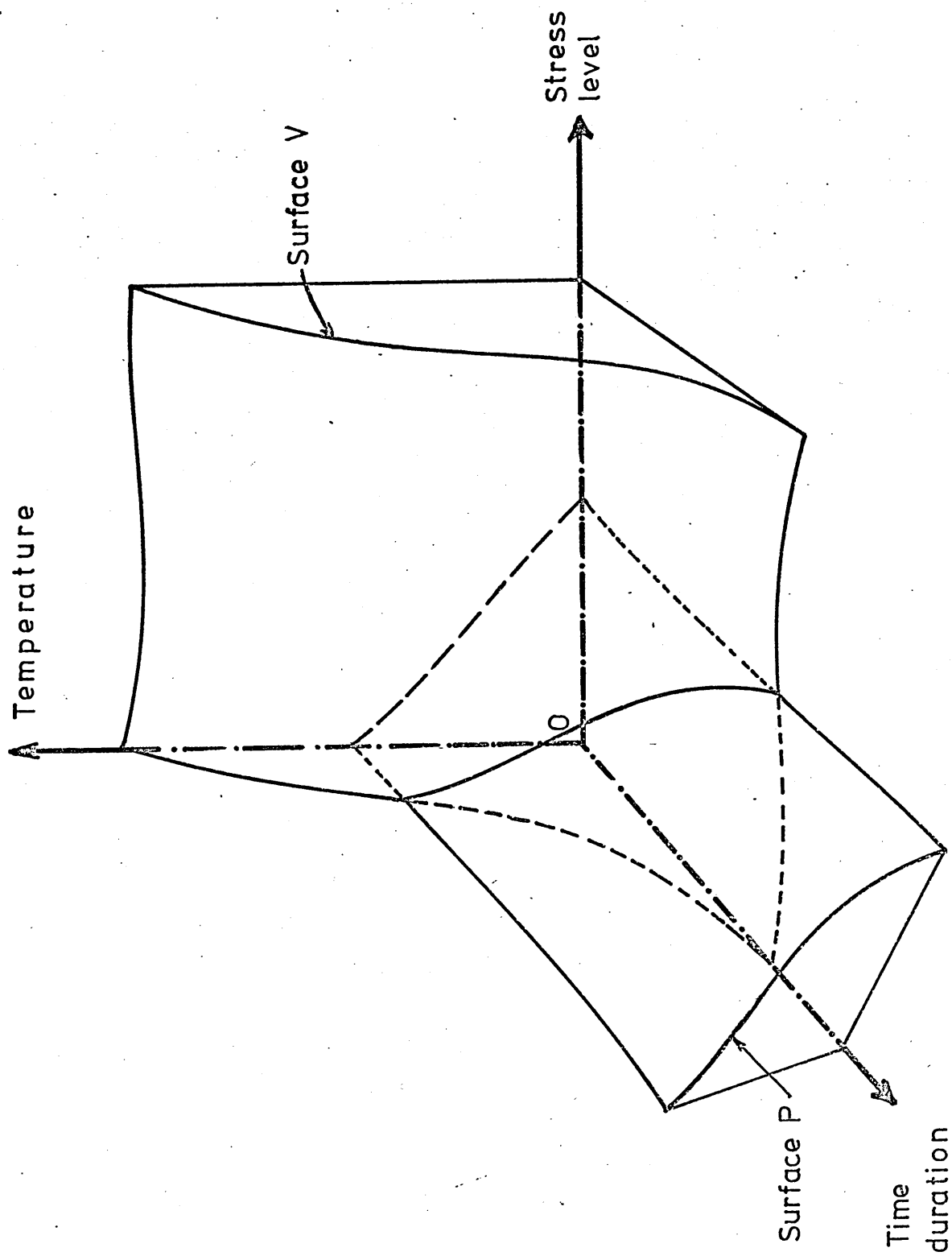



FIG. 4. Schematic diagram indicating regions of importance of different modes of inelastic behavior. plastic flow effects significant for processes above surface P; viscoelastic effects significant for processes above surface V. Below both surfaces the elastic idealization applies. From Boley and Weiner [17]

a three-dimensional to a one-dimensional problem where the solidified shell behaved as an assembly of four separate simply supported beams. The system of equations obtained in their work are highly nonlinear. The authors solved the system of equations, for the special case of slow cooling rates, using a linearising perturbation method. Thus they derived a particular expression for the stress in the solidifying skin, and the time required for an air gap to form between the ingot skin and the inner mould surface. For the case of a constant cooling rate, Richmond and Tien's calculations  showed the stress to be uniform through the ingot skin at all the times, beginning with a compressive value and becoming less compressive as solidification proceeds. The time at which an air gap forms was proposed by the authors to be the time at which the stress became zero. However, for higher cooling rates, the authors found that the stress in the outer surface of the ingot became tensile prior to air gap formation.

II.2.4 Coupled Thermoelastic model

This model deals with a boundary value problem which is of considerable mathematical difficulty, as it combines the theories of elasticity and heat conduction under transient conditions. Grill et al⁽²¹⁾, developed a mathematical model based on the thermoelastic coupled model. This mathematical model has been formulated to follow a transverse

slice of a steel slab through the mould and used to calculate the interactive heat flow and gap formation between the shell surface and the mould wall. To perform these calculations the authors sub-divided the model into two sections which could be evaluated independently: firstly, a section which calculated the temperature distribution in the slice accounting for the effect of the air gap between the slab surface and mould wall and, secondly, a stress distribution section which computed the deformation of the solidified shell and the stress distribution resulting from the temperature changes and the action of the ferrostatic pressure. They predicted a hot spot on the surface of the slab within a few centimetres of the corner on both the wide and narrow faces which was due to the shape of the gap. The temperature and location of the hot spot was seen to depend on the gap behaviour which varied markedly with changes in casting variables. In cases where the gap was wide, the hot spot reached temperatures as high as 1340°C where steel is weak and nonductile. Under these conditions the gap may collapse under the force of the ferrostatic pressure and later a narrower more stable gap configuration forms with lower hot spot temperatures⁽²¹⁾.

II.2.5 Solid contraction model

This simple model is based on the thermal contraction of metals during solidification. Waters⁽²²⁾ estimated an apparent linear coefficient of solidification shrinkage of the ingot metal, β , from the following relation:

$$\beta = \frac{1}{2} \left[\frac{(\gamma_1)^2}{(\gamma_2)^2} - (1 + 2 \Delta\theta\alpha) \right] \quad (\text{II.1})$$

where γ_1 is the radius of the mould and γ_2 the radius of the ingot at room temperature, α is the linear coefficient of expansion of ingot metal and $\Delta\theta$ is the difference between solidification temperature of the ingot and room temperature. For continuously cast lead ingots in a mould 25.26mm diameter, the measured ingot diameter at room temperature was found to be 25.20mm. From the above equation (II.1) Waters calculated a value of β to be -0.0068. He concluded that, in case of lead, there is no solidification contraction, but an apparent expansion of the solidified ingot. This was explained as possibly being due to plastic flow of the newly formed ingot skin.

Lewis and Savage⁽²³⁾ calculated gap widths using the formula:

$$J_a = \frac{D\alpha}{2} (\theta_s - \theta_o) \quad (\text{II-2})$$

where J_a is the gap width, D is the diameter of the ingot, θ_s is the solidus temperature, θ_o is the mean ingot surface temperature and α is the linear coefficient of expansion.

From the heat flux formula (II-3) air gap widths were calculated in order to compare them with those calculated from thermal contraction formula (II.2).

$$H = \frac{\theta_s}{\frac{d}{k_s} + \frac{m}{k_m} + \frac{Ja}{k_a} + \frac{b}{V_w^{0.8}}} \quad (11.3)$$

where d is the solidified thickness (cm, k_s is the metal thermal conductivity (cal/cm⁰Cs), k_a is the air thermal conductivity (cal/cm⁰Cs), b is a constant equal to 455, k_m is the mould thermal conductivity (cal/cm⁰Cs), m is the mould thickness (cm) and V_w is the velocity of the cooling water (cm/s). The heat flux and ingot surface temperature data were taken by the authors from Savage and Prichard⁽²⁴⁾. Lewis and Savage compared widths made by both methods and their results are shown in fig. 5. For continuously cast steel ingots in an 80mm diameter mould, the ~~two~~ methods both gave gap widths of the order of 10^{-2} mm. The values obtained from thermal contraction (see fig.5) appear to be two or three times larger than those derived from heat transfer data. The authors explained this difference from the idea of hindered contraction where the partially solidified skin does not contract naturally. This phenomenon prevents the contraction of the cooler surface of the ingot. The effect of hindered contraction causes the ingot skin to change its shape and sometimes to tear in order to try and accommodate itself to the strains which are created by non-uniform

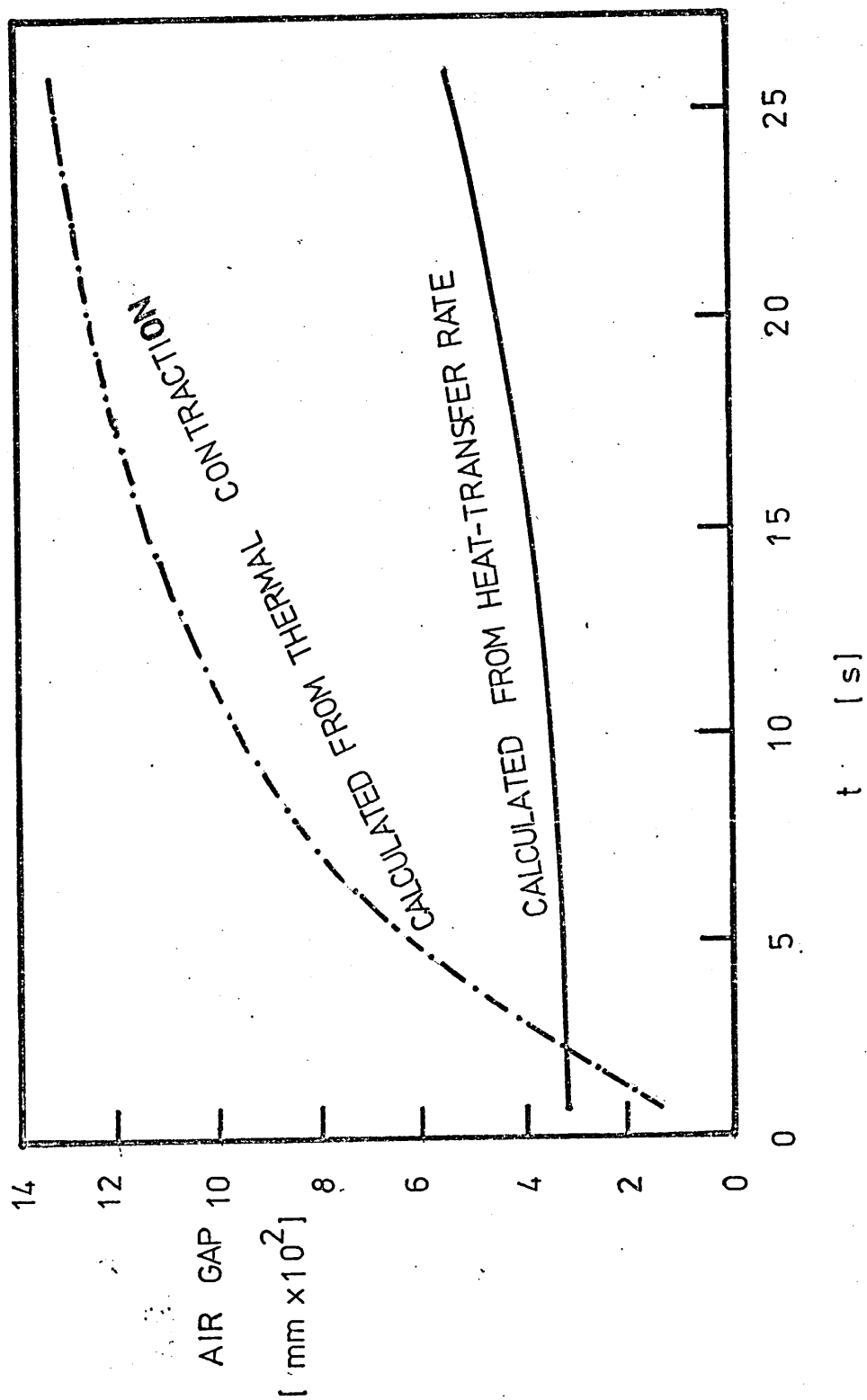


FIG. 5 Estimated Air Gap Between Ingot and Mould. (After Lewis and Savage(23))

contraction.

Skvortov⁽²⁵⁾ claimed that the air gap between the billet surface and the mould wall occurred mainly at the corners and the convex portions of the billet when different mould geometries were used. He explained that this was due to non-equilibrium between the shrinkage and ferrostatic forces acting on the solidified shell. The interaction of these forces determines the moment at which a gap forms between the billet surface and the mould wall and the extent of the stresses arising in the shell. Since the force acting on the narrow face of the billet is always less than the force acting on the wide face, then the gap must form at the narrow face first then at wide face⁽²⁵⁾.

11.3 Influence of cooling rate on solidification

The process of unidirectional solidification of binary alloys has been analysed by several authors^(25,26,27). Tien and co-workers^(25,26) have developed approximate solutions to^{the} unidirectional solidification problem considering two different kinds of boundary conditions: an imposed constant surface temperature lower than the liquid temperature and a surface temperature which continuously decreases its initial value with solidification time. For this latter case, they considered the influence of cooling rate by classifying cooling rates as either fast or slow. They defined a fast rate

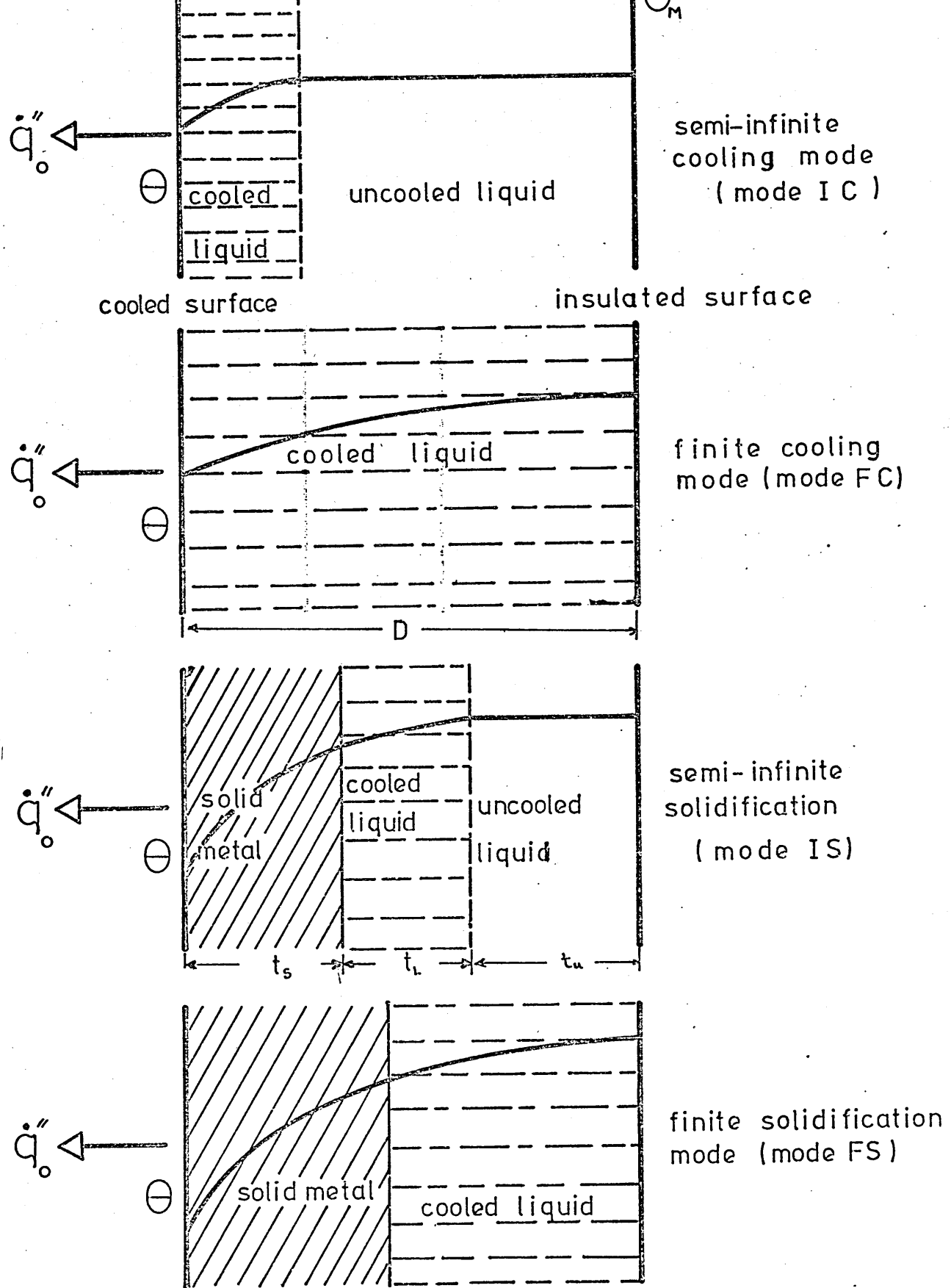


Fig.6 Cooling modes for a pure metal or alloy.(After Hills et al(28))

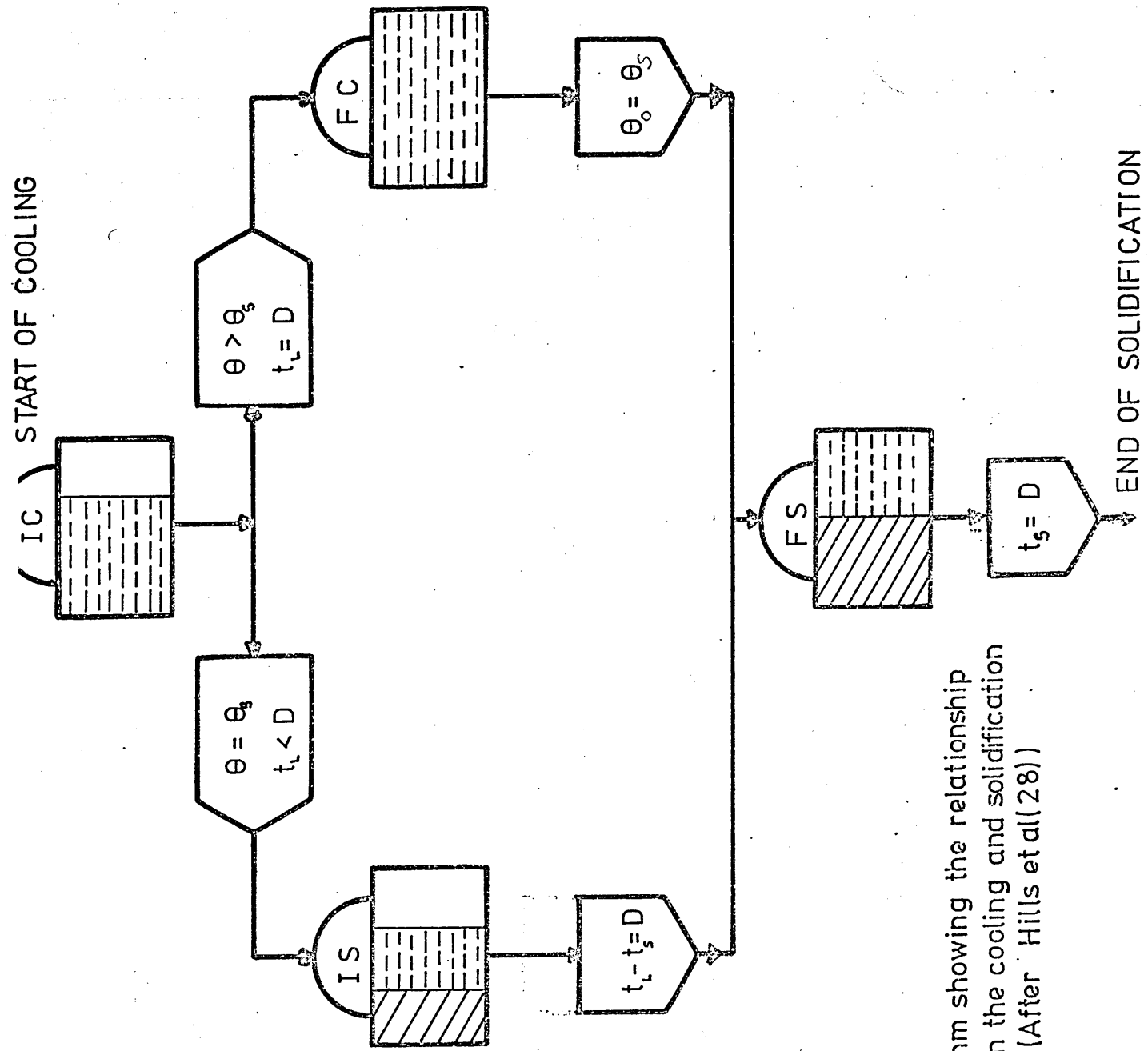


Fig. 7 Algorithm showing the relationship between the cooling and solidification modes. (After Hills et al(28))

of cooling as one for which the solid skin forms before the liquidus front reaches the centre of the slab and thus defined a slow rate of cooling as one for which the rate at which the surface temperature decreases is sufficiently slow for the liquidus front to reach the centre of the slab before solidification at the surface of the slab is complete. They present approximate solutions of the heat conduction equation for both these boundary conditions. They compared theoretical values predicted by their theory with experimental results obtained for the unidirectional solidification of aluminium 4% copper alloy. They obtained qualitative agreement only and attributed the lack of better agreement to some of the assumptions made.

Hills et al⁽²⁷⁾ have attacked the solidification of binary alloys in a different way. Their formalism takes into account the influence of superheat on the mode of solidification. They applied the integral profile method in order to describe the heat transfer process in the liquid metal region in terms of a characteristic variable. Two layers are defined: a layer of cooled liquid and a layer of solidified metal (see figure 6). The layer of cooled liquid initially expands into uncooled liquid metal. (Mode IC). Under slow cooling conditions, this mode ends when the cooled liquid layer has expanded to the neutral surface after which the entire liquid layer cools (Mode FC). Under fast cooling conditions, Mode IC ends when the surface is cooled to the solidification temperature, after which the solid and liquid layers expand

together (Mode IS). Modes FC and IS are both followed by Mode FS in which the solid layer expands, the layer of cooled liquid contracting against the neutral surface. Fig. 7 shows the algorithm which determines which solidification route is followed under any given conditions.

III EXPERIMENTAL APPARATUS

III EXPERIMENTAL APPARATUS

III-1 Moulds

Transparent moulds were selected in order to allow visual observations of the changes that would occur at the mould/ingot interface during solidification of metallic alloys. Initial experiments were carried out in pyrex beakers, and these were followed by experiments in two types of mould - type A and type B.

III.1.1 Beakers

The beakers used to melt and solidify in-situ metals were of pyrex glass 36mm diameter and 55mm long, i.e. 100ml in volume. Pyrex glass can withstand temperatures up to 600°C without deformation but not sudden temperature changes. These properties made the pyrex beakers adequate for melting of alloys which have a low melting^{point} and allowed visual observation of the changes taking place at the interface.

III.1.2 Mould A

The subsequent mould used was that shown in plate 1. Mould A consisted of a rigid square U-frame of mild steel 40 x 55mm in cross section. This mould was designed for melting and solidifying in situ rectangular prismatic ingots of the following dimensions 45 x 130 x 135mm.

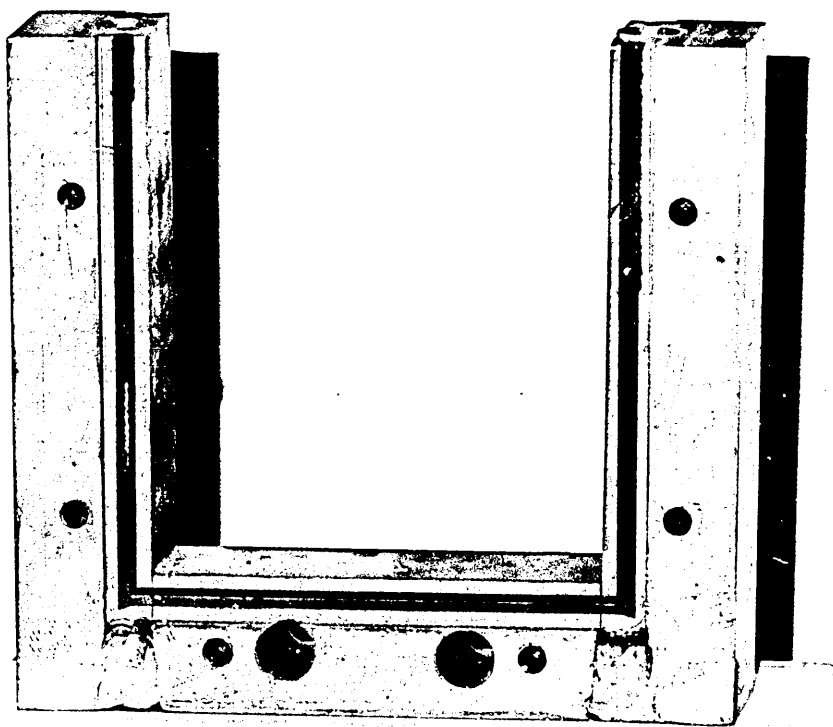


PLATE 1

The front face of the U-frame consisted of a pyrex glass 6mm thick. The back face consisted of a rectangular steel plate 3mm thick. Both plates were held against the U-frame by means of bolts screwed to the frame and the edges sealed with asbestos string. One vertical orifice was drilled in each side of the frame at 1mm from the inner mould face, and to a depth of 150mm from the top of the frame. Two horizontal holes were also drilled from side to side 25mm from the centre of the lower part of the frame. These holes were made for positioning the electrical heaters that would supply necessary power to melt in-situ the ingot.

III.1.3 Mould B

Mould B fig. (8) was a rectangular mould, the front face being either a pyrex or a silica glass plate 155 x 170 x 6mm. The remainder of the mould was made by welding from mild steel plates to give a mould cavity 40 x 135 x 170mm in volume. At the back wall two orifices 15mm diameter and 150mm long were drilled at a position 30mm from the centre of the plate and 30mm from the inner face of the wall. One other orifice of 1.5mm diameter and 100mm long was also drilled vertically and parallel to the wall surface. This orifice, which was used to locate a

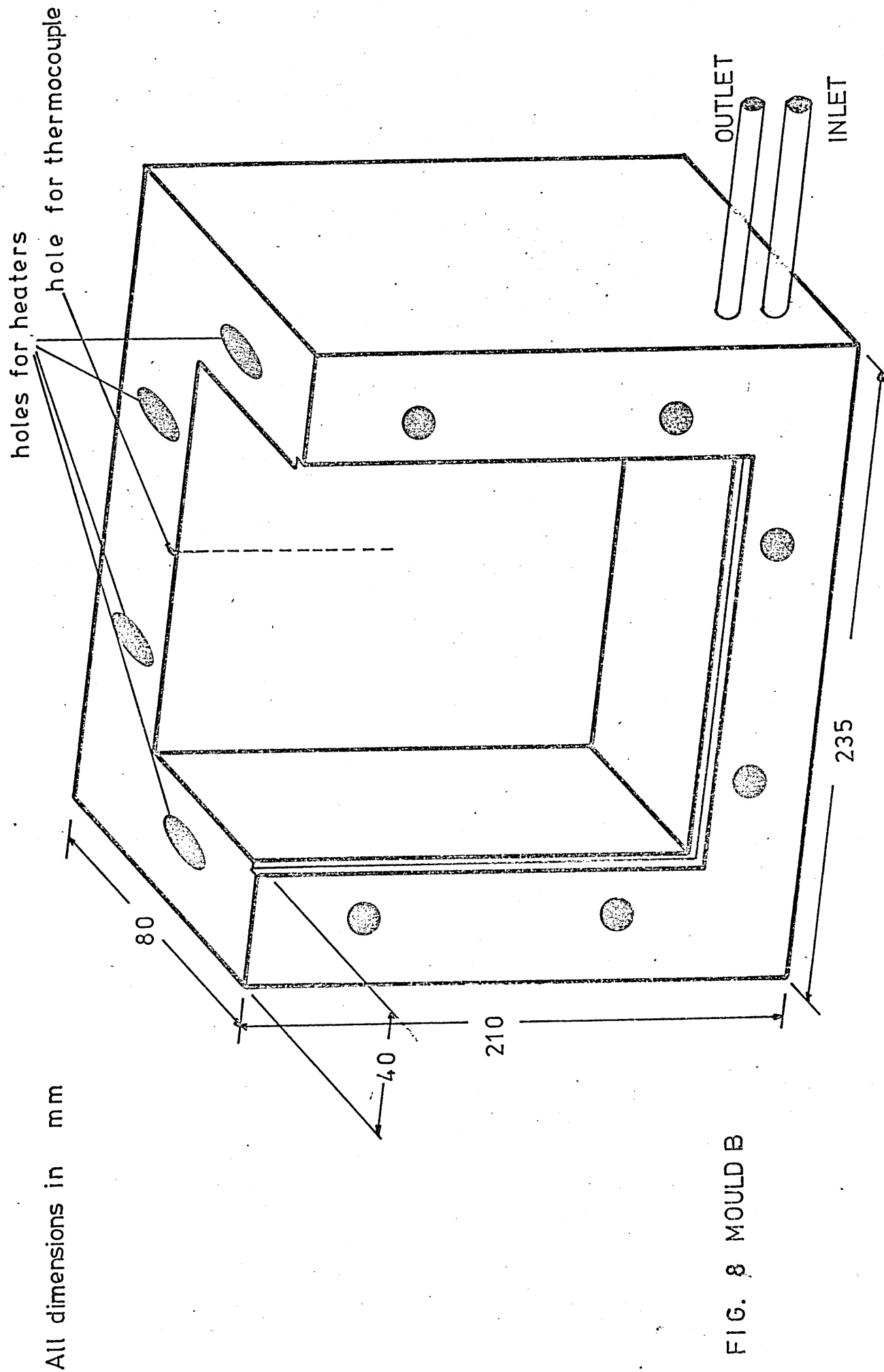


FIG. 8 MOULD B

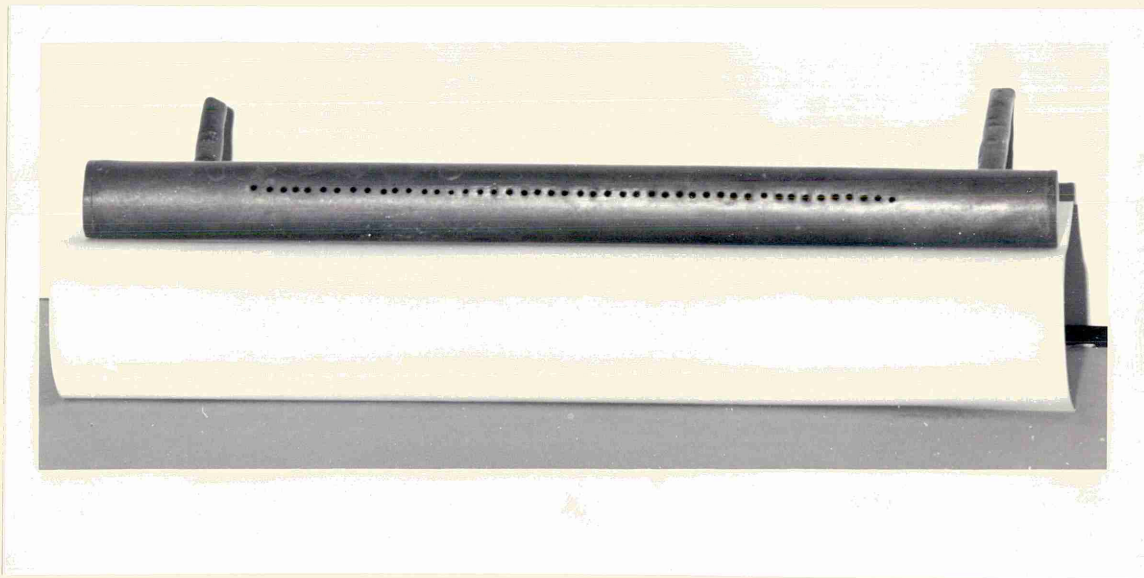
thermocouple, was placed 1.0mm from the inner mould surface and at the mid-point of the back wall of the mould. The front faces of the side walls of the mould were machined to provide a recess into which an asbestos string could be placed to provide an adequate seal for the plate of pyrex glass or fused silica. Six small threaded holes were machined into the front faces of the mould to hold retaining screws for the glass plate. A series of horizontal grooves were machined in the outer face of the metal walls of the mould. These grooves were interconnected to form continuous channels in the side and back walls of the mould. A plate was then welded over the outer faces of the side and back walls to enclose these channels to form cooling passages for either water or air.

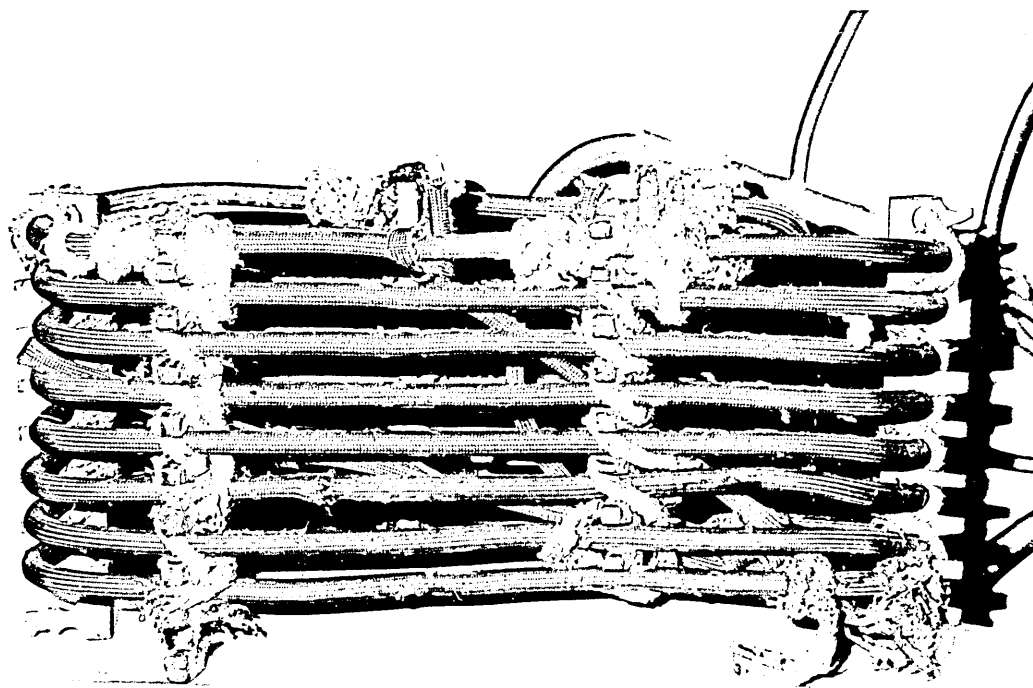
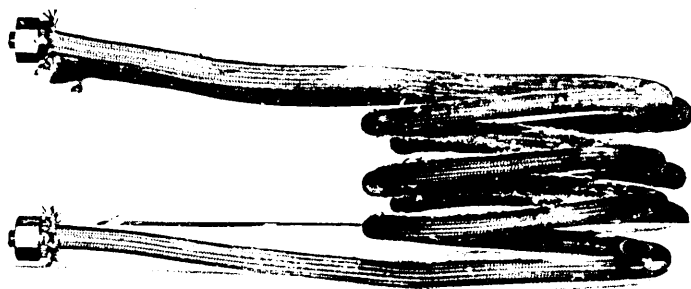
III-2 Cooling system

In the metallic section of the mould which formed the two sides the back and the base this consisted of the cooling passages for the back and the sides previously described. Copper tubing was brazed to the lower part of one of the sides (see fig.8), to provide an inlet and an outlet for the passage of either air or water through this section of the cooling system.

To provide cooling for the front face a multiple nozzle, shown in plate 2 was constructed from a copper tube 300mm long and 30mm diameter which was closed at both ends. Along the length of this tube a row of small holes, 2mm diameter was drilled at a 3mm separation between the centres of the holes. Entry of air or water to this cooling nozzle was effected by welding 10mm diameter tubes to openings made opposite to the fine holes and 20mm from each closed end. Initial flow studies showed that the most even flow distribution of cooling water was achieved when only one of these tubes was used to supply the water. By means of this multiple nozzle it was possible to obtain a nearly laminar flow over the glass interface of the mould B when water was used.

An aluminium trough 500mm and 150mm high was made to collect the water discharged by the nozzle. Three aluminium rods were welded between two opposite sides of the trough at 100mm from the base. These rods supported the mould to prevent direct contact with the water being collected. Also, the trough was filled with water up to 80mm high providing a sufficient water depth to quench all the liquid metal in case of rupture of the mould glass wall. By means of siphon the level of water





inside the trough was maintained constant during the experiments in which the front was water cooled.

III.3 Temperature Measurement

Two different thermocouple arrangements were used in this work as shown in fig.9a and 9b. The thermocouples were chromel-alumel encased in a stainless steel sheath 1.5mm in external diameter and supplied by Pyrotenax Ltd. The conductors and sheath were bonded together at the extreme tip to obtain a quick response. The thermocouples were fixed to a support which held them in place inside the mould cavity. The arrangement is shown in plate 4. The thermocouples were arranged so that their length lay normal to the heat flow direction. In the first arrangement fig. 9a, the thermocouples were connected to a Credshire-500 data logger. The data logger recorded the EMF's on a tape at rates of up to four thermocouples in five seconds. The temperatures were calculated using the linear relationship:

$$\Delta\theta = \theta - \theta_0 = \alpha V$$

where θ is the temperature, θ_0 is the room temperature, α is the slope from the curve given in fig.10 and V is the E.M.F. read by the data logger. The second arrangement

All dimensions in mm

Front thermocouples

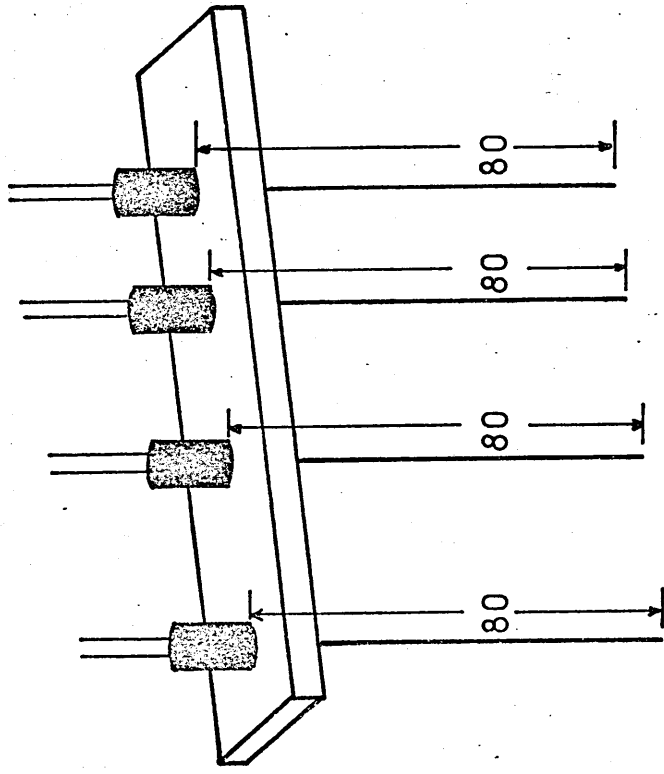
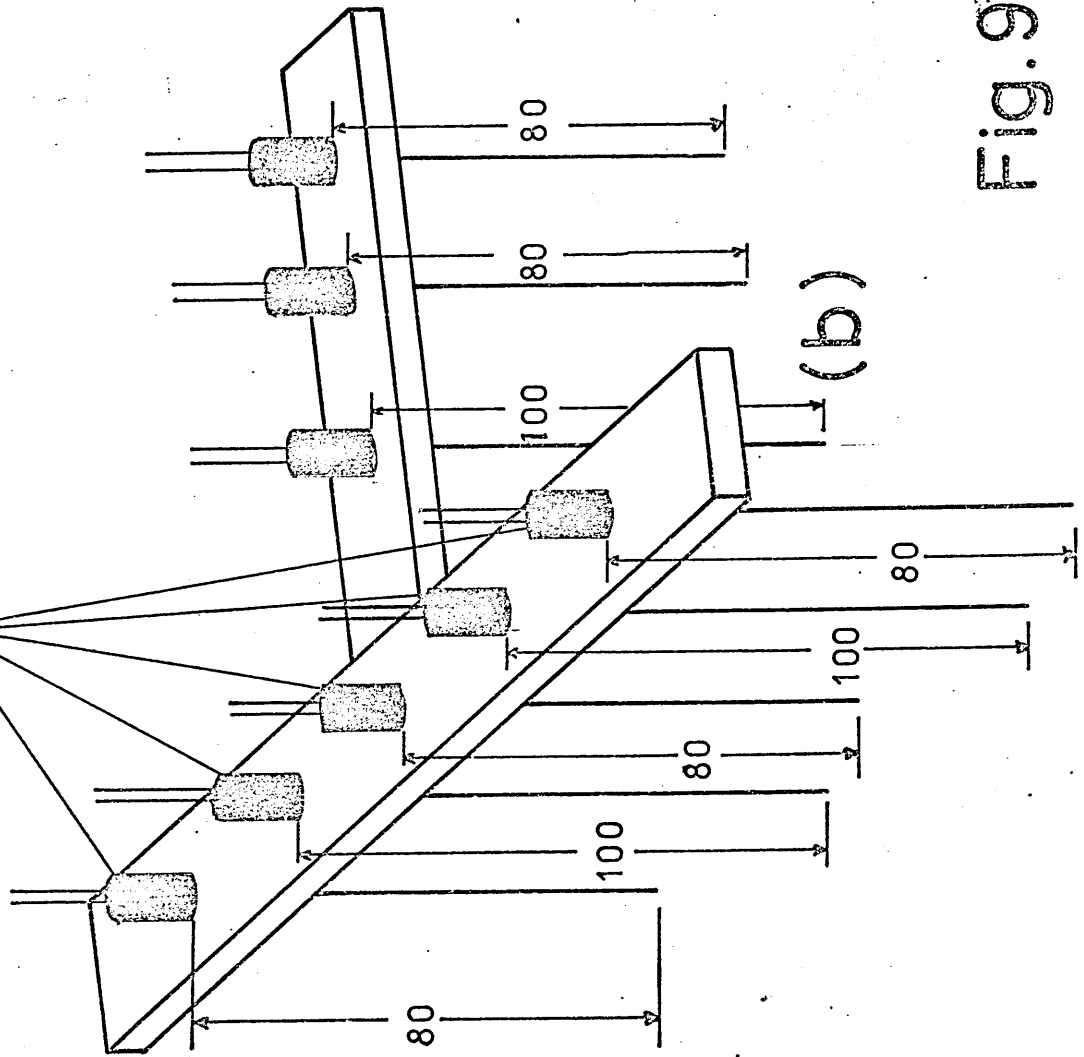


Fig. 9

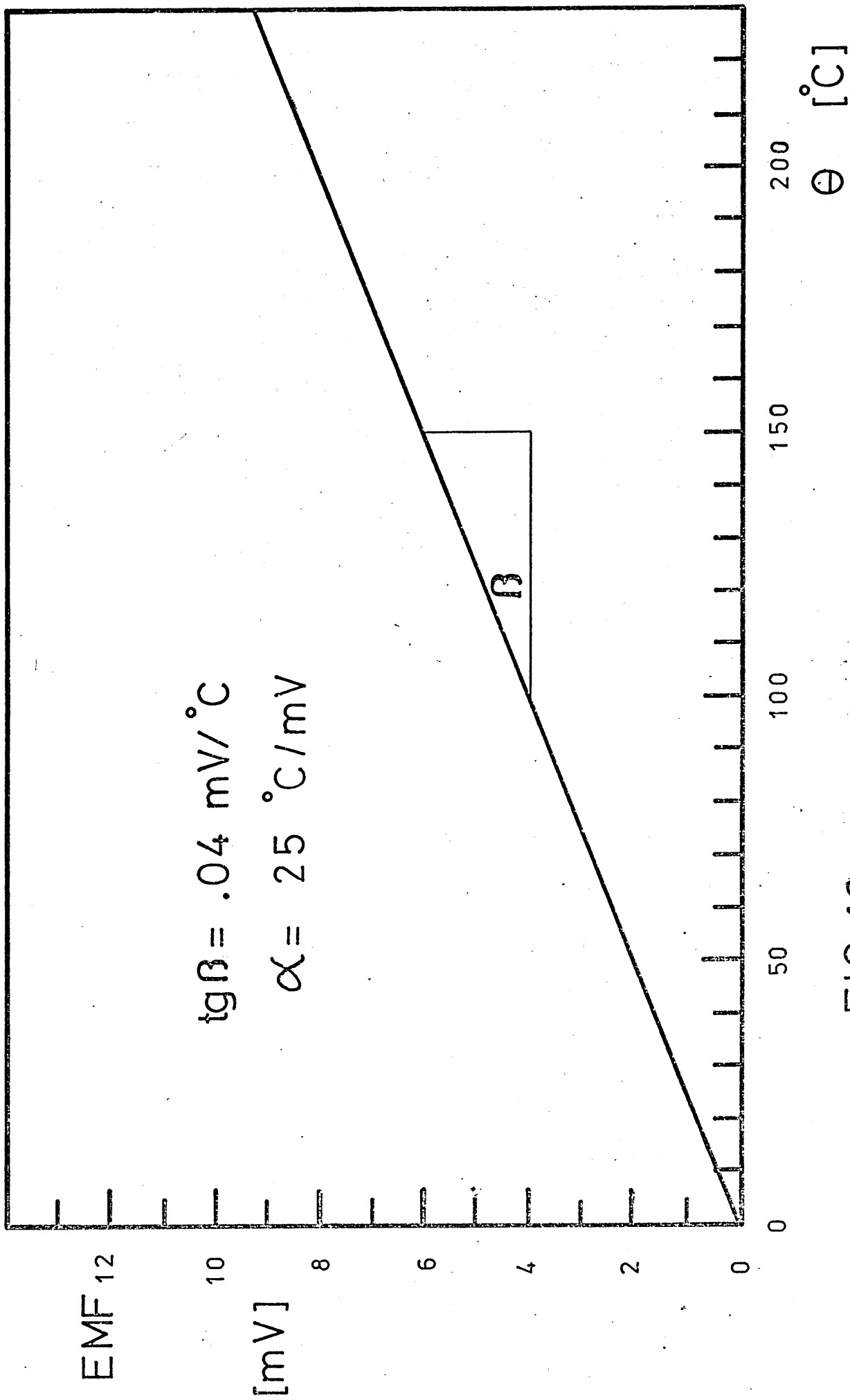


FIG.10

fig.9b the thermocouples were connected to a computerised solartron data logger which computed the temperatures differences, $\Delta\theta$, based on the linear relationship indicated above. For both arrangements, the corrections for the room temperature was made by adding the room temperature to the temperature difference.

III-4 Heating

A Radyn-C50 6kW R.F. induction heater with two coils of different geometric form was used to heat the beakers and mould B. The coil used was cylindrical for the beakers and rectangular for mould B. The two coils are shown in plate 3 . The coils were made out of copper tubing 5mm diameter covered with insulating tape.

Mould A was heated with four electrical heaters each of 1000 watts capacity and supplied with power delivered from a variac transformer.

III.5 Equipment for air gap width measurements

III.5.1 Interferometer

A Michelson interferometer shown schematically in fig.11 was developed in an attempt to measure the air gap width. The interferometer was constructed as a normal interferometer except that one of the mirrors was replaced

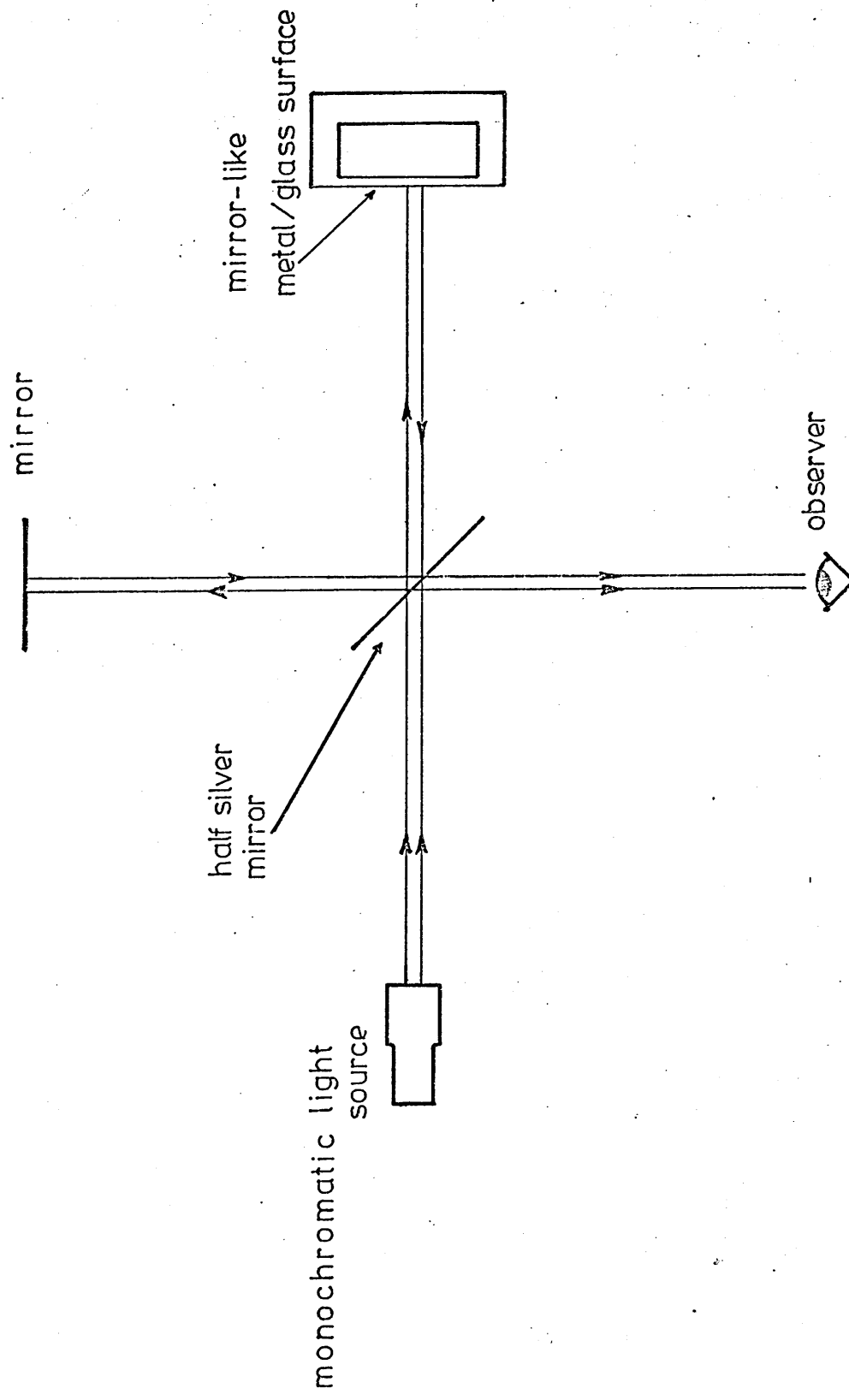


Fig. 911

by the metal/glass interface in mould B. This interface behaved as a mirror surface. The principle of the above method consisted in comparing the interference pattern produced when the metal inside the mould was liquid to the interference pattern produced as the metal solidified. The changes produced in the interference patterns give a characteristic displacement which is later related to parameters such as wave length of the light used and optical distances of the instrument.

III.5.2 Laser

A laser beam was used in a second attempt to measure the gap width by reflexion at the metal surface. The beam was focused at a point of the metal/glass interface as shown in fig. 12. The width of the gap can then be calculated from the relative displacement of the reflected beam from the metal with respect to the beam reflected from the glass.

III.6 Metals and alloys used

The metals and alloys used in this work were chosen from metals which have low melting points and a relatively high percentage of volume contraction during solidification. In experiments carried out in beakers the following metals and alloys were used: pure lead, pure tin, Wood's metal

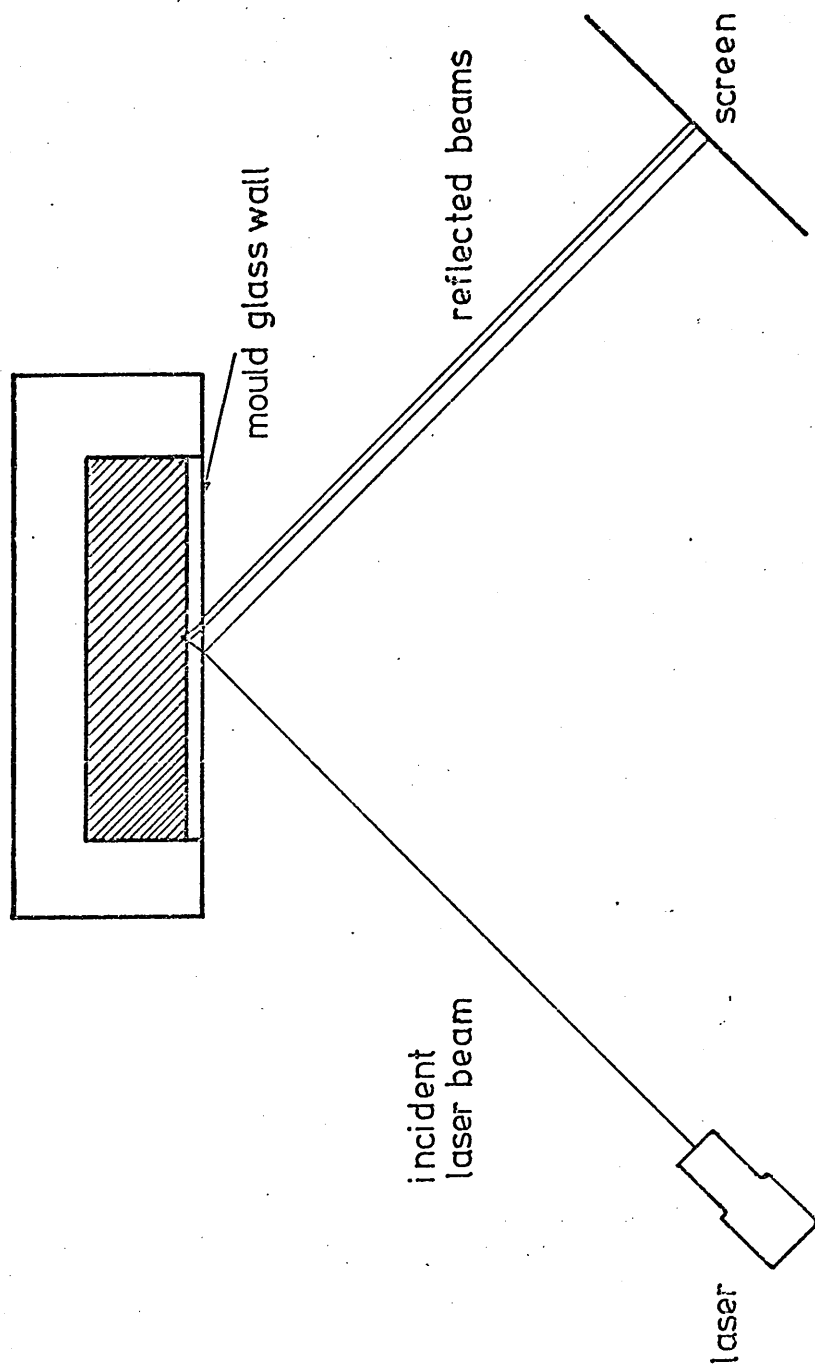


Fig. 12

(25% Pb, 12.5% Sn, 50% Bi, 12.5% Cd) Sn 43% Bi, Pb 5% Sn and 50% Pb Sn alloy. In the experiments which were carried out in moulds A and B metals and alloys used were pure tin, pure lead and 50% lead-tin alloy. All the metals used either individually or in an alloyed form were of normal commercial purity. All the alloys and pure metals used in the present work were melted in-situ except for the first experiment in mould A. In this case a 50% lead-tin alloy was sand cast into a rectangular mould. The ingot obtained was subsequently machined to the dimensions of mould A.

IV EXPERIMENTAL PROCEDURE

IV. EXPERIMENTAL PROCEDURE

IV.1 Experiments in beakers

A series of experiments were carried out in transparent pyrex glass beakers. The objective was to ascertain the feasibility of being able to follow visually air gap formation which it was thought would take place at the metal/glass interface. These experiments were performed with different pure metals and alloys (pure lead, pure tin, Wood's metal, Pb 5% Sn, Sn 43% Bi and 50% Pb Sn alloy). Both, the pure metals and the alloys were melted in-situ using a R-F induction heater equipped with a cylindrical coil which fitted the beaker's geometry. The coil could be removed after melting allowing direct visual observation of the solidification process at the metal/glass interface. Before the melt was allowed to cool it was stirred vigorously to homogenise the temperature. The solidified metal was observed to stick to the glass walls until solidification was completed. The metal shrank from the glass walls due to thermal contraction once it had solidified producing an audible click. On several occasions this latter effect caused the beaker to shatter.

Since it was not possible to observe the air gap formation in these preliminary trials a series of further experiments in a different shaped mould were carried out.

IV.2 Experiments in mould A

A series of experiments were carried out in the mould A design plate (1) with the object of observing the formation of an air gap at a flat metal/glass interface during solidification. Observations were made using pure metals and alloys (pure lead, pure tin and 50% lead-tin alloy).

The first experiments were performed with a rectangular 50% lead-tin alloy ingot which was sand cast and subsequently machined to fit into the mould. The machined ingot was then melted in the mould using electrical heaters inserted into the holes drilled into the mould sides.

After melting, a flat mirror-like metal/glass interface was obtained and remained until solidification took place at the interface. A less reflective but still smooth interface formed during the solidification process allowing visual observation of the changes occurring to be made. The metal was observed to remain stuck to the glass until solidification was completed but then shrank away from the glass, due to the thermal contraction of the completely solidified ingot, producing an audible click.

During these initial experiments with mould A, it was found that the production of a mirror-like glass/metal interface did not require the separate casting and machining of an ingot. During the melting of metal in the mould, it was found that dirt and films of oxide and dross were deposited at the inner glass surface. However, it was possible to clean these away with an asbestos brush and a steel scraper. After cleaning the glass in this way, a mirror-like interface was obtained as in the initial experiments, and this in-situ melting and cleaning procedure was adopted in all subsequent experiments. Several pure metals and alloys were melted and their solidification studied in this way. In all these experiments the ingots remained stuck to the glass surface until well after solidification was complete. In an attempt to change the nature of the mould/metal interface at the glass surface, a silicone oil was sprayed onto the inner glass surface before an ingot was melted in situ. The result was that an oil film together with an oxide film formed at the glass surface during melting destroying the mirror-like interface and obstructing any visual observation.

Since no air gap formation had been observed in the above experiments a new mould design was developed. The new design maintained the transparent front wall but allowed the cooling rate to be controlled and temperatures to be

recorded. In addition an interferometry apparatus was developed in an attempt to measure any small separations that might occur at the metal/glass interface during solidification.

IV.3 Preliminary experiments in mould B

IV.3.1 Use of the interferometer

Complete details of the equipment were given in section III.5.1 and shown schematically in fig.11.

The mould B and the interferometer apparatus rested on a strong steel table the top of which was a Syndanyo platform 1000 x 800 x 25mm. The side walls of the mould were either air or water cooled but the front glass plate was cooled by natural convection. The cooling air for the side walls was taken from a compressed air line and delivered through a plastic tube connected to the cooling channel in the mould walls. When water was used for cooling, it was taken from the tap and delivered in a similar manner to the air. Temperatures were recorded at four different points in the metal and the mould using the initial thermocouple rig (fig.9a), described in section III.3. The thermocouples were connected to the Credshire-500 data logger.

Prior to each experiment, the mould and the 50% lead-tin alloys were heated up some 40° to 50° above the melting point of the alloy and the melt was stirred vigorously for temperature homogenisation. The inner metal/glass interface was then cleaned obtained a mirror-like interface and attempts were made to obtain the reference interference pattern, at this cleaned interface. Unfortunately, it proved impossible to obtain any interference pattern due to both natural convection of the liquid metal inside the mould cavity and the mechanical vibrations produced by the cooling air or water through the side walls of the mould.

The interferometry method was thus discarded and a further method based on the reflexion of a laser beam was used to examine any small separations that occurred at the metal/glass interface.

IV.3.2 Use of the laser beam

Otherwise applying the experimental procedure already described in the previous section, a laser beam was made to impinge at a certain angle onto the glass plate once the metal had been melted. Two reflected beams were formed, one reflected from the external glass surface and one from the glass/metal interface. When solidification occurred at the

interface a third reflected beam from the metal appeared. All these beams were collected onto a screen, producing three sharp spots. It was observed that the spot produced by the beam reflected from the metal surface moved away from the other spots immediately after solidification occurred. The metal surface then suddenly became granular scattering the reflected beam and producing a diffuse spot which obliterated any further measurement.

These experiments showed that some changes occurred at the metal/glass interface on solidification but did not allow measurement to be made of the width of any air gap that might form. Further experiments were, therefore, based on a combination of thermal analysis and visual and photographic observation of the metal/glass interface during cooling and subsequent solidification of the metal or alloy.

IV.3.3 Preliminary experiments using the thermal analysis method and visual observations

These experiments were conducted under a range of different cooling conditions achieved by use of the multiple jet and the side wall cooling passages. The cooling conditions used are specified in table III, which also defines the

TABLE I I I

SIDE FRONT WALLS PLATE	A natural convection			B air cooling		C water cooling	
	1	2	3	4	1	2	3
1 natural convection	1 A	2 A	3 A	4 A	1 B	2 B	3 B
2 air blowing from top downwards							
3 air blowing from bottom upwards							
4 film water cooling							

cooling conditions preliminary experiments

code that will be subsequently used to specify the different conditions.

Mould B was equipped with a pyrex glass front, as in the previous experiments and with an eight thermocouple rig (fig.9b) connected to the Solartron data logger. The lead-tin eutectic alloy was used in all these preliminary experiments and was melted and solidified in-situ. Melting and heating were carried out using R-F induction unit connected to a movable coil. As in the previous experiments the alloy and the mould were heated to some 40° to 50°C above the melting point. Oxide films that appeared at the mould glass/metal interface during melting were cleaned using the asbestos brush and steel scraper. The molten metal was subsequently stirred vigorously to even out any temperature variations. Subsequently the air pressure valve was opened releasing the pressurized air to the multiple jet and/or to the side wall cooling passages at a measured gauge pressure of 5.5 bar. At the same time the recording of the temperature was started and visual observations made. A typical set of cooling curves for a 1B run is illustrated in fig.13.

Since air gap formation could be followed visually in some of the experiments, a final modified arrangement was developed, in which the major solidification variables could be controlled more precisely.

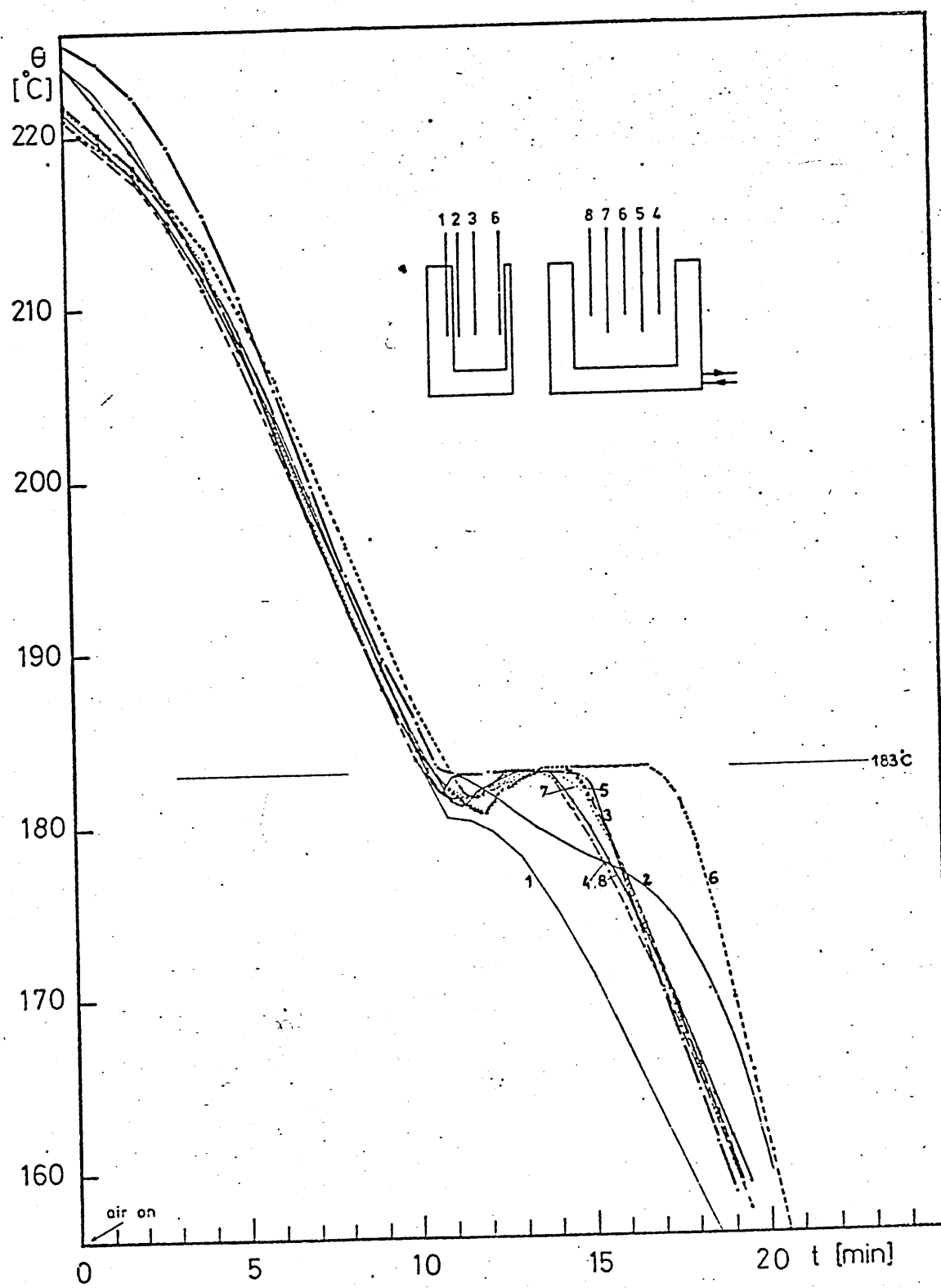


Fig. 13

IV.4 Final Assembly

IV.4.1 Experimental procedure

The final assembly (plate 4) was used to conduct a series of experiments with different controlled cooling conditions applied to both the mould walls and the front silica plate which replaced the pyrex plate used in the previous experiments. The cooling conditions are specified in table III. The pure silica glass plate allowed the front to be water cooled, adding a new set of cooling conditions to the ones obtained in the preliminary runs.

Actually, the experiments were carried out using the experimental procedure described in section IV.3.3, except that, when water was used to cool the front silica wall, the multiple jet was repositioned in order to balance the higher rate of heat extraction from the coolest side of the mould, i.e. the side of the mould where the inlet and outlet tubes were situated.

IV.4.2 Thermocouple calibration and temperature corrections

IV 4.2.1 Thermocouple calibration

As discussed in section III.3 the thermocouples used in this work were stainless steel sheathed chromel-alumel 1.5mm diameter. Thermocouple No. 3 was calibrated using the lead-tin arrest as standard.

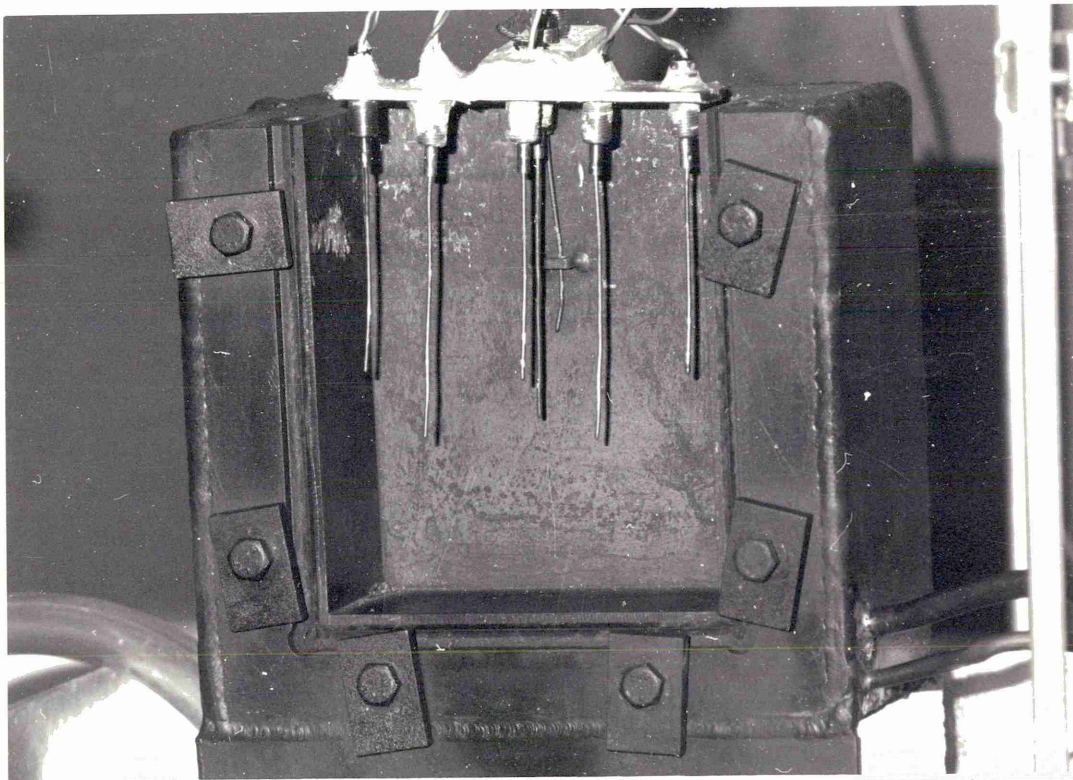


PLATE 4

The calibration was performed in a fireclay crucible. 200cc of the molten alloy was removed from mould B and poured into the crucible. Thermocouple No. 3 was immersed in the molten alloy and temperature recordings were made during the cooling and solidification of the alloy.

IV.4.2.2 Temperature corrections

In the calibration as well as in all the temperature measurements made with the melt, the thermocouple sheaths, and the measuring apparatus were all earthed to a common earth. In addition, the leads from each thermocouple were kept 'floating' and were wired independently to the measuring instrument. No common positive or negative pole was used.

One thermocouple, thermocouple No. 3, was calibrated using the solidification arrest obtained in the separate fireclay crucible section (IV.4.2.1). The remaining thermocouples within the experimental apparatus were calibrated by adjusting their readings to indicate the same arrest temperature in each solidification experiment.

V RESULTS

V.1 Air gap formation studies

Visual observations and thermal records were made during solidification of pure metals and alloys (pure tin, pure lead and 50% lead-tin alloy) in the preliminary experiments carried out in mould B. These experiments were conducted under cooling conditions specified in table III.

It was found that the pure metals stuck to the glass surface but the lead-tin alloy always became separated after complete solidification occurred. This separation could be observed visually but, in addition always occurred with an audible click. The 50% lead-tin alloy was thus chosen for the remainder of the experiments that were carried out in mould B with the pyrex glass in place. The cooling curves of this alloy* obtained from the solidification of a sample in a fireclay crucible remained consistent over several melting and cooling cycles. A typical cooling curve of the alloy is shown in fig. 14. Atomic absorption chemical analyses of a sample taken from the middle of the back face, 4cm from the bottom of the solidified ingot under the 3C cooling conditions, i.e. water at the side walls and air from bottom upwards at the front, showed a tin content of 52.5 mass %.

V.2 Thermal analysis results

This work comprises the experimental runs 1 to 13 where the solidification of molten lead-tin alloy (50% PbSn) and

* A portion of the curve below the liquidus temperature is shown, so that the curve does not show the liquidus arrest which occurred at 212°C.

pure tin, initially at some 50°C and 20°C above the respective solidus arrests, has been studied.

Cooling curves are given for the 13 runs for each of the eight thermocouples used, together with the isochrones for different times for the metal glass interface. These cooling curves and isochrones are shown in figures 15 to 28 and each is classified as defined in table III.

V.3 Photographic Records

Cine recordings were taken for the experiments 4A, 4B and 4C carried out with 50% lead-tin alloy. Plates 5 to 17 show 12 frames which have been taken from the film of the 4C experiment and plates 18 to 27 show 9 frames taken from the film for the 2C experiment. The cine camera was operating at 16 frames per second for all cine recordings.

V.4 Visual Observations

It was observed during the preliminary experiments that the metal remained stuck to the front plate until after solidification had been completed. When it subsequently separated it produced an audible click.

When separation occurred prior to solidification being completed, it started from the sides of the front face and worked towards the centre. Such separation only occurred when water was used to cool the side walls of the mould and water always leaked into the cavity resulting from the separation.

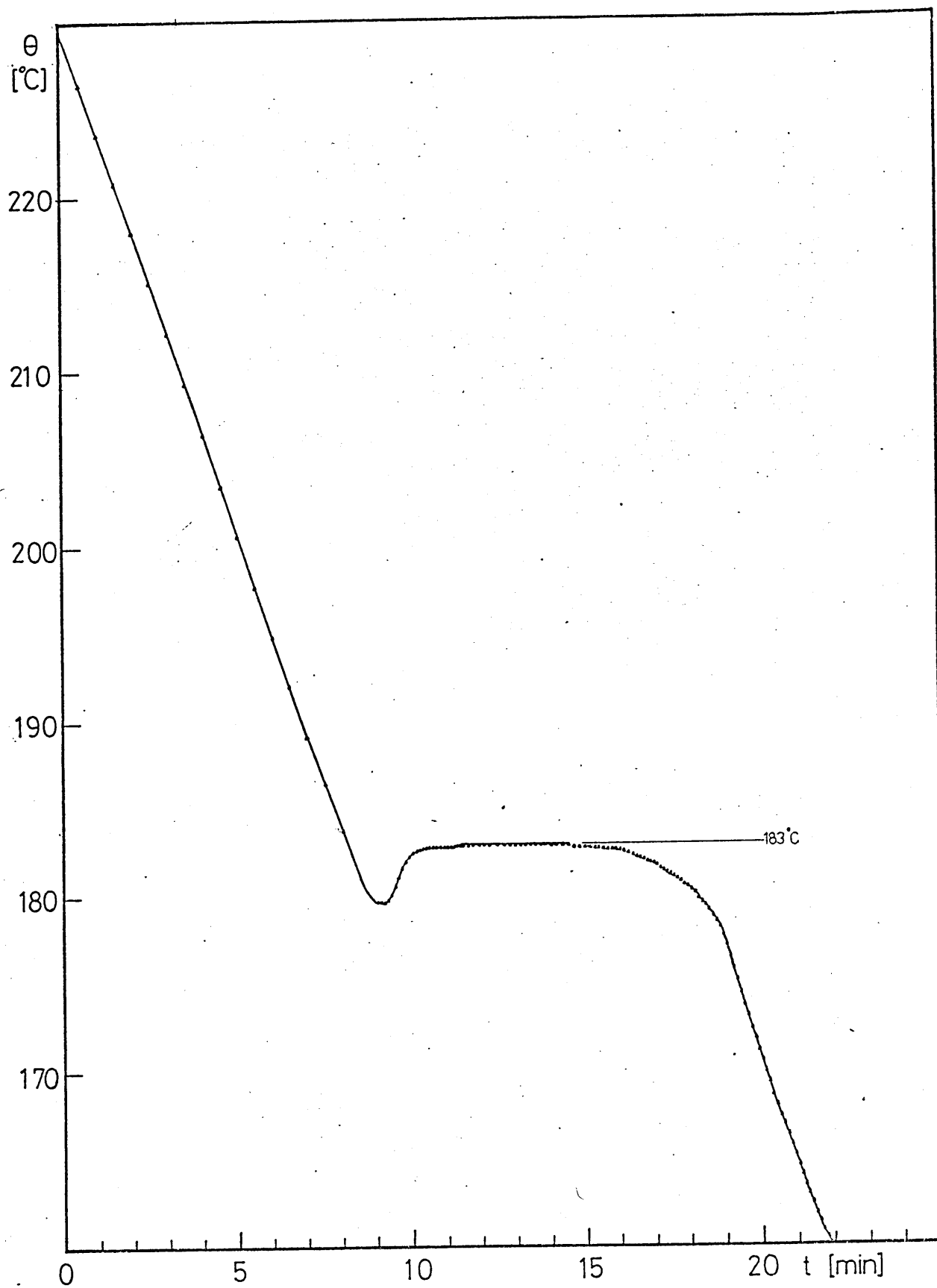


Fig. 14 50% Lead-Tin alloy cooling curve.

Cooling curves and isochrones for different times, for the set of runs carried out during solidification of 50% lead-tin alloy in mould B.

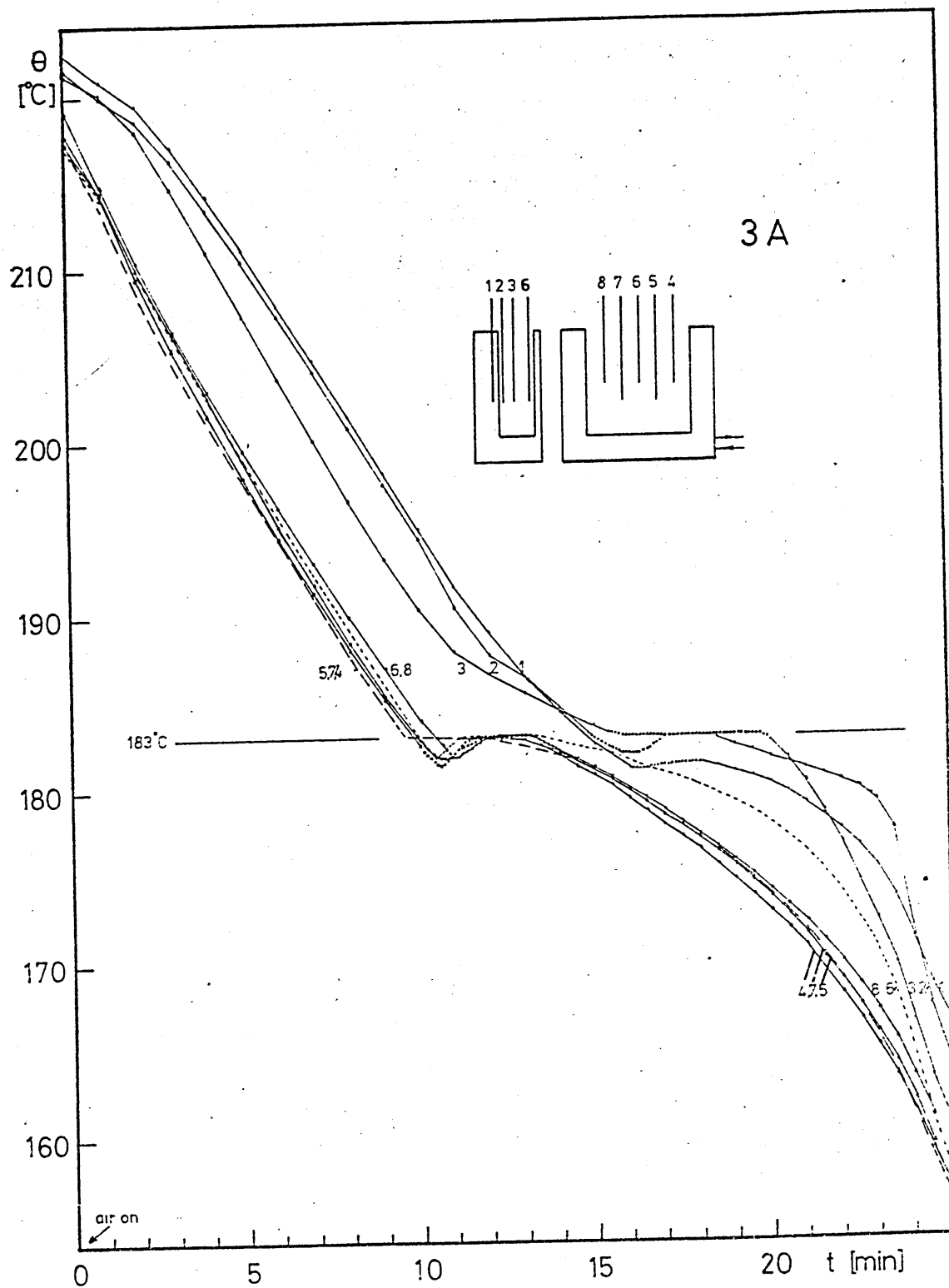


Fig. 14 a

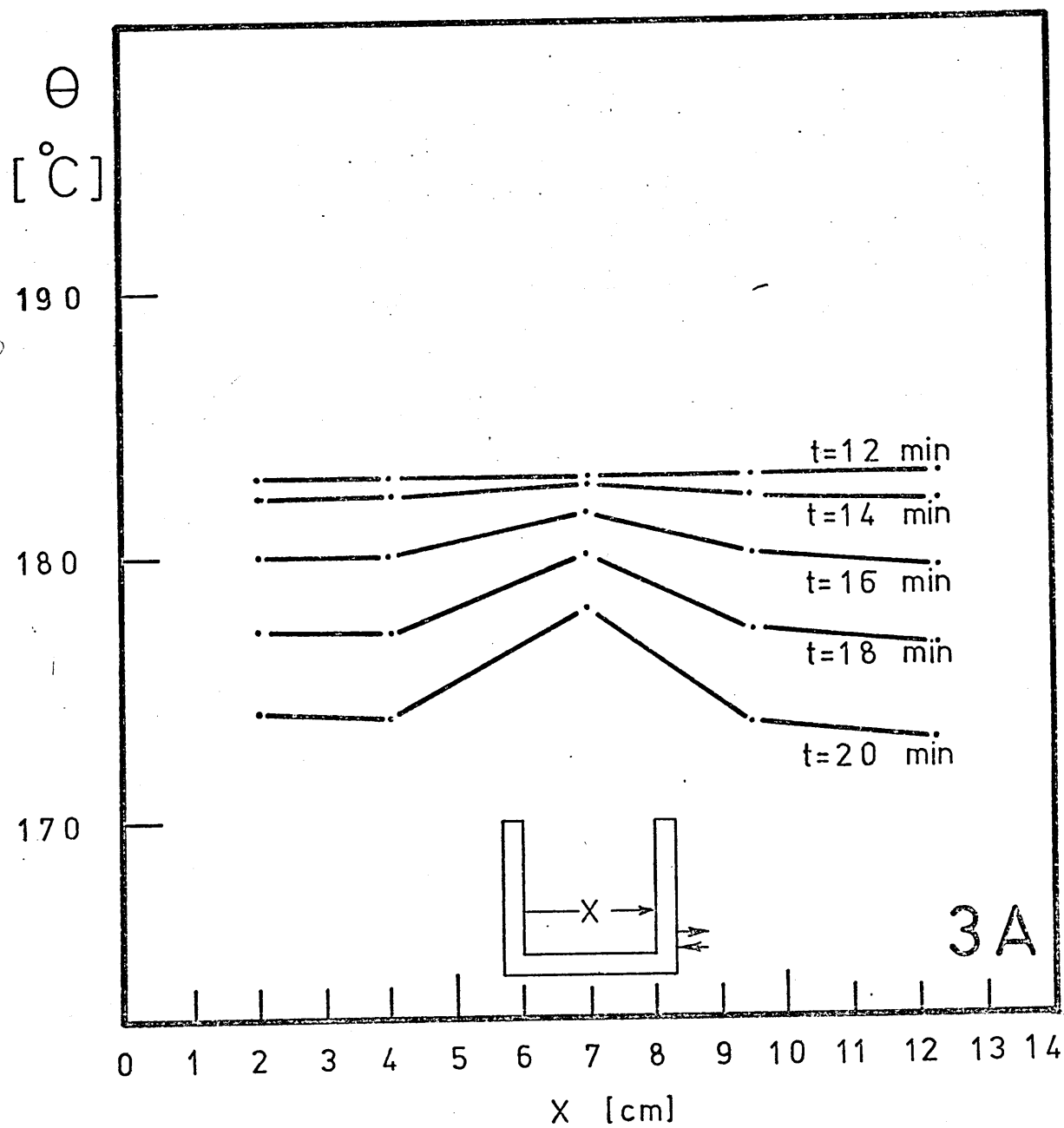


Fig. 14 b

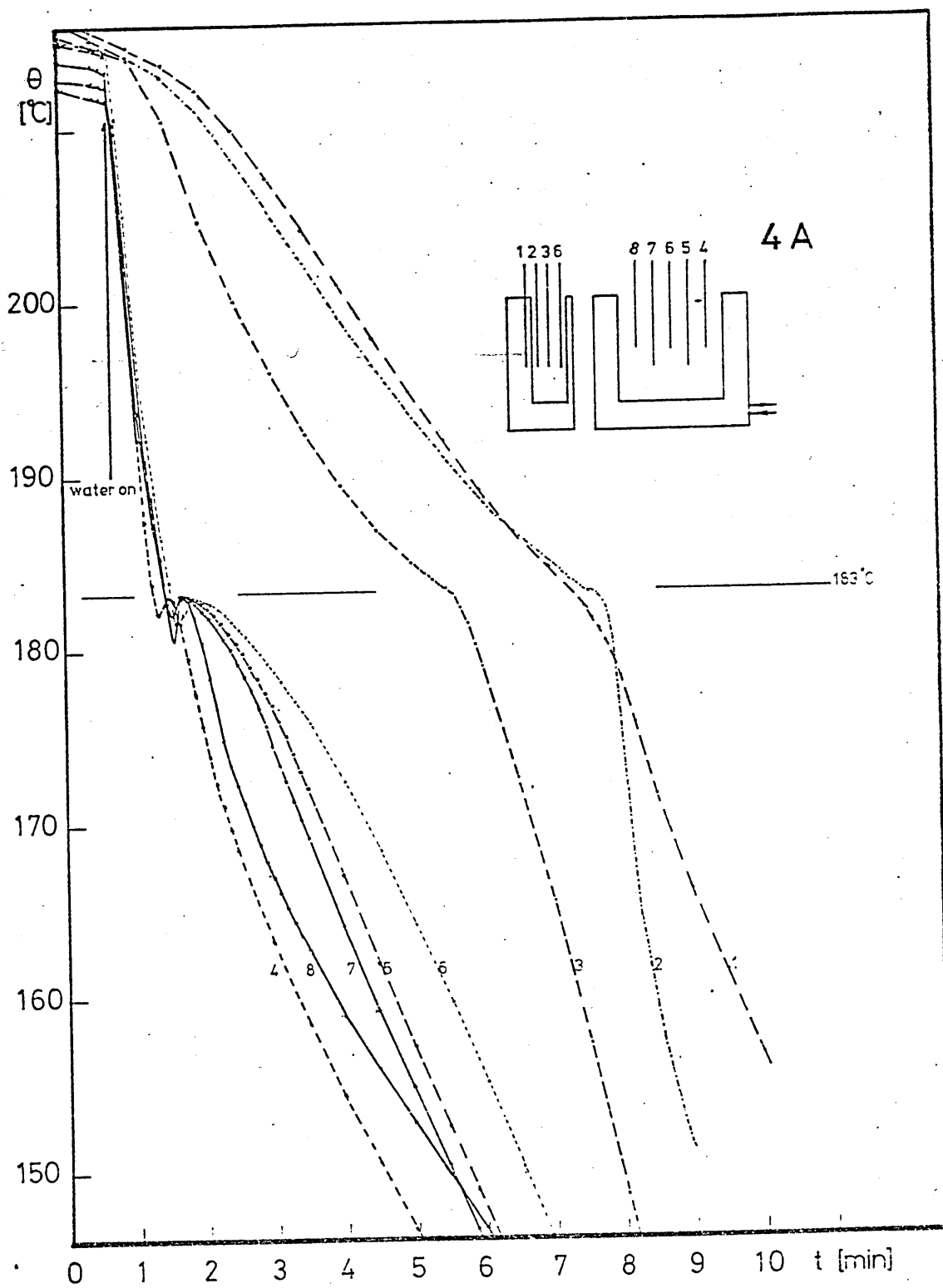


Fig. 15a

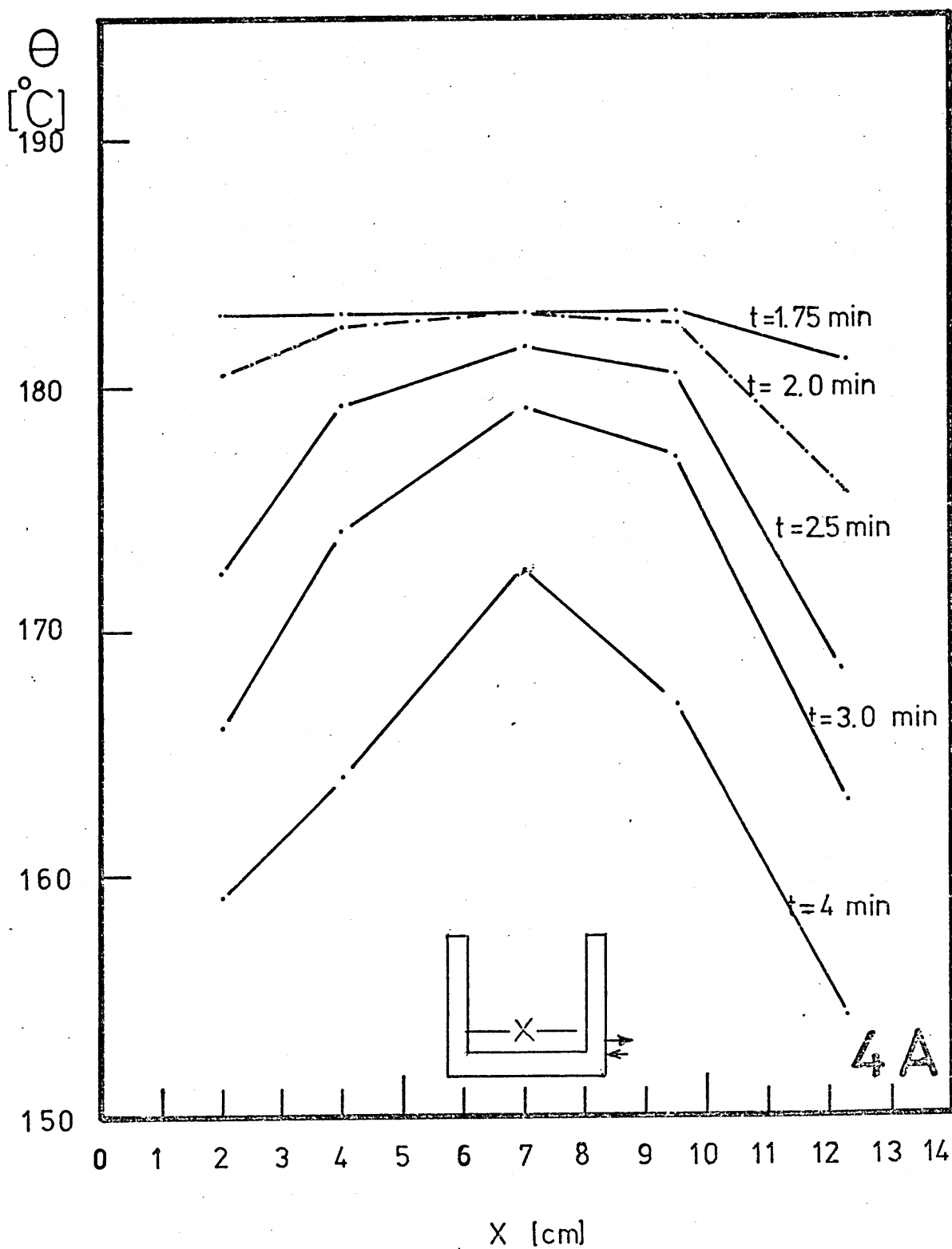


Fig. 15b

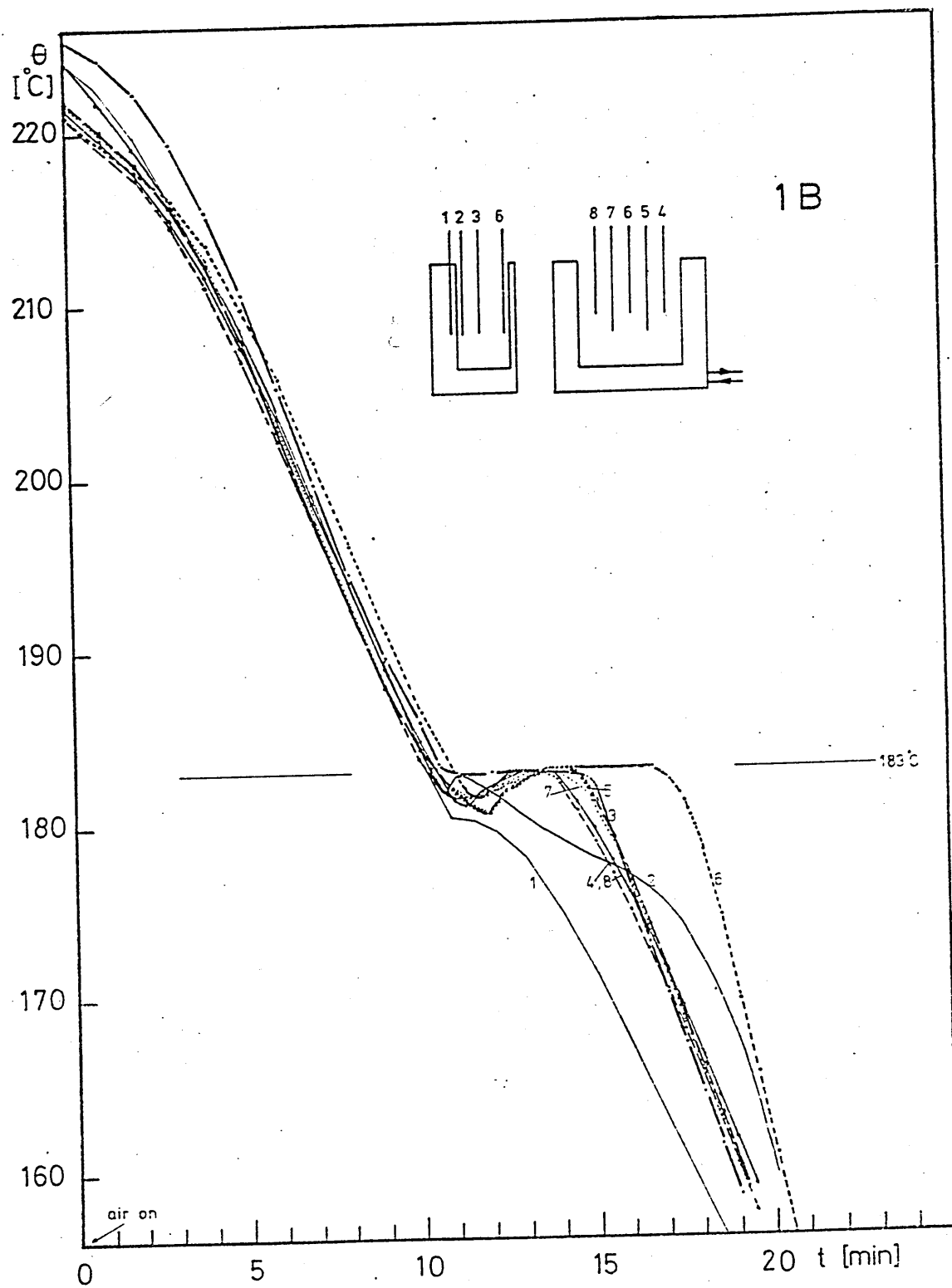


Fig. 16a

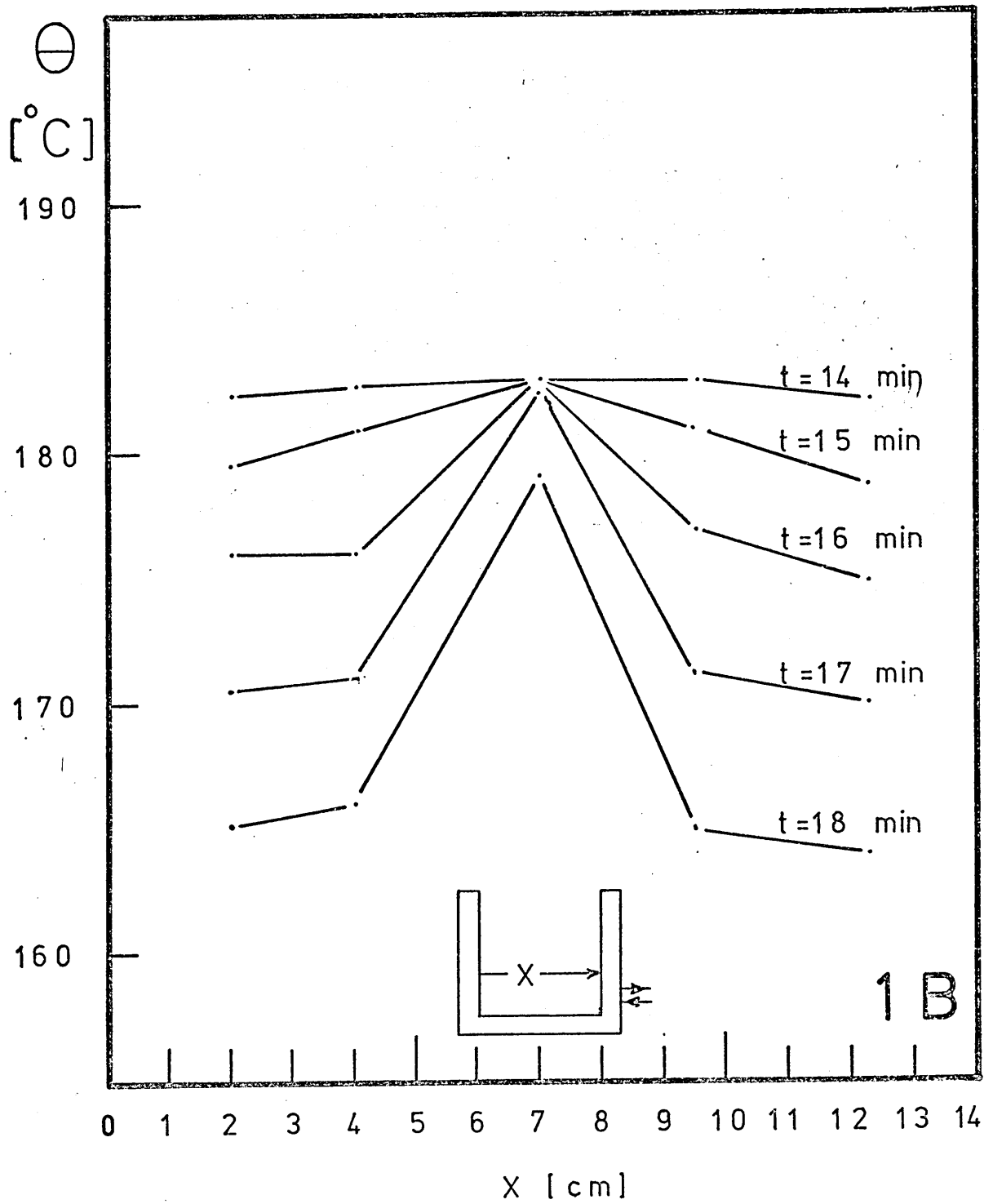


Fig. 16 b

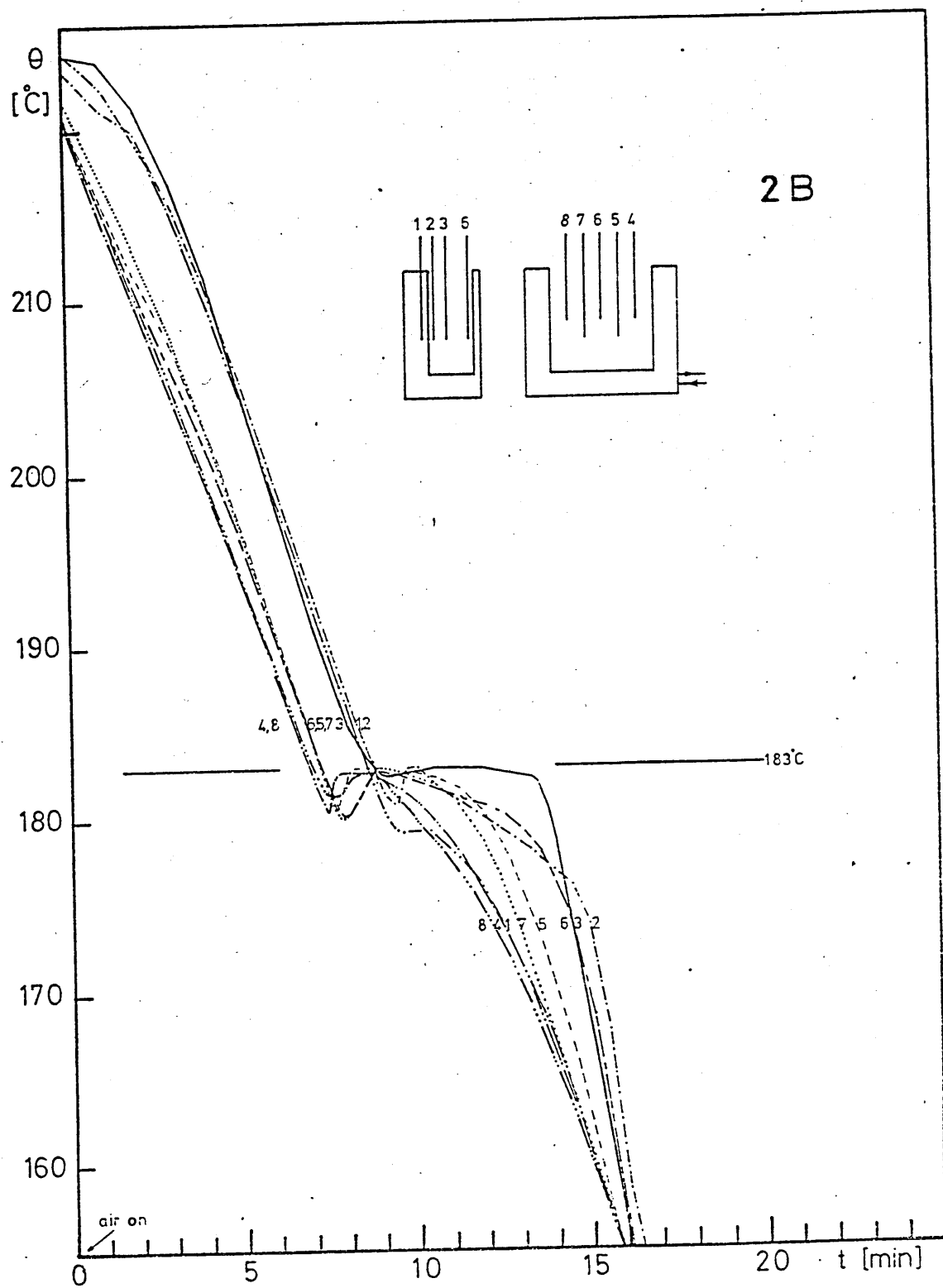


Fig. 17a

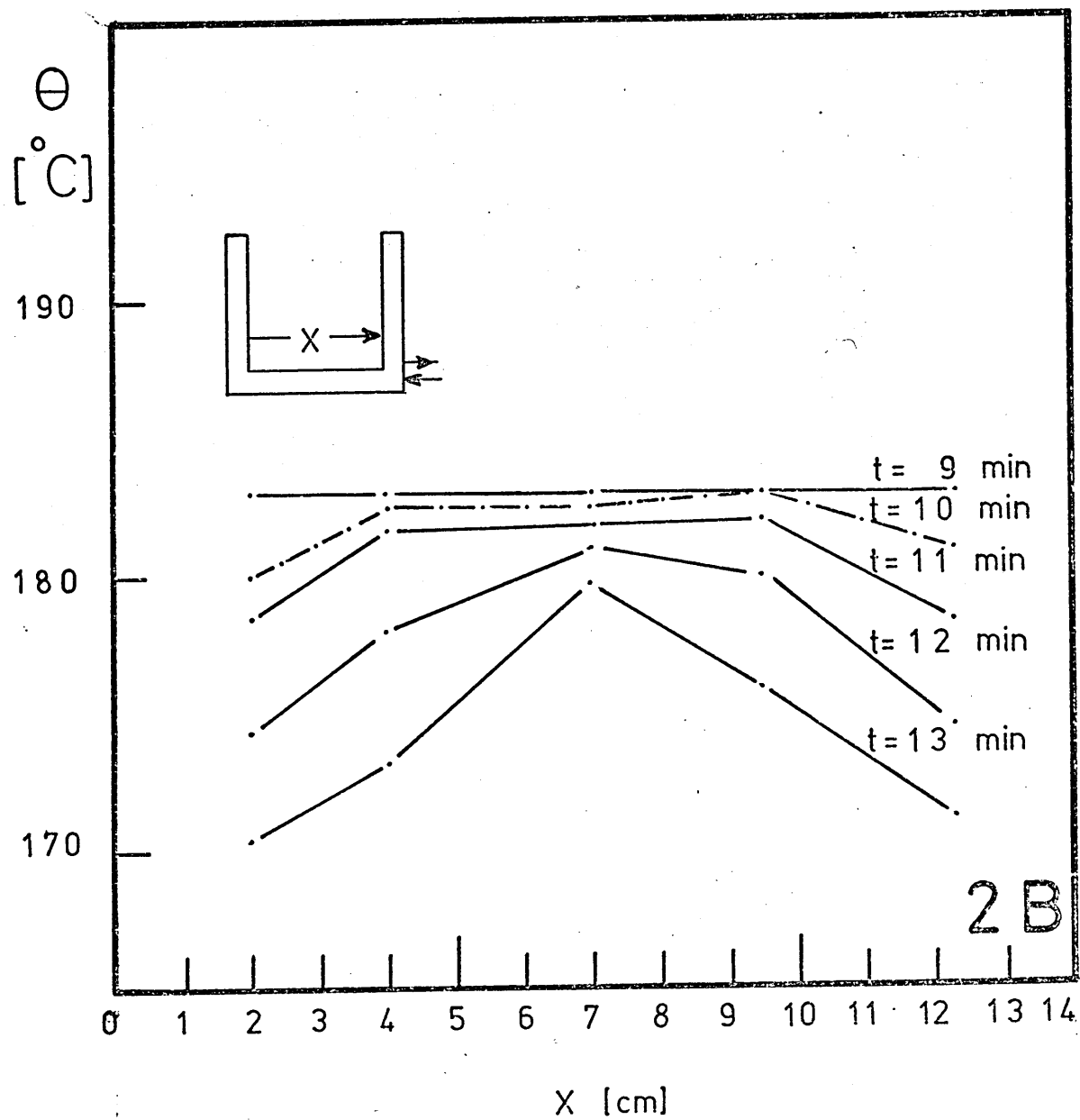


Fig.17 b

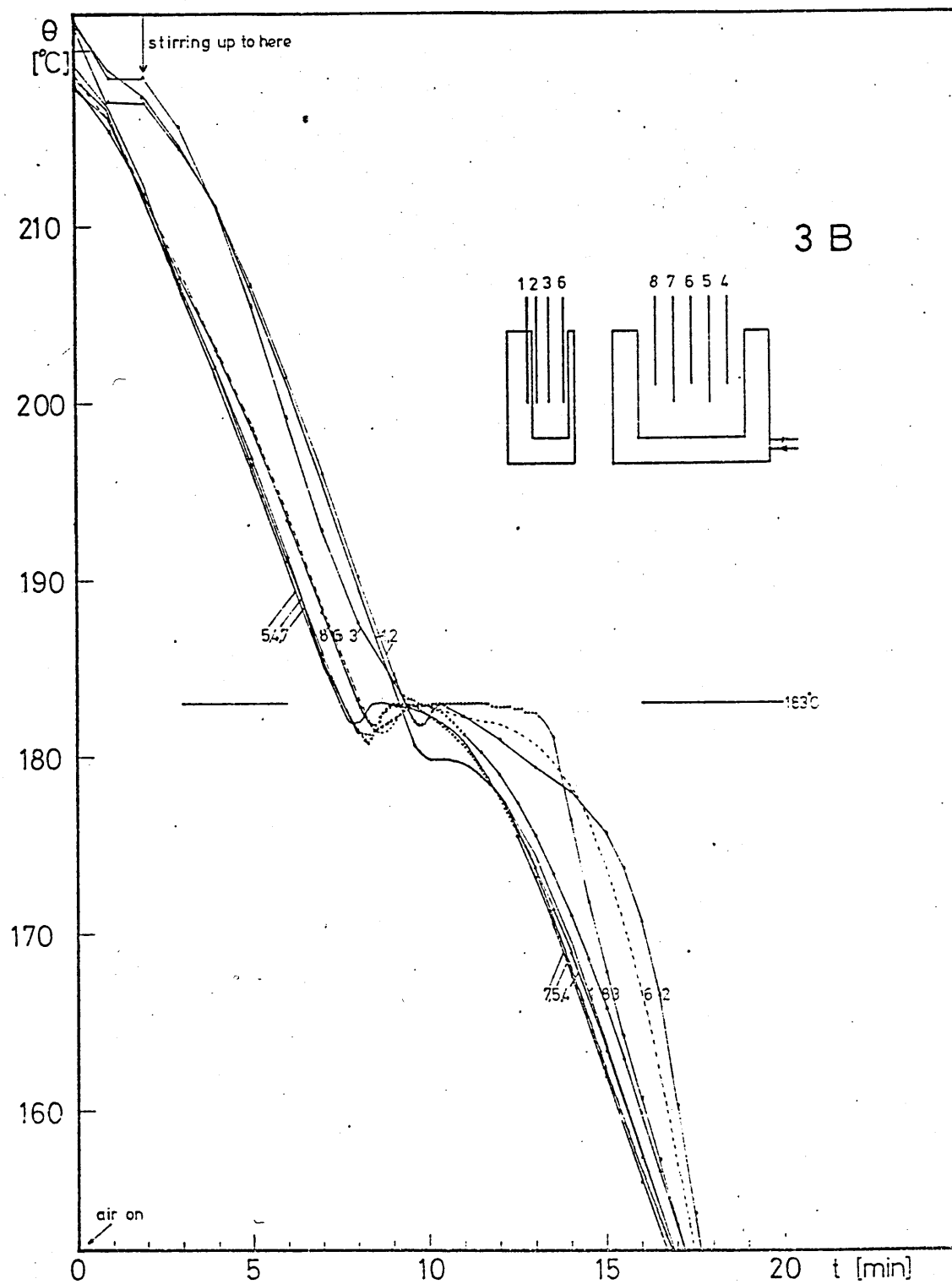


Fig.18 a

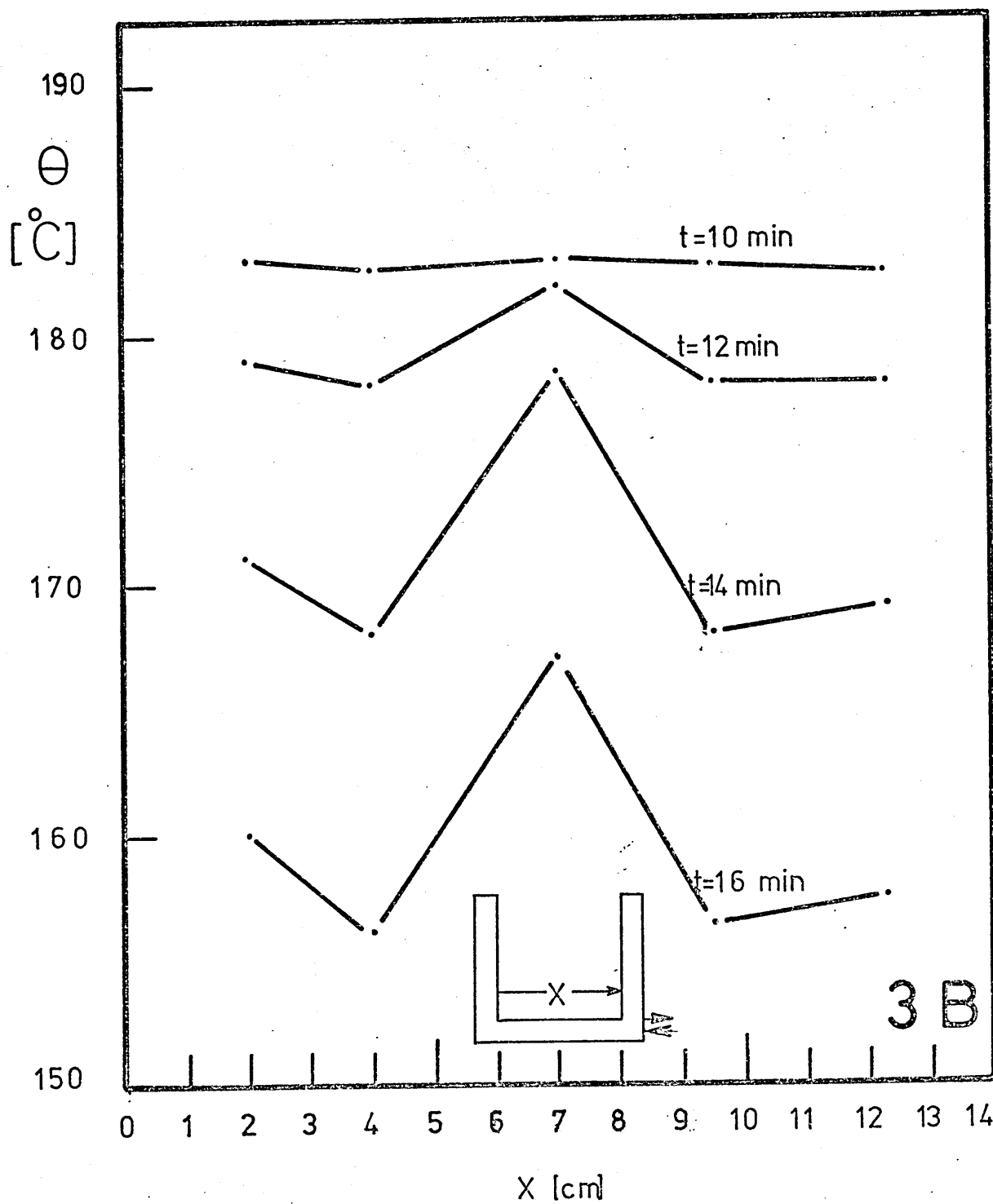


Fig. 18 b

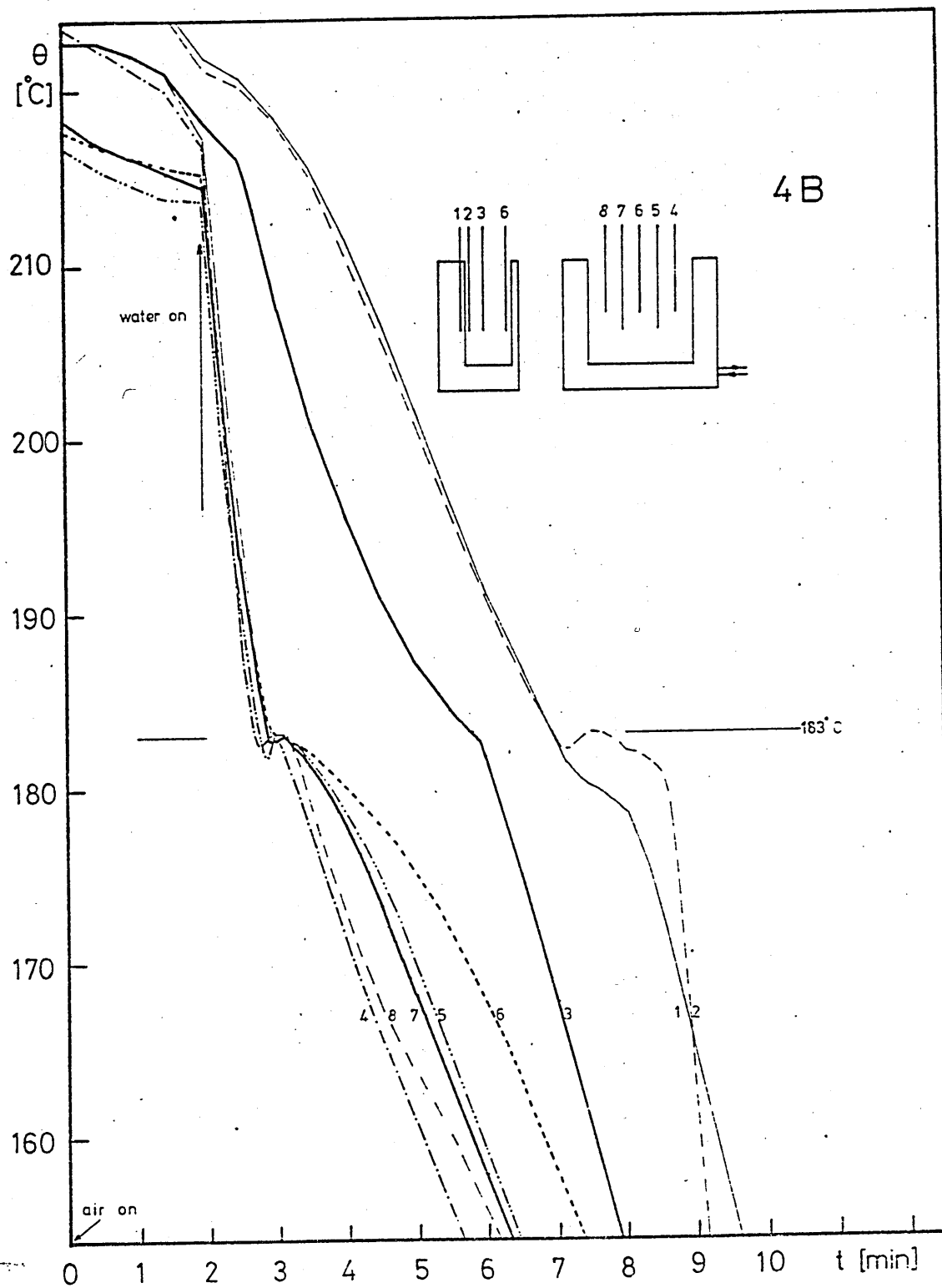


Fig. 19a

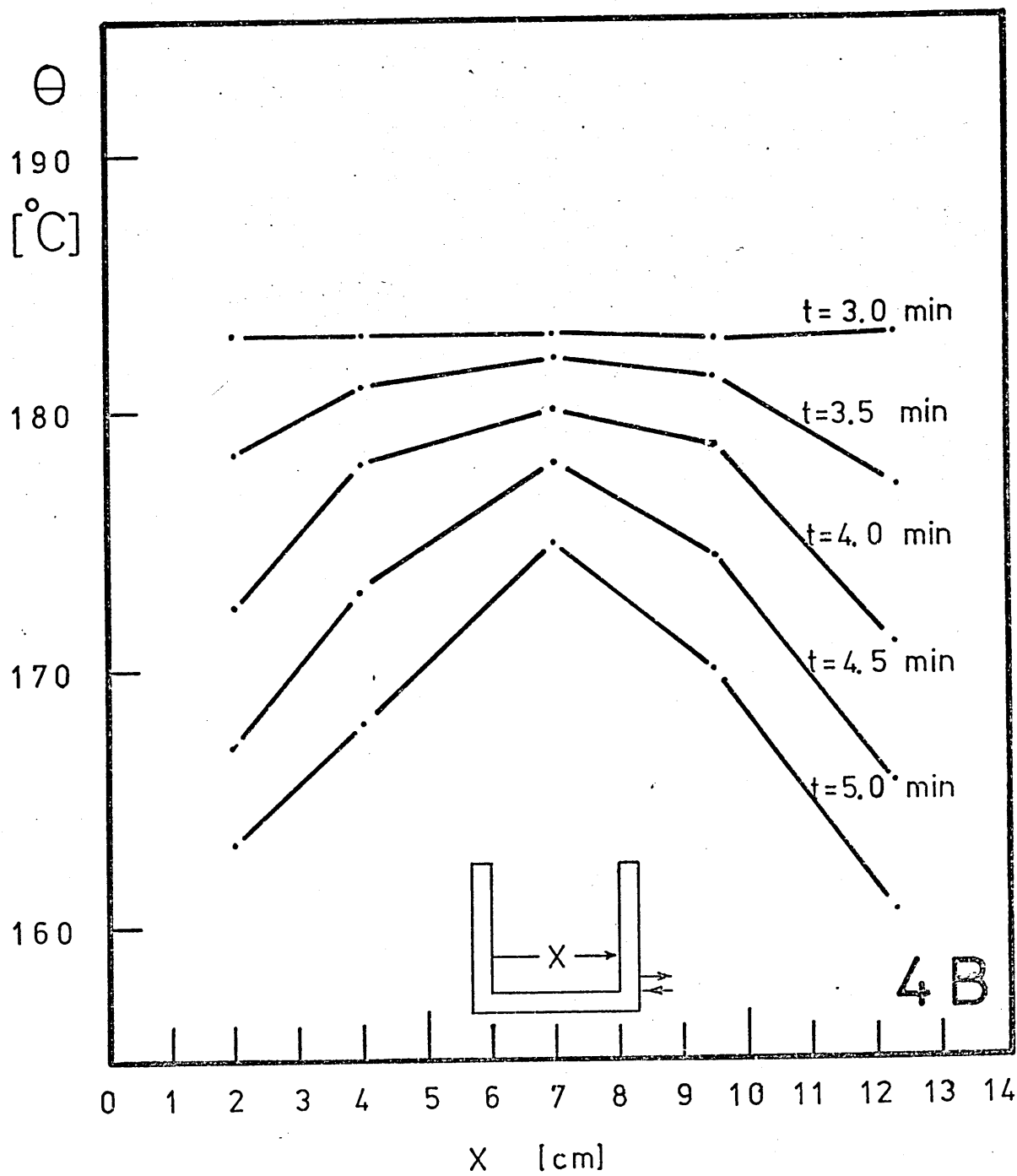


Fig. 19 b

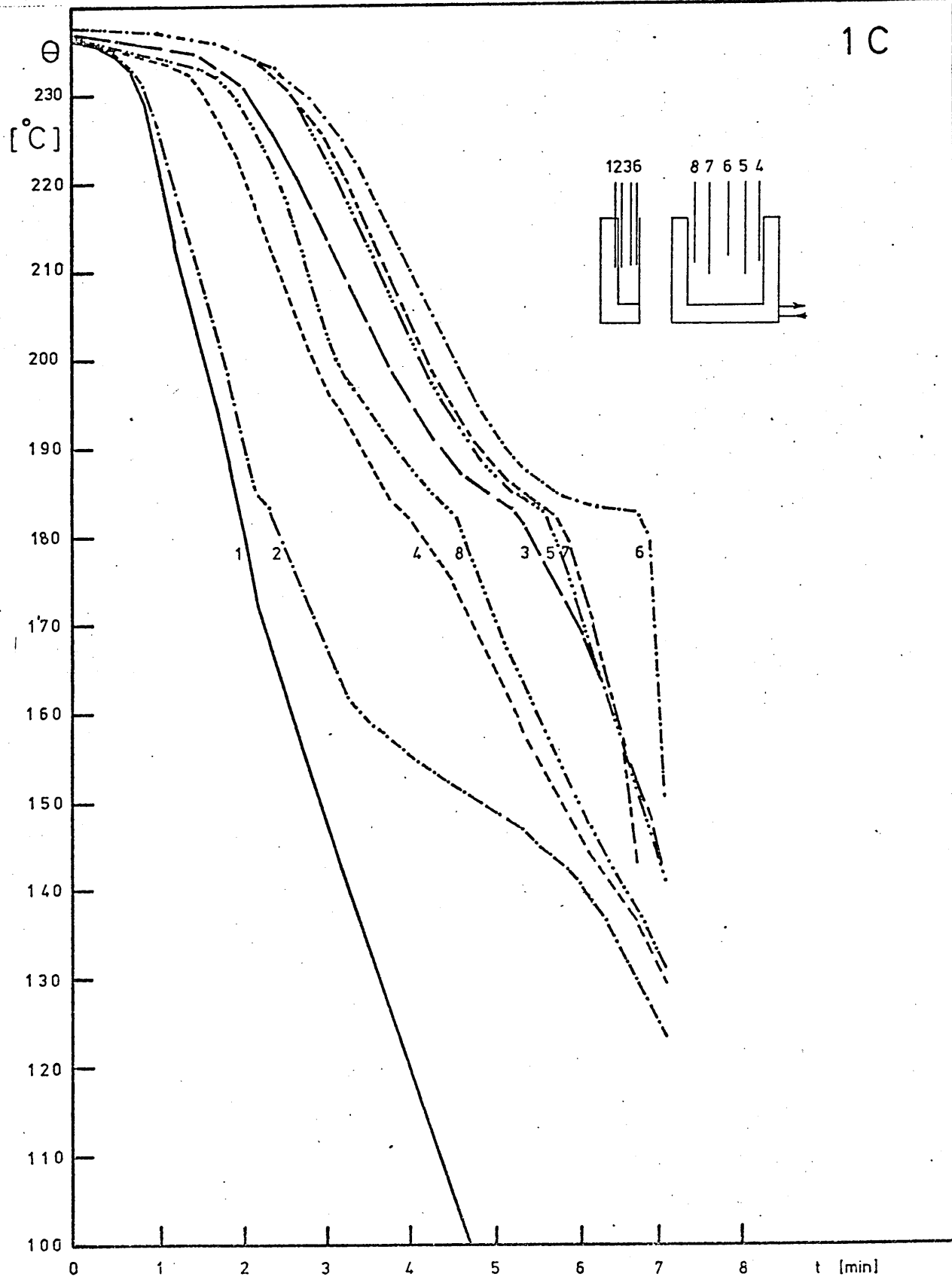


Fig. 20 a

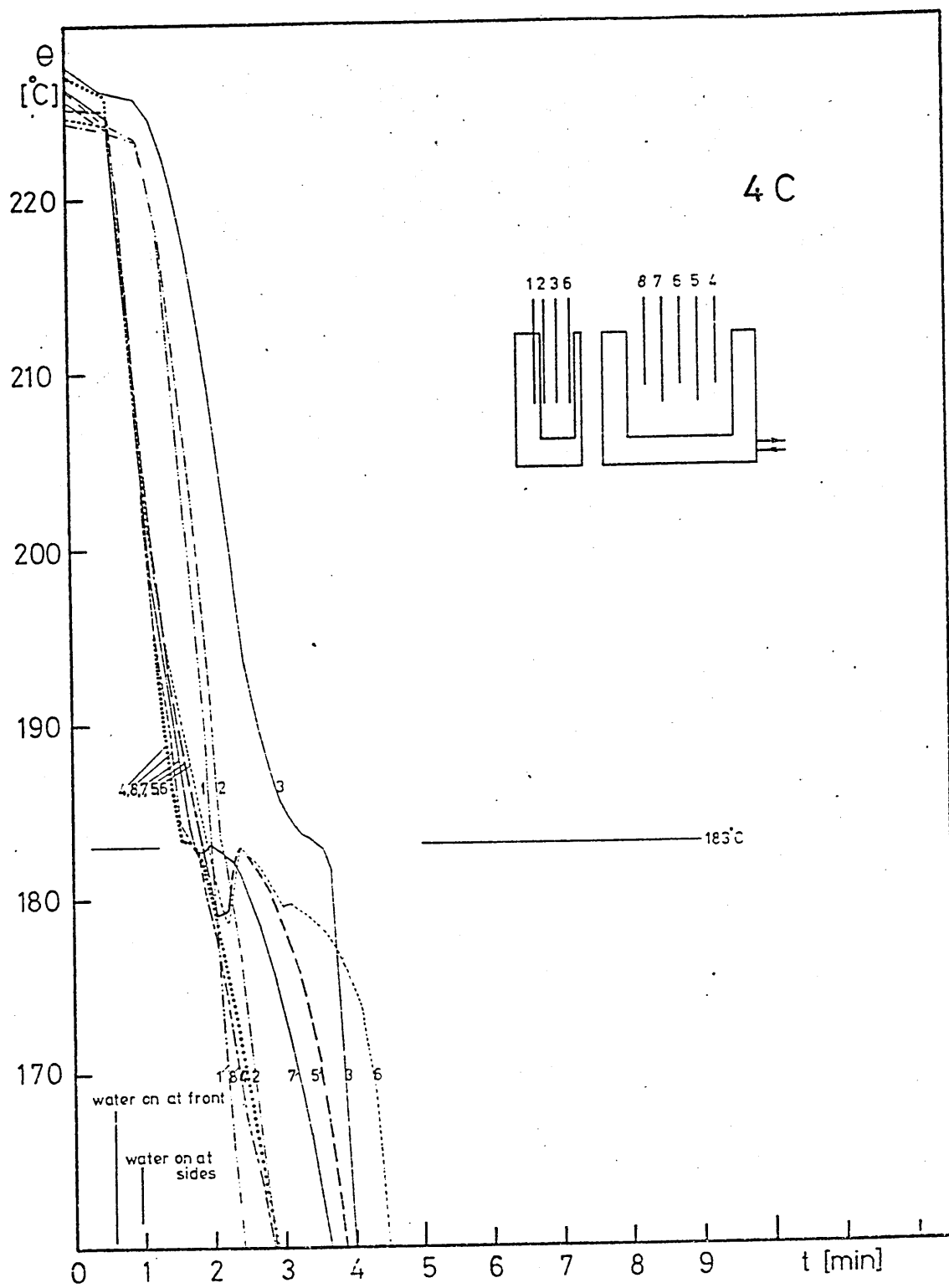


Fig. 21 a

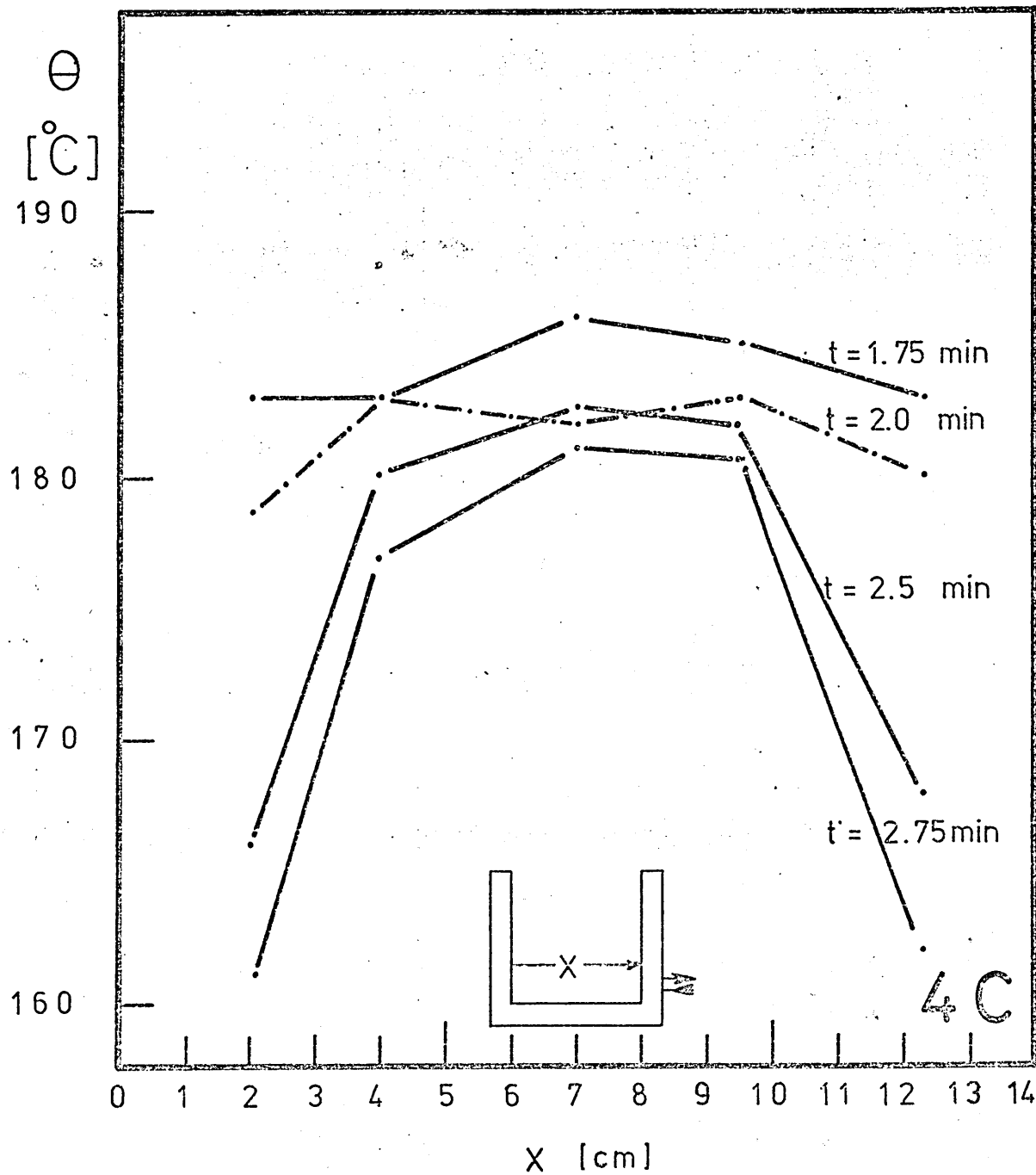


Fig. 21 b

Cooling curves and isochrones for different times,
for the set of runs carried out during solidification
of pure tin in mould B.

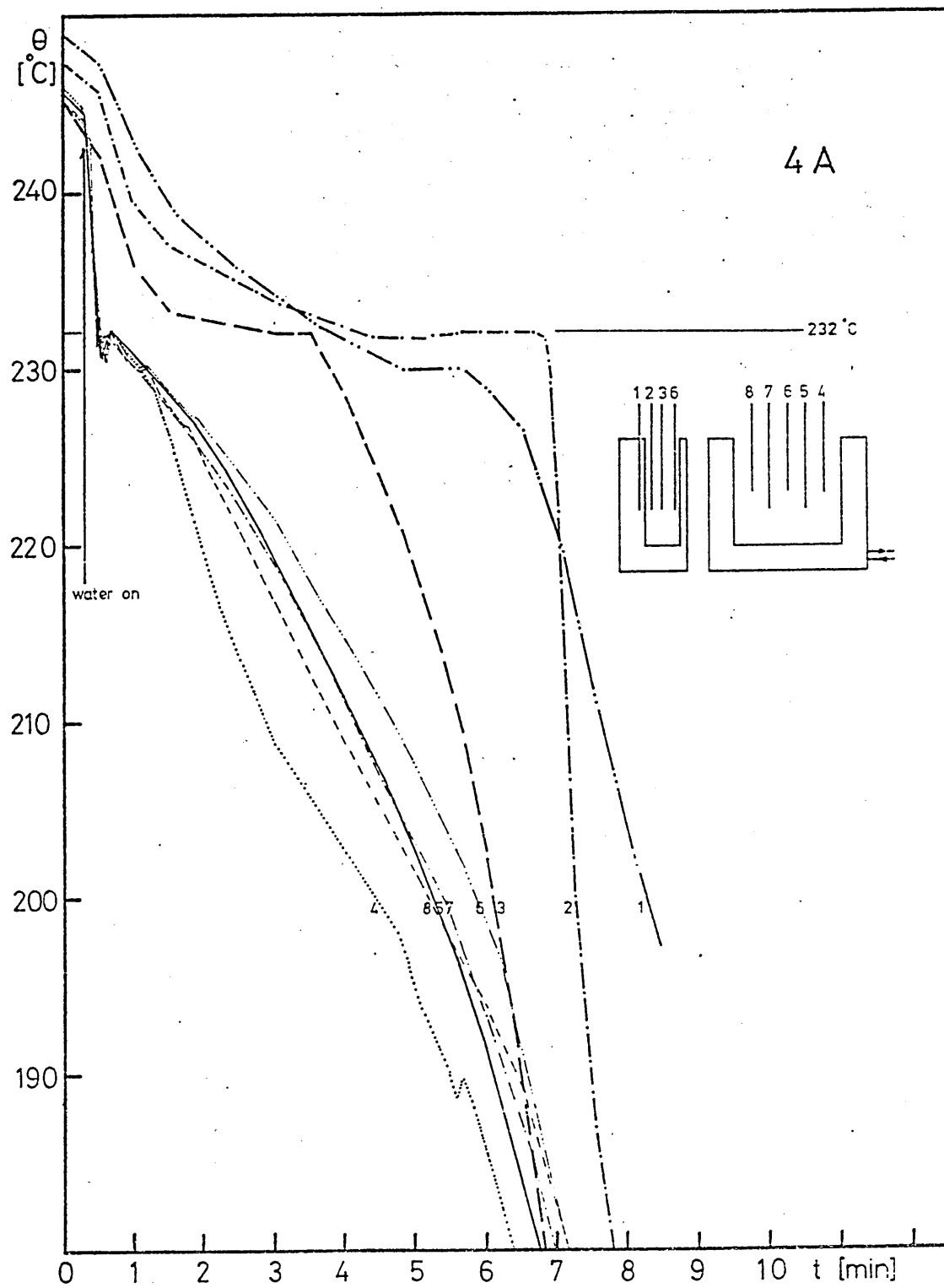


Fig. 22a

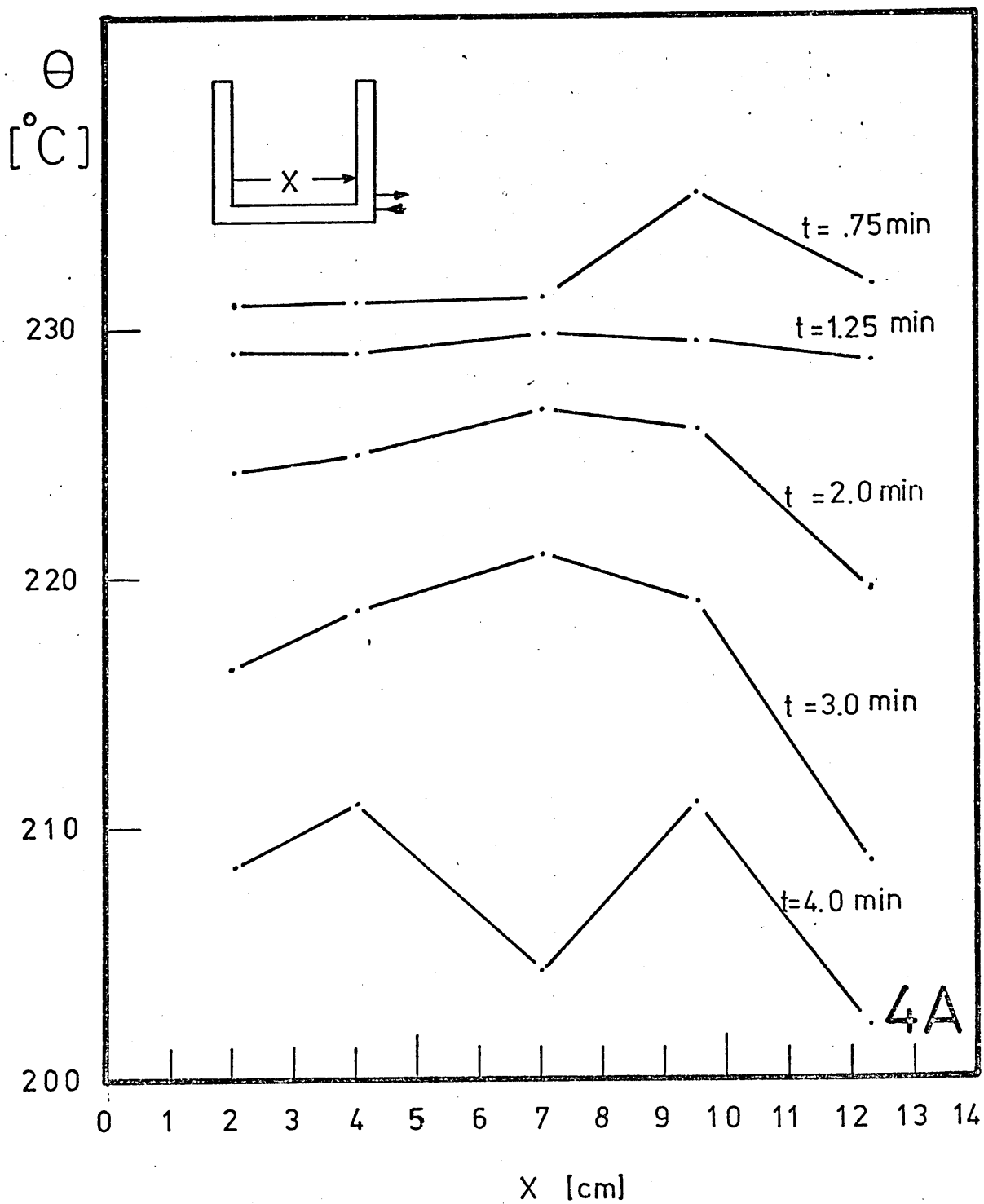


Fig. 22 b

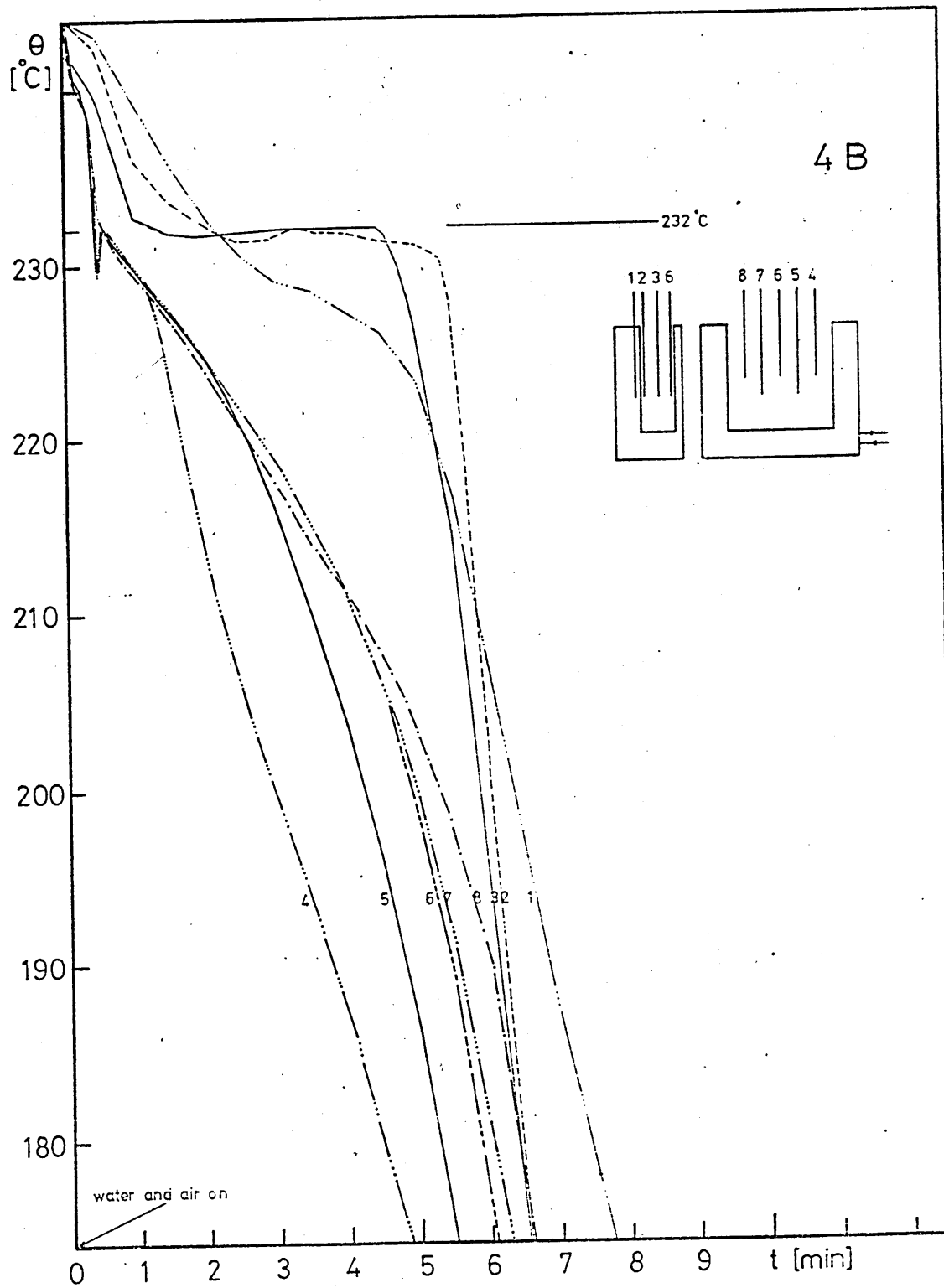


Fig. 23 a

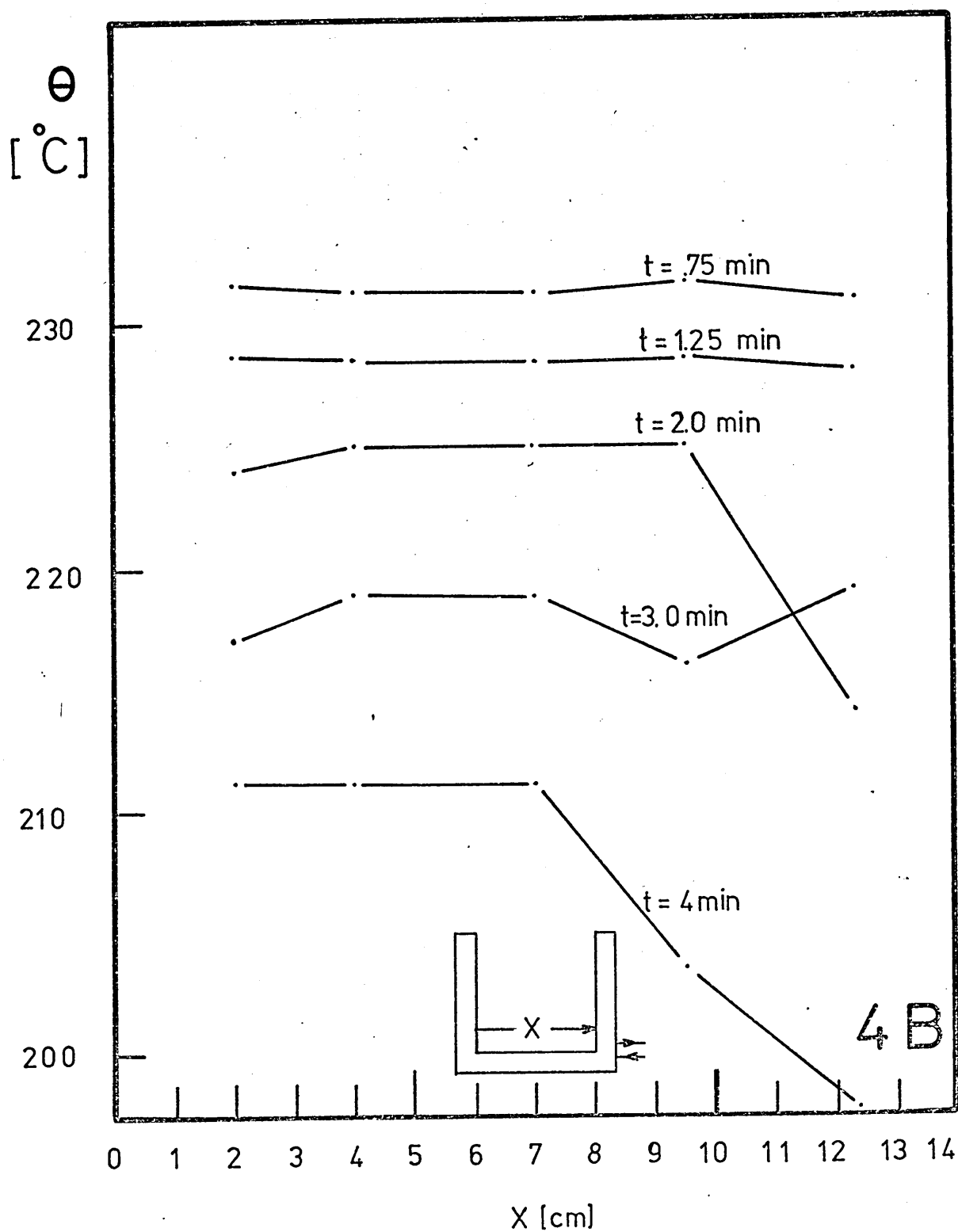


Fig. 23 b

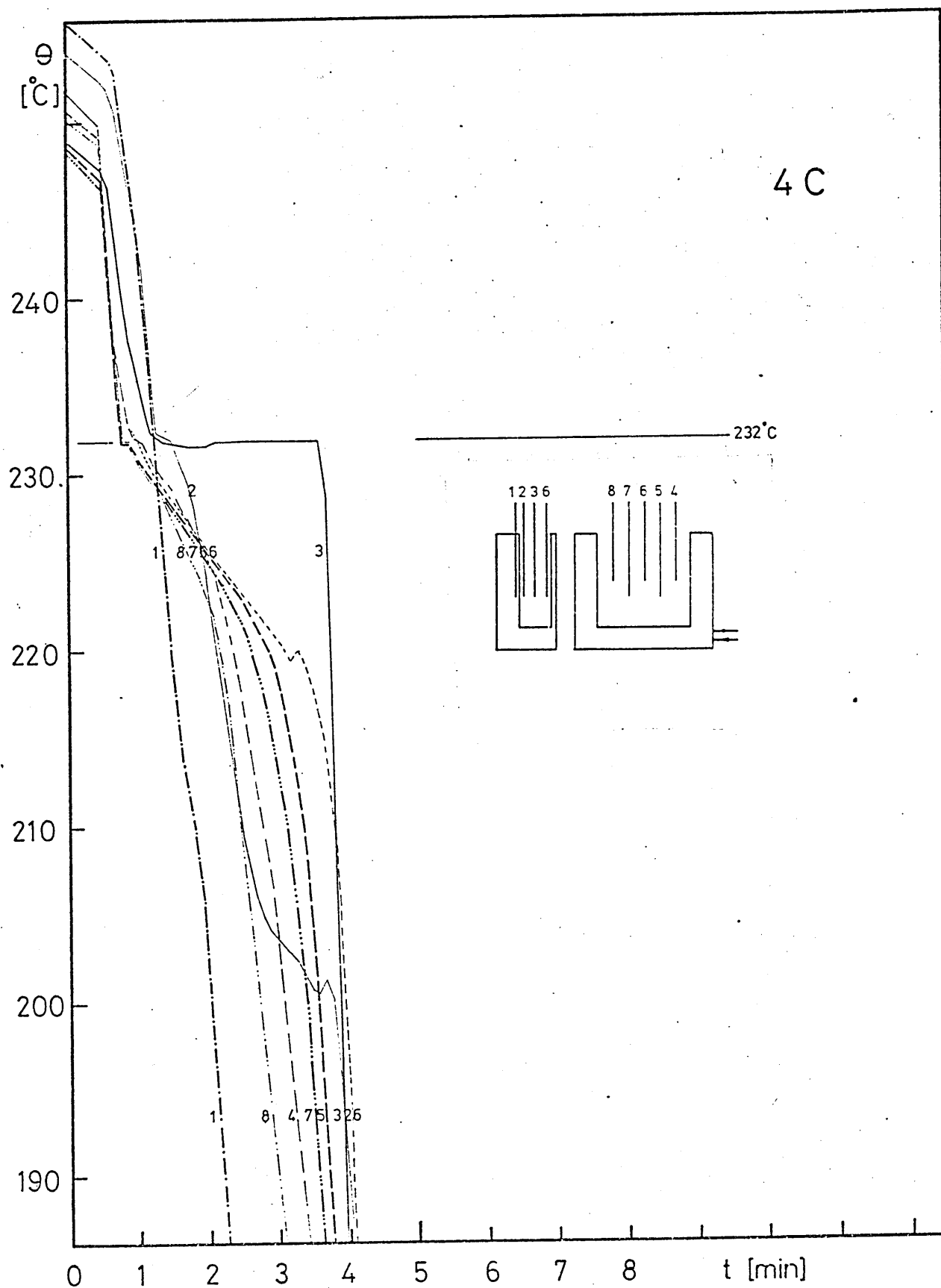


Fig. 24 a

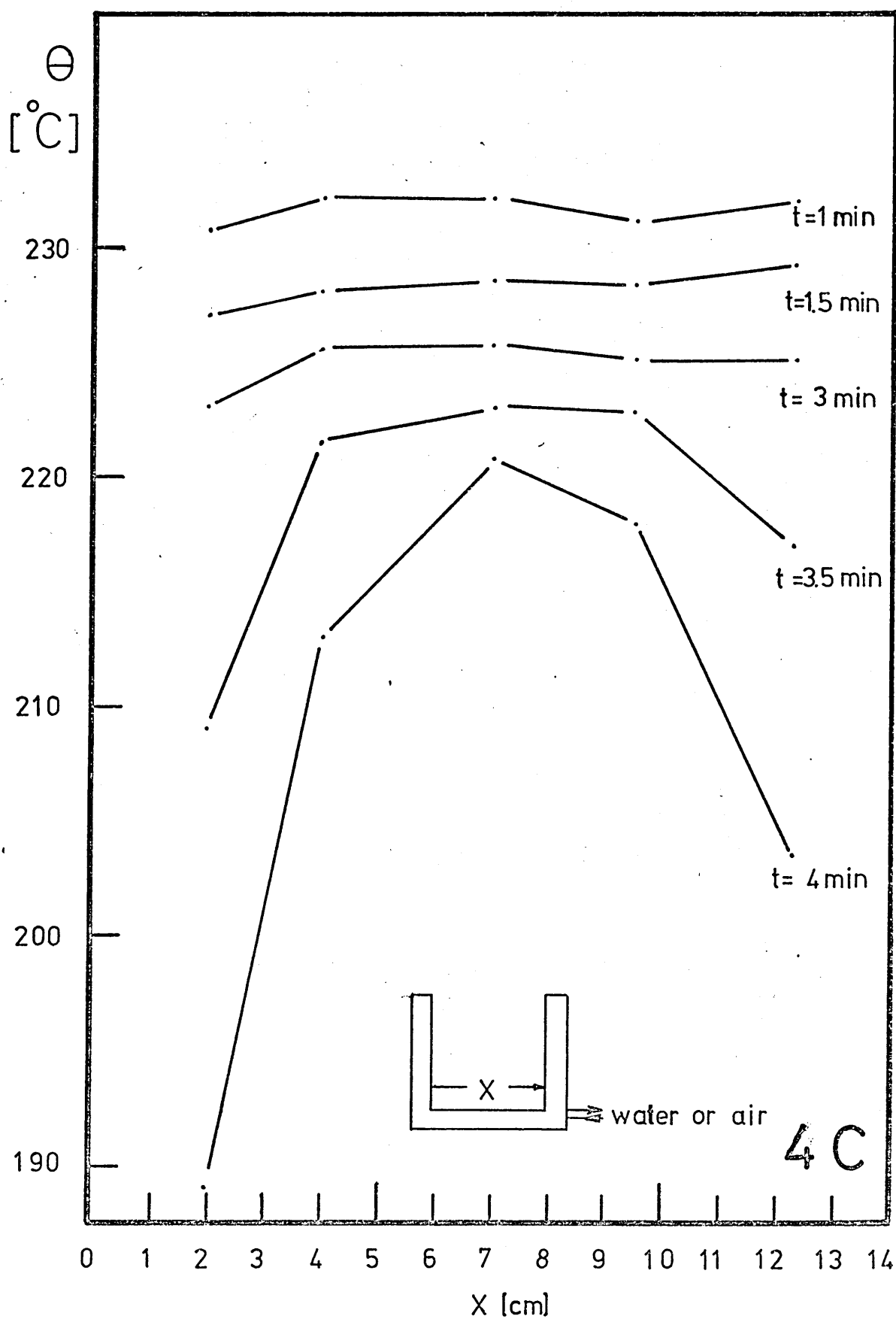


Fig. 24 b

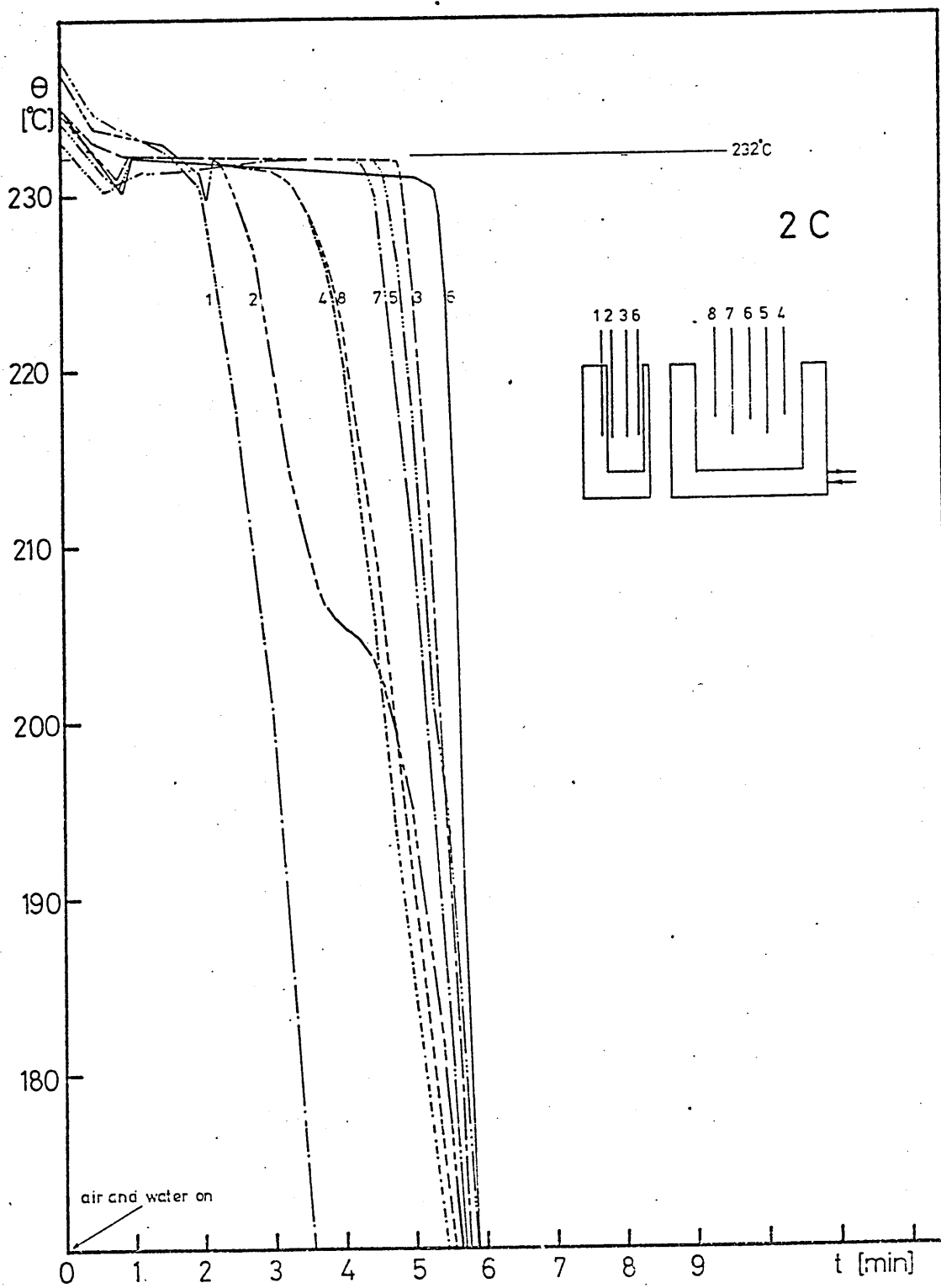


Fig. 25 a

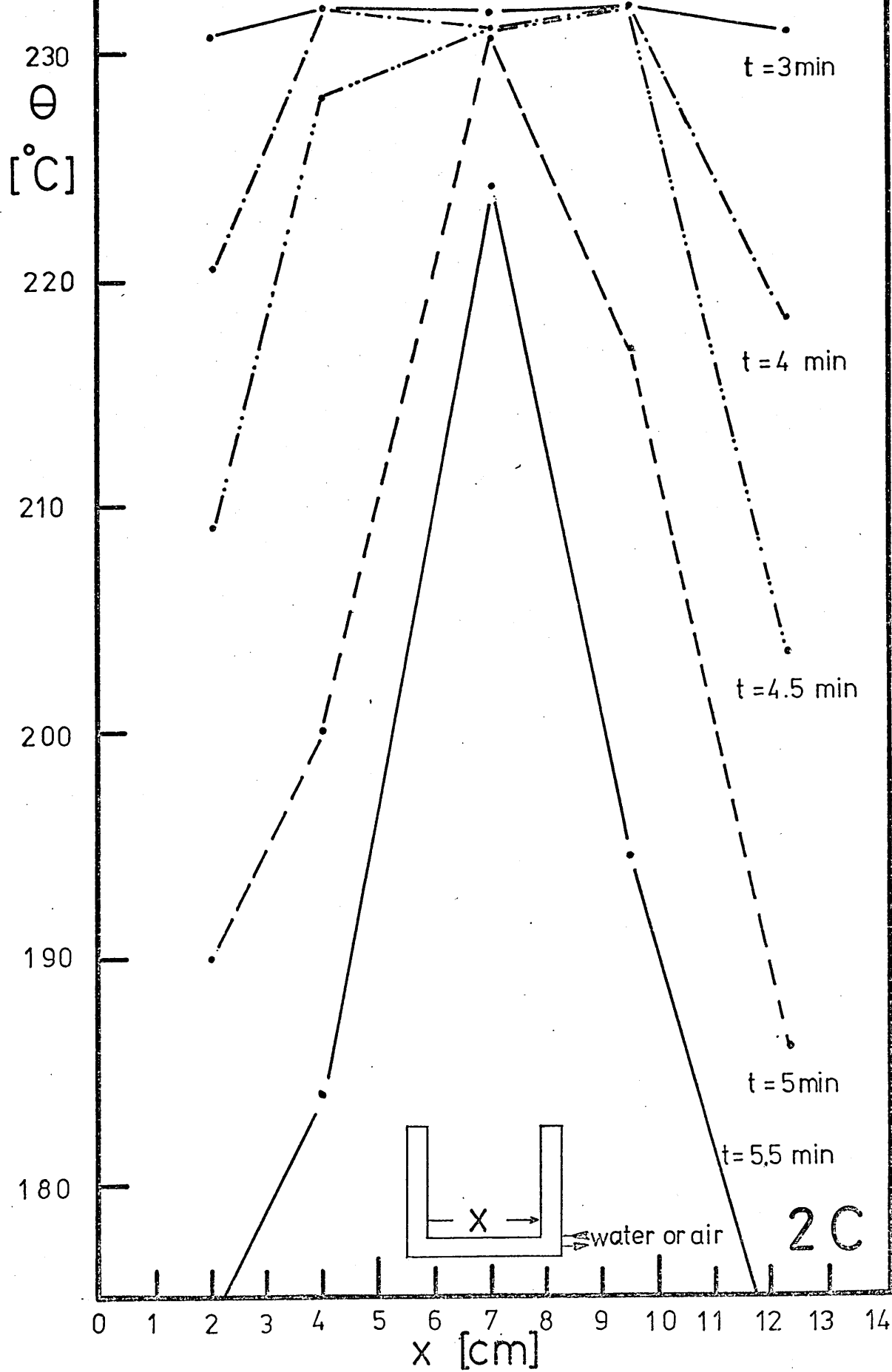


Fig. 25 b

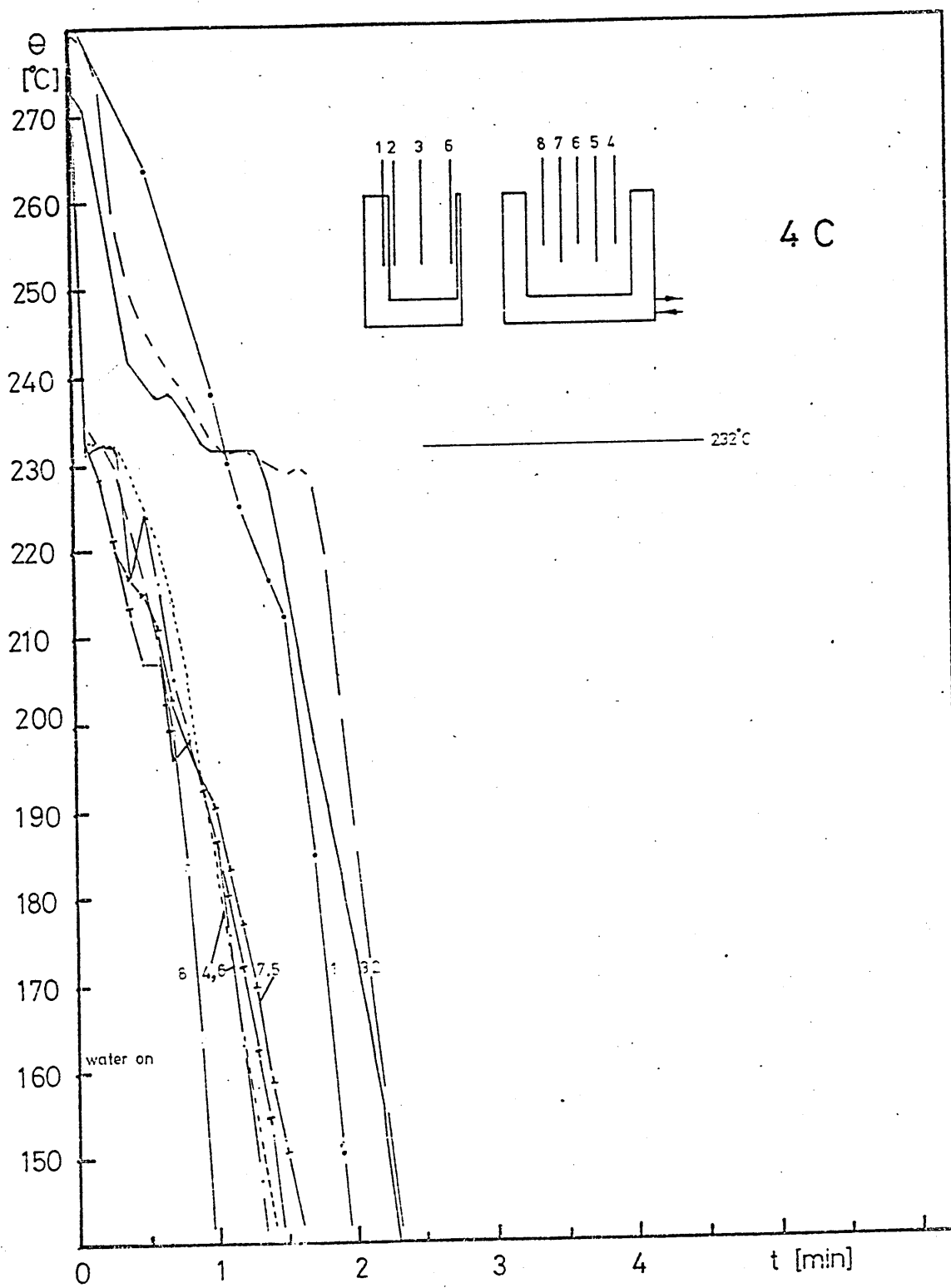


Fig. 26 Cooling curves for pure tin, front: steel plate.

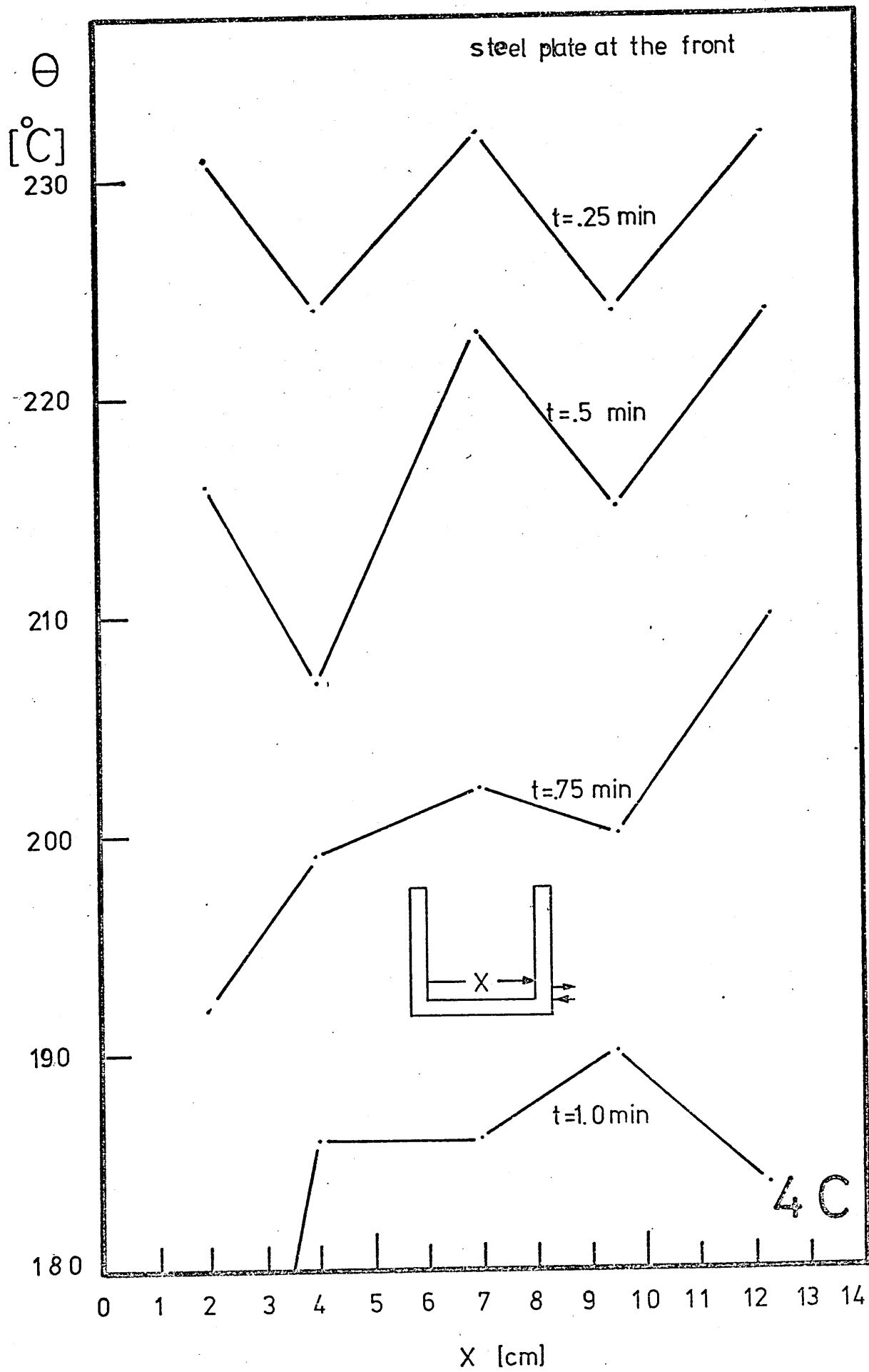


Fig. 27



PLATE 5 ($z = 0' 00''$)

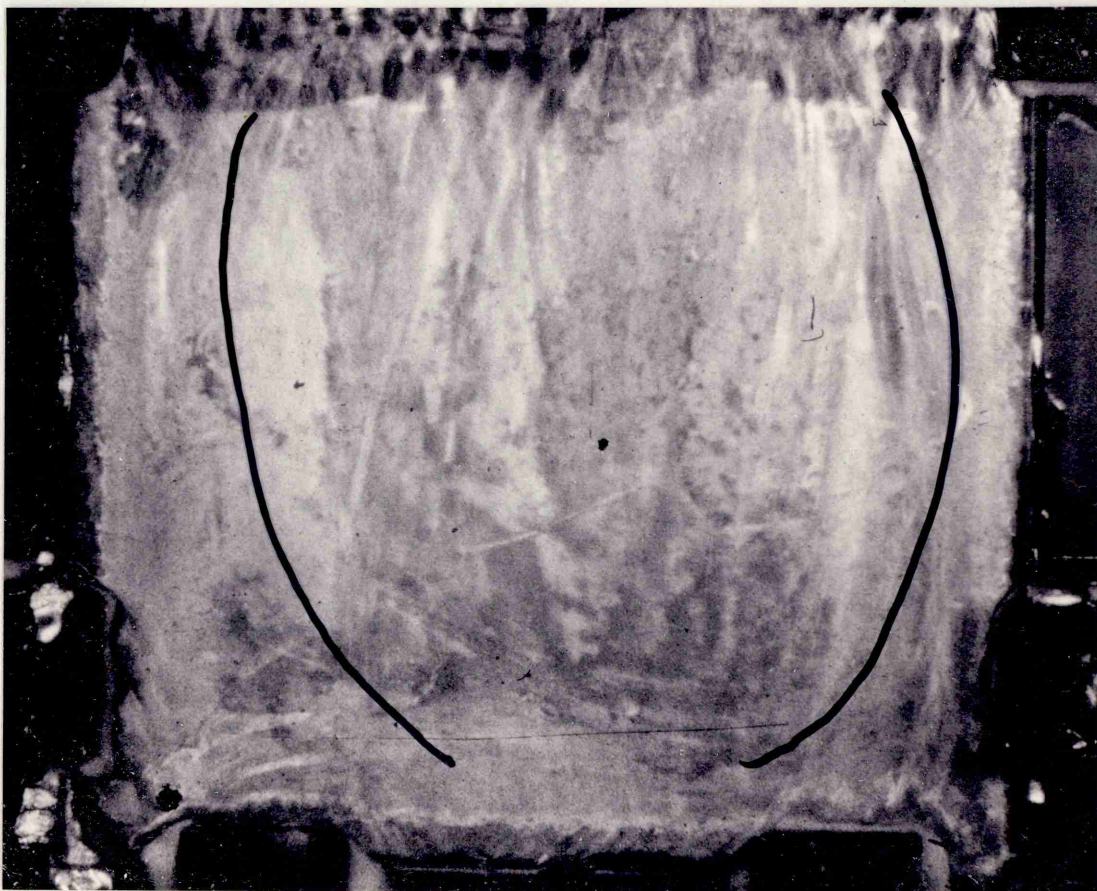


PLATE 6 ($z = 2' 29''$)

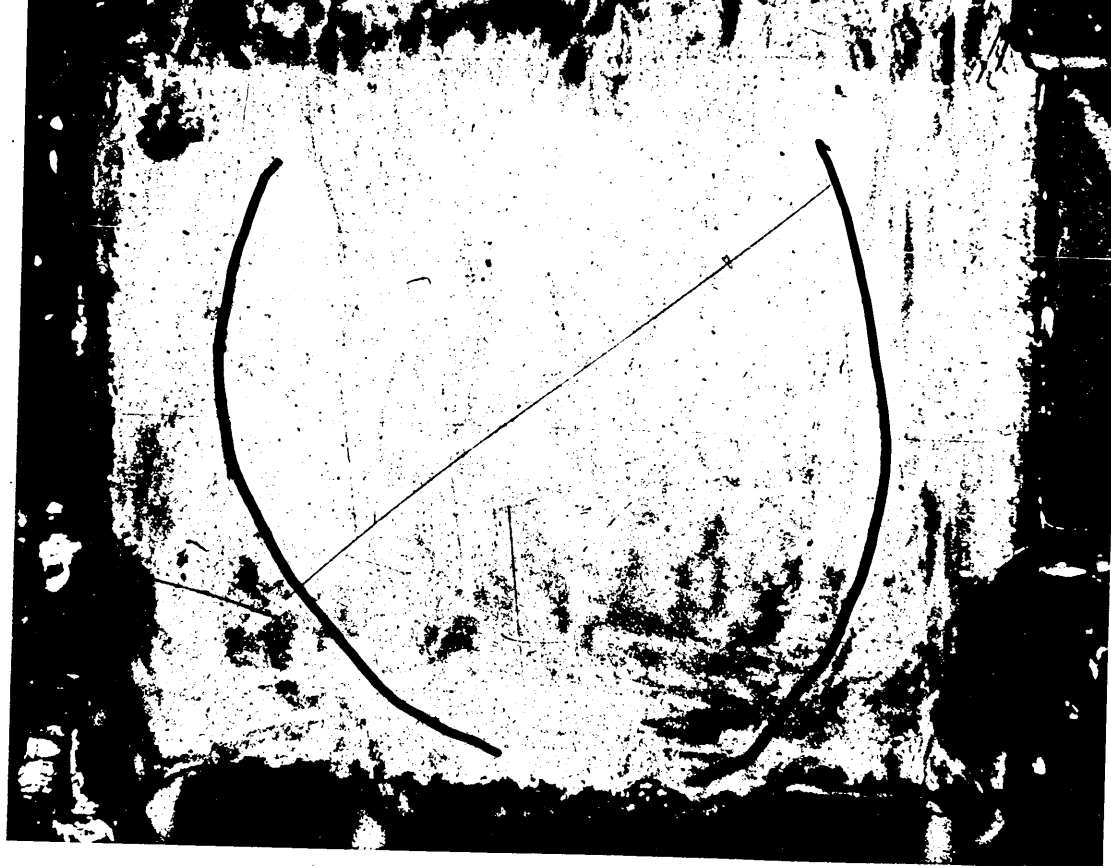


PLATE 7 ($\zeta = 2' 42''$)

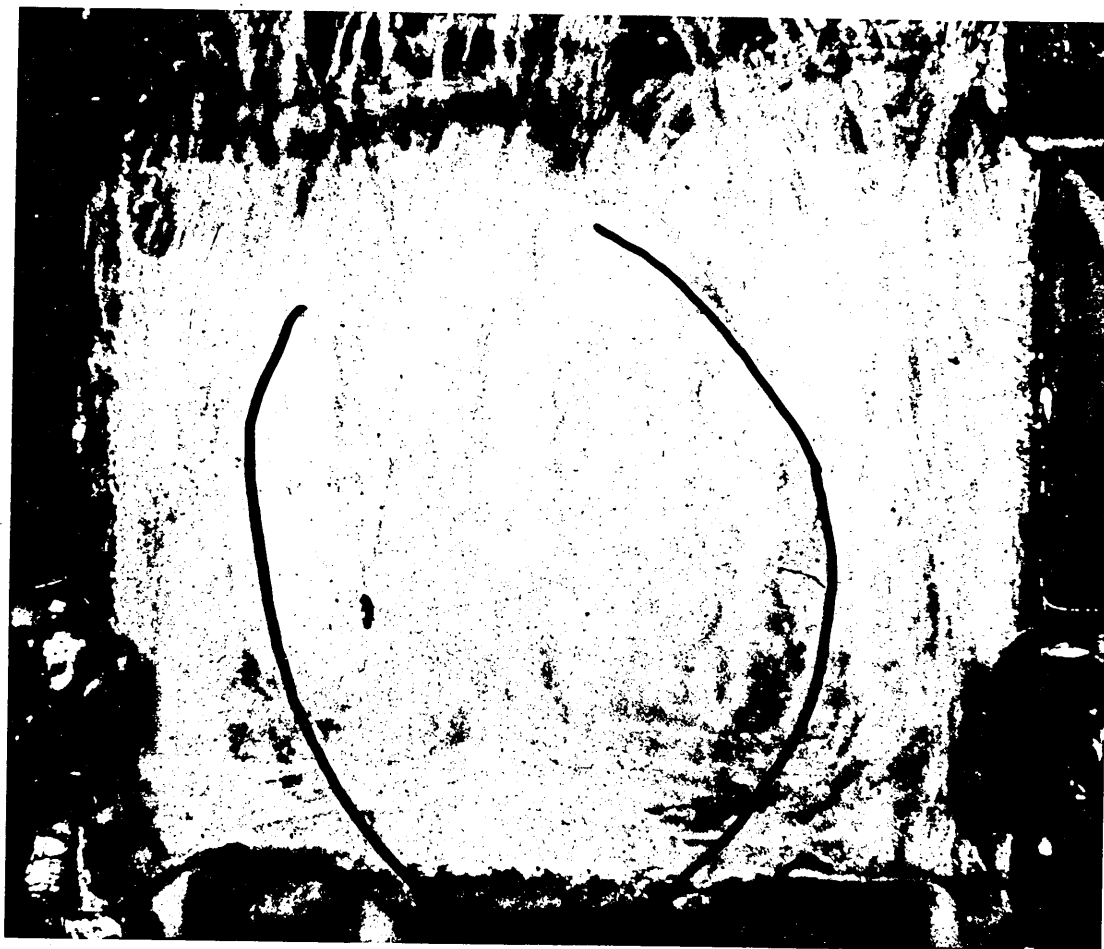


PLATE 8 ($\zeta = 2' 45''$)

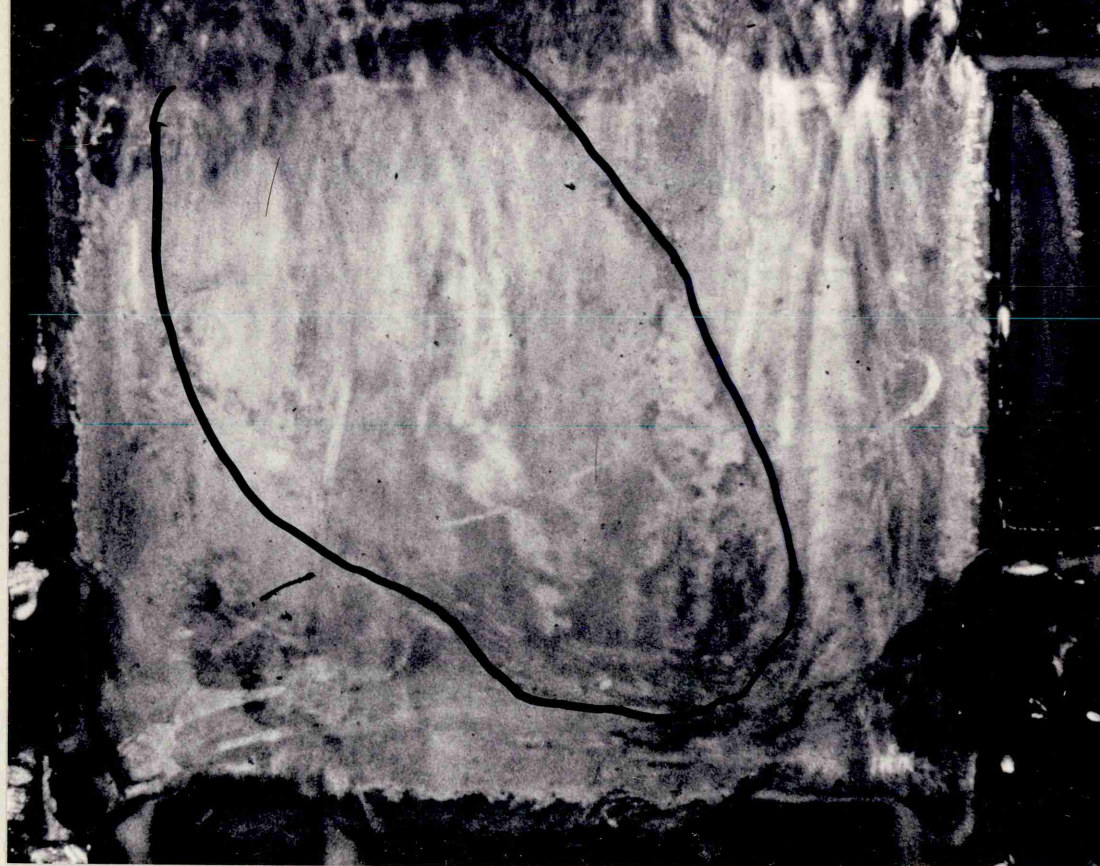


PLATE 9 ($\zeta = 2' 48''$)

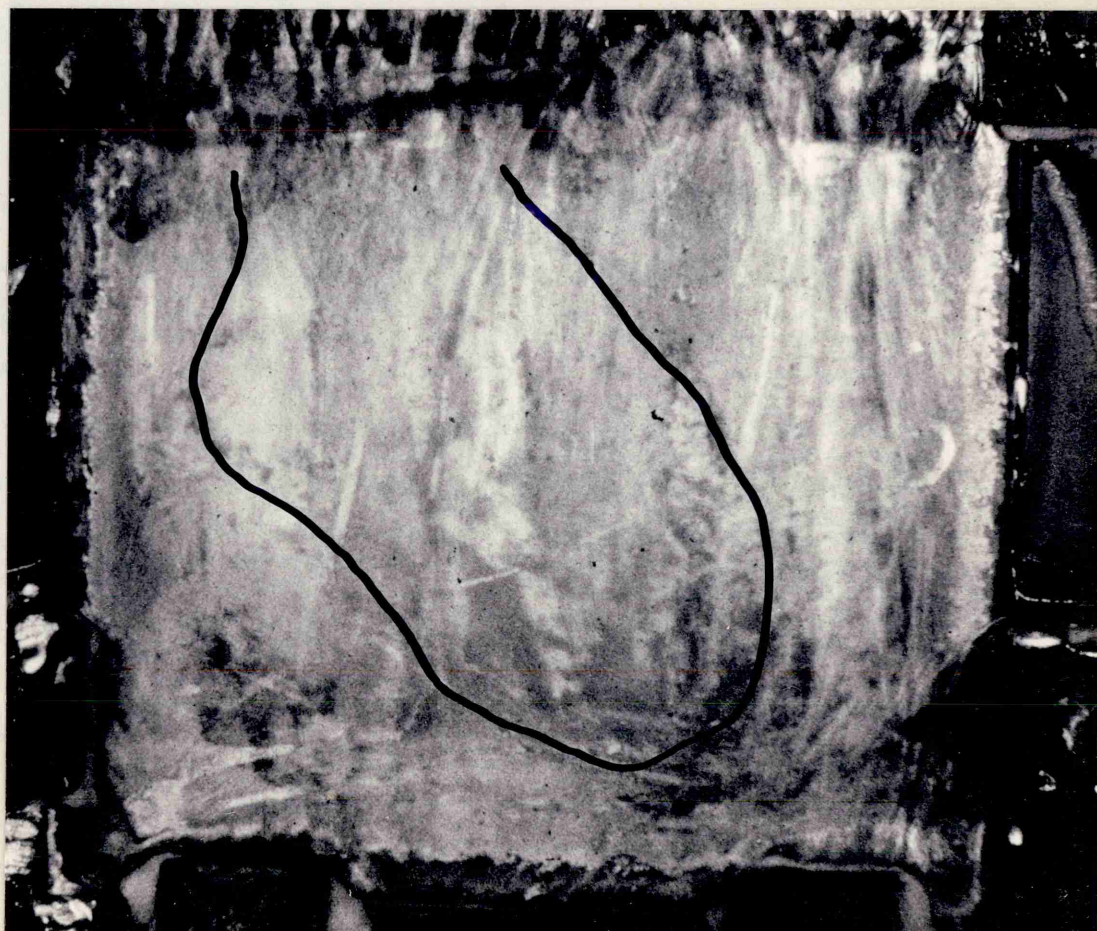


PLATE 10 ($\zeta = 2' 51''$)



PLATE 11 ($\lambda = 2' 54''$)



PLATE 12 ($\lambda = 2' 57''$)



PLATE 13 ($\zeta = 3' 00''$)



PLATE 14 ($\zeta = 3' 03''$)



PLATE 15 ($\zeta = 3'06''$)



PLATE 16 ($\zeta = 3'09''$)



PLATE 17 ($\zeta = 14' 40''$)

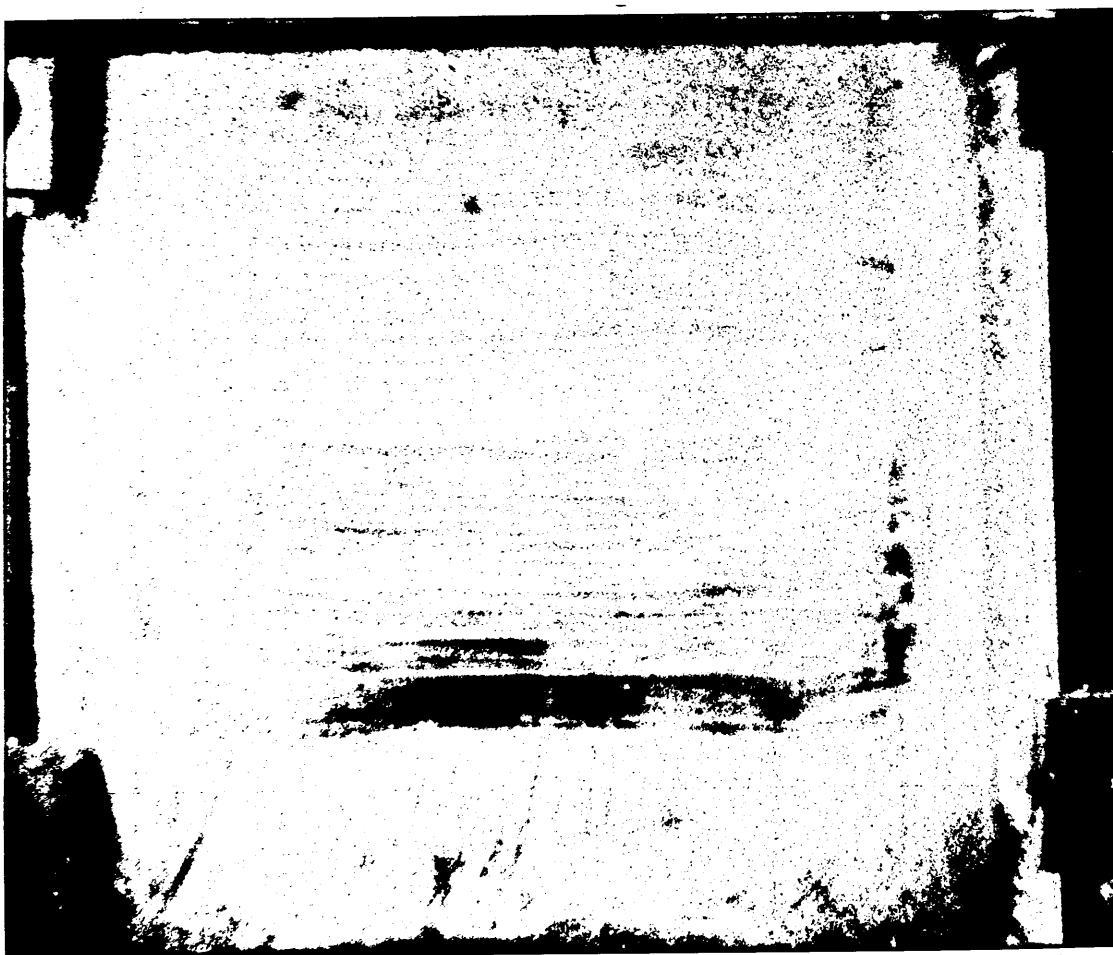


PLATE 18 ($\zeta = 14' 54''$)



PLATE 19 ($\zeta = 15' 08''$)



PLATE 20 ($\zeta = 15' 22''$)



PLATE 21 ($\zeta = 15' 36''$)

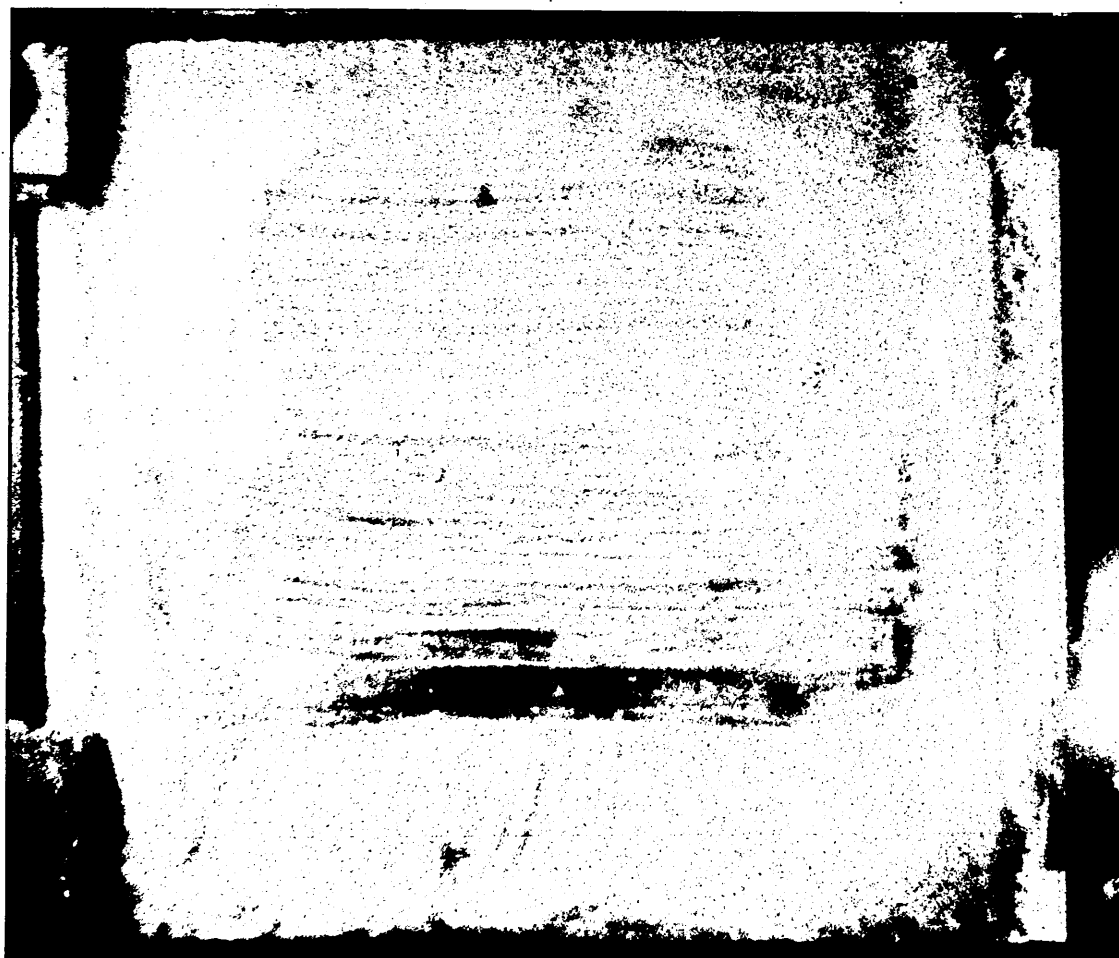


PLATE 22 ($\zeta = 15' 50''$)

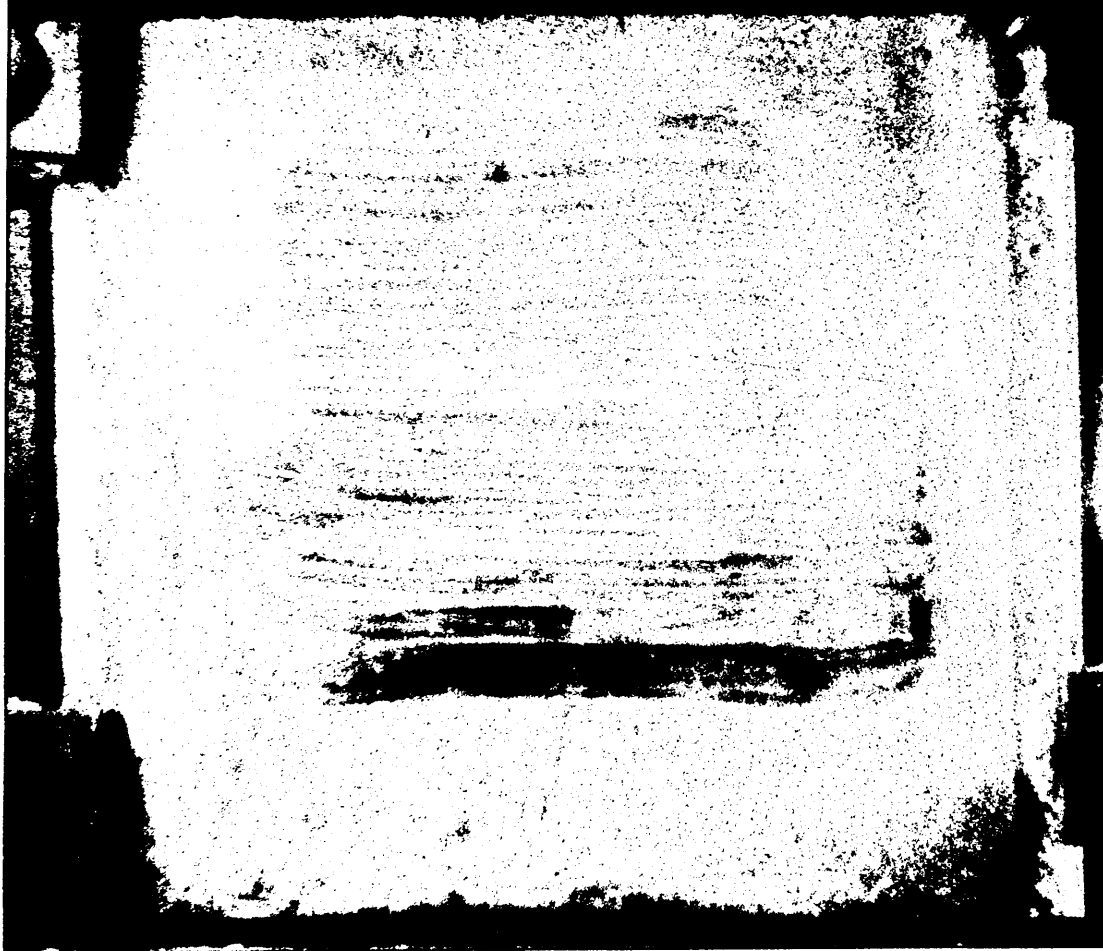


PLATE 23 ($\zeta = 16' 04''$)



PLATE 24 ($\zeta = 16' 1.8''$)

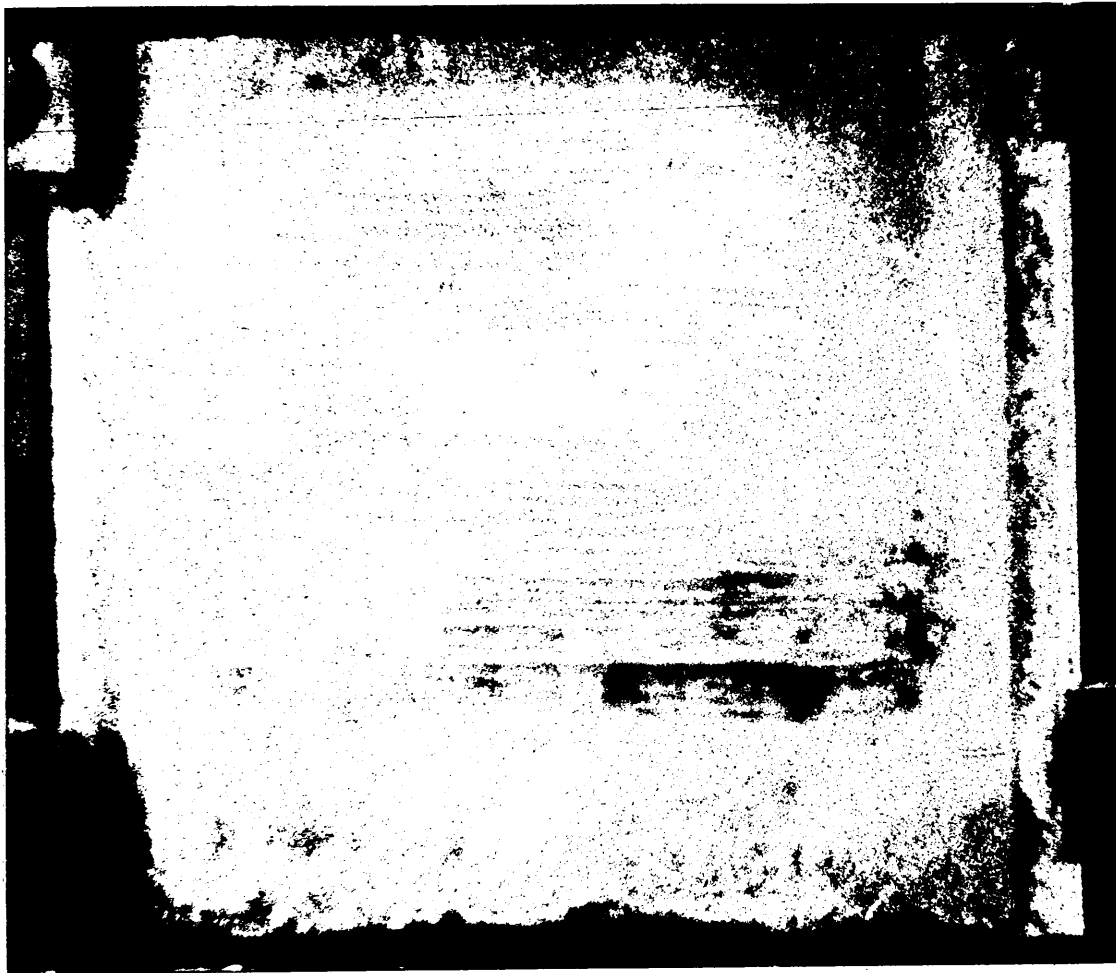


PLATE 25 ($\zeta = 16'32''$)

VI DISCUSSION

VI.1 Thermal analysis

VI.1.1 Combined effects of superheat and cooling conditions

The melt superheat and the applied cooling conditions define the mode of solidification of the pure metal or alloy.

Hills et al^(27,28) have developed a model to describe the solidification of pure metals and alloys in the presence of superheat. Their model describes the progress of any given solidification process through an algorithm that consists of various solidification modes. The algorithm and solidification modes are shown in fig.28. This algorithm is more complicated than the one shown in figures 6 and 7 because it includes the effect of the layer of partially solidified metal consisting of dendrites and liquid. Many more Modes and routes can occur as shown in the algorithm in Figure 28. The cooled liquid layer is shown as a dotted layer in this latter algorithm, the partial layer is horizontally hatched, and the fully solidified metal is obliquely hatched. The solidification modes relevant to this work are S1, S1F, S2, S2F, S3, S3F and Z3F. Modes S3 and S3F involve a growing layer of solidified metal, within which a layer of partially solidified metal exists but does not extend to the neutral surface within the casting. In the other relevant modes that involve an outer solidified layer, the partially solidified layer extends to the centre of the casting so that the dendritic net extends throughout the entire region inside the solidified shell. The cooling

conditions used in this work have been classified in accordance with the routes through this algorithm, as shown in Table IV, from the evidence presented in the thermal analysis curves.

Relating this table to the occurrence of air gap formation in the experiments suggests that it is only in the cooling routes S1-S2-S3-S3F-Z3F and S1-S1F-S2F-S3F-Z3F that an air gap can form when an alloy is solidified. It is only when the solidification process follows these routes that a solid layer exists at the outer surface of the ingot whilst liquid metal still exists at the centre. Under these conditions, the solidified shell can exert a contraction force bigger than the force exerted by the metallostatic head and thus give rise to the formation of a gap.

TABLE IV

	side		
	front	walls	plate
	A	B	C
1	S1-S1F-S2F-Z2F-Z3F	S1-S1F-S2F-Z2F-Z3F	(S1-S2-S2F-S3F-Z3F)
2	"	"	"
3	"	"	"
4	S1-S2-S2F- S3F-Z3F	S1-S2-S2F- S3F-Z3F	S1-S2-S2F-S3F-Z3F

(symbols as defined in table III and figure 28)

It can be seen from figure 28 that, when other routes are followed, the partial layer will extend over the whole region of the casting (mode Z2-Z2F-Z3F) allowing the dendrites to bridge throughout the entire cross section of the ingot. Although the dendrites will not be strong, resistance to their deformation, once they have formed an interlinking network, will probably be at least of the same order of magnitude as the metallostatic head (10^4 N/m^2), and will prohibit the formation of an air gap before solidification is more or less complete. Table IV shows that experiments 4A, 4B and 4C reproduced conditions which the above analysis suggests will favour the formation of an air gap.

The remainder of the experiments will not create the conditions required for the formation of an air gap. For a pure metal, the air gap will only form provided the outer layers of solidified metal have been cooled sufficiently for them not to creep, before too great a thickness of solid metal has been formed. This implies that, even for pure metals, those cooling modes that do not establish a large temperature gradient across the metal layer will not show the formation of an air gap. Examination of the algorithm in fig.28 suggests that it is the pure metal cooling route involving mode 2 that gives sufficient cooling. Once again, experiments 4A, 4B and 4C involve appropriate cooling conditions.

VI.1.2 Effect of Undercooling

Undercooling at the liquidus arrest point has been observed by a number of workers. Hunt and Chilton⁽²⁹⁾ found that the degree of undercooling at the solid liquid interface during the solidification of a lead tin eutectic alloy varied linearly with the solidification rate. In the range of solidification rates that correspond to this investigation their results show that the degree of under-cooling would vary between 0° and 1.5°C . However, Moore and Elliott⁽³⁰⁾ have reported lower values than those obtained by Hunt and Chilton about 0° to 0.8°C under similar conditions. Undercooling was detected in the present investigation during the solidification of both pure tin and the lead-tin alloy, as indicated in each set of cooling curves. Furthermore, the presence of undercooling indicated the extent to which the front face was cooled uniformly when water was used as the coolant since, with uneven cooling conditions, the undercooling took place at different times at different thermocouple positions. The degree of undercooling observed in the present investigation varied with the cooling rates over the range 0° to 3°C .

This undercooling is presumably due to a nucleation delay at the start of solidification. Ruddle⁽³¹⁾ claims that, undercooling only occurs in pure metals and alloys near to the mould walls and, once recalescence has taken place, the solidification proceeds at the equilibrium solidification temperature, no undercooling occurring in the interior of the

casting. During the solidification of both pure tin and lead-tin alloy in this investigation no undercooling was detected for thermocouple No.3 placed in the middle of the ingot.

VI.1.3 Solidus Arrest

The solidus arrest point (at the eutectic temperature for the alloy investigated) was slightly below the equilibrium temperature. For the thermocouples placed at the front face of the mould the difference between the equilibrium solidus temperature and the observed values was small (2° to 3°C) and although the results were scattered showed some dependence from experiment to experiment on cooling rate. This result has also been reported by a number of previous authors Doherty and Feest⁽³²⁾, on the other hand, observed, during a study of solidification of copper nickel alloys, that the solidus arrest occurred some 10°C below the equilibrium value and that it always occurred at the same temperature even though the cooling rate was varied from $10^{\circ}\text{C}/\text{min}$ to $38^{\circ}\text{C}/\text{min}$.

Although the solidus temperature observed in this work differed from the equilibrium value, the difference was small and the results were scattered and varied from thermocouple to thermocouple in any one experiment. The random nature of this variation suggested that it was due to random differences between the thermocouples and their connections rather

than to variations of solidification rate. Thus, in order to correlate the readings of the different thermocouples in any one experiment, a standard correction was applied to all of the temperatures indicated by each thermocouple in order to bring the arrest point indicated by each thermocouple to the eutectic temperature.

VI.1.4 Study of the cooling curves after the solidus arrest

Many workers have observed inflections in the mould heating and cooling curves for positions at the mould interface for both static and continuous casting moulds. These inflections have usually been attributed to and assumed to be consistent with, the formation of an air gap. Figures 21a, 22a and 24b presented in section V.2 show inflections in the cooling curves of the thermocouples No.6 and No.4. These inflections occurred at the same moment to within approximately 1/10 th of a second, that the solidifying metal was observed to separate from the glass face.

VI.2 Visual Observations

Plates 5 to 25 indicate the development of the separation gap during the solidification of the tin alloy. The plates 5 to 16 were taken during an experiment in which the front glass plate and the side walls were cooled with water, i.e. a 4C run, and in which cooling started ($\tau=0$) when the metal and mould were some 50°C above the solidus temperature of the lead-tin alloy. The thermal history for this run is shown in figures 19a and 19b. Plate No.6 was taken at a much later

stage in the freezing process.

The entire process of separation of the metal from the glass surface took 35 seconds and is shown in plates 5 to 16.

The separation process was rendered more apparent by cooling water leaking into the cavity through the asbestos string seal.

The set of plates 17 to 25 were taken during a preliminary run in which the front face was cooled with forced air before the side walls were water cooled. The run was thus a modified 3C run. The lead-tin alloy and the mould were initially heated some 60°C above the solidus temperature. The system was then cooled to 200°C by blowing air at the front face and by allowing the side walls to cool by natural convection. After the 14th minute the side walls were cooled with water. This situation represents a S1-S1F-S2F-Z2F-Z3F cooling route and this does not, in line with the analysis presented in section VI-1-1, allow the formation of an air gap. Indeed the front face is cooled significantly less than the other surfaces and thus becomes the thermal centre of the ingot. The growth of the partial layer and then completely solidified layers could be followed across the glass plate from the side walls and is recorded in film and in the sequence of plates 17 to 25. Light areas can be seen at the sides together with horizontal dark bands which correspond respectively to the solidified and partial layers

of the alloy at the front face. A contraction gap is observed to occur against the front face as the completely solidified ingot pulls away from the glass plate. This type of separation was seen fundamentally different from the air gap formation, since it does not occur early in the solidification process, and does not involve the distortion of a thin solidified layer against the action of metallostatic pressure.

This work has shown that the air gap only forms when the cooling rates are fairly high, and then forms at the corners of the mould moving towards the centre of each face. This observation agrees with that of some earlier work^(5,21) but disagrees with almost all the theoretical predictions that have been made. These suggest that the gap will form at the centre of the ingot or at billet faces, by the inward bowing of the solidified shell.

Considerable thought has been given to the effect on the results due to the water that leaked into the air gap, once it had formed. If the water could be considered to have affected the air gap formation processes it could only have done so during the later stages, because it was not until the air gap had formed that the water could enter into the region of the interface. Moreover, it was felt that no mechanical effect could be involved since the water, and any steam produced from it, could easily escape. Thus the only effects that the water could have had would result from its influence on heat transfer processes. The water would enhance

40

somewhat, the heat transfer rates over those across an actual air gap since it has a higher conductivity than the air. However, the effect on the overall heat transfer process will be very small because this process is dominated by the thermal resistance of the glass plate (see section VI-3). That this is so can be seen because the temperature cooling curves Fig.21a do show a small rise when the 'air gap' forms indicating that the heat transfer rate must have been slowed down in spite of the presence of the water.

These curves thus show that, if the water had any effect on the evolution of the air gap, it could only have had a relatively minor one.

VI.3 Estimated values of heat transfer coefficients

VI.3.1 Natural convection

For a plate cooled by natural or free convection in laminar flow conditions, i.e. $10^4 < Gr_x \times Pr < 10^{10}$, S. Ostrach⁽³⁵⁾ developed the following correlation for the average value of the Nusselt number:

$$Nu_L = 0.902 \sqrt[4]{\frac{Gr_L Pr^2}{4(0.861 + Pr)}} \quad (VI.1)$$

Taking the properties of the air as shown in table V for the average boundary temperature of 120°C

$$Pr = \frac{c \mu}{k} = 0.696$$

and

$$Gr_L = \frac{\beta g}{\nu^2} (\theta_0 - \theta_Q) L^3 = 6.0 \times 10^7$$

Where L is the height of the glass plate we calculate the product $Pr \times Gr_L$ to test for laminar flow conditions.

$$Pr Gr_L = 4.2 \times 10^7$$

Since $Pr Gr_L < 10^{10}$, the natural convection processes are laminar and we can substitute values in (VI.1) giving

$$\frac{hL}{k} = Nu_L \approx 42$$

from which

$$h \approx 9.5 \text{ W/m}^2 \text{ } ^\circ\text{K}$$

The overall heat transfer coefficient from the inner surface of the glass or mould wall to the air is calculated by the following relation

$$\frac{1}{h_{\text{overall}}} = \frac{1}{h_{\text{conv}}} + \frac{d}{k} \quad (\text{VI.2})$$

from which

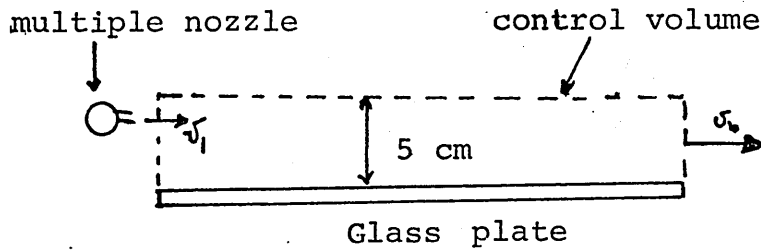
$$h_{\text{overall}} \cong 9 \text{ W/m}^2 \text{ } ^\circ\text{K}$$

Considering the side walls cooled by natural convection and starting at the same initial temperature as the glass plate the overall heat transfer coefficient from their inner surface to the air is

$$h_{\text{overall}} \cong 9.4 \text{ W/m}^2 \text{ } ^\circ\text{K}$$

VI.3.2 Forced convection (bottom upwards and top downwards)

The air flow over the outer surface of the glass plate results from the action of the multiple nozzle. Air is entrained into the jets produced by the nozzle to provide a curtain of air flowing past the surface. The mean velocity of this air can be estimated from a rough momentum balance carried out a control volume that extends over the thickness of the air curtain.



Observation of the apparatus showed that the thickness of the air curtain was about 5cms.

The velocity of the air at the exit of the nozzle is calculated using the Bernoulli equation.

$$\frac{p}{\rho_{air}} = \frac{1}{2} v_1^2$$

and from the momentum balance over the control volume a bulk air velocity of $v_b = 3.7$ M/S was found. Since $Re_L < 10^5$, the forced convection processes are laminar and we can substitute values in the correlation given by Pohlhausen⁽³⁶⁾ and quoted by Geiger and Pourier⁽³⁷⁾, e.g. VI.3, for $Pr > 0.6$ and $Re < 10^5$.

$$Nu_L = 0.664 Pr^{0.343} Re_L^{0.5} \quad (VI.3)$$

We can substitute values in VI.3, giving

$$Nu_L \approx 105$$

from which

$$h_{con} \approx 24 \text{ W/m}^2 \text{ } ^\circ\text{K}$$

J. Gryzadoridis⁽³⁸⁾ has studied experimentally the influence of forced flow in a natural convection process. He claims that the influence only becomes significant when Re_L^2 is of the same order of magnitude as the Grashof number, i.e. $0.1 < Gr_L / Re_L^2 < 3$. In the present case $Gr_L = 6.0 \times 10^7$ and $Re_L = 3.2 \times 10^4$ so

$$\frac{Gr_L}{Re_L^2} = 0.06$$

Thus it can be concluded that natural convection at the glass plate will have a negligible effect on the forced convection process.

The same heat transfer coefficient will thus apply whether the air is blown up or down the plate. Equation VI.2 is used to calculate this overall heat transfer coefficient from the inner glass surface to the air:

$$h_{\text{overall}} \approx 21 \text{ W/m}^2\text{K}$$

VI.3.3 Film water cooling

The heat transfer coefficient at the glass surface when it is cooled by a falling film of water can be calculated, assuming a constant film thickness, using the correlation given by Pigford⁽³⁹⁾ and quoted by Bird et al⁽⁴⁰⁾.

$$\left[\dot{q}_{\text{aver}} \right]_{x=0} = \frac{3}{2} k (\theta_o - \theta_a) \frac{1}{(9\beta L)^{1/3} \Gamma(4/3)}$$

where $\beta = \frac{\mu^k}{p^2 c_g \delta}$ and $\Gamma(4/3)$ is the

Gamma function of $4/3$ and is approximately equal to one.

Assuming that the surface temperature of the plate is constant, this equation gives

$$h_{\text{film}} \approx 7900 \frac{\text{W}}{\text{m}^2 \text{ } ^\circ\text{K}}$$

and the overall heat transfer coefficient from the inner surface of the glass plate to the film of water becomes

$$h_{\text{overall}} \approx 204 \frac{\text{W}}{\text{m}^2 \text{ } ^\circ\text{K}}$$

These two values show that the heat transfer process is controlled by the thermal resistance of the silica glass plate.

VI.3.4. Heat transfer coefficient from the mould to the cooling water passages

To calculate the heat transfer coefficients from the mould to the fully developed flow in the side passages of the mould we used the correlation given by Sider and Tate⁽⁴¹⁾ and quoted by Szkel and Themelis⁽⁴²⁾ for $\text{Re} < 2000$ and $L/d > 10$. A mean surface temperature of 120°C was assumed and the property values of the water were calculated assuming a bulk temperature of 60°C . A water flow of 2.2 lit/min corresponds to

$$\text{Re} = 102$$

$$\text{and } \text{Pr} = 2.5$$

then substituting values in

$$Nu_L = 1.8 (Re \ Pr \frac{L}{d})^{1/3} \left(\frac{\mu_{av}}{\mu_s} \right)^{0.14} \quad VI.5$$

an average heat transfer coefficient of

$$h_{av} = 4125 \text{ W/m}^2 \text{ } ^\circ\text{K}$$

was estimated.

The overall heat transfer coefficient from the inner surface of the mould to the cooling water is calculated using the formula VI.2;

$$\frac{1}{h_{overall}} = \frac{1}{h_{aver}} + \frac{d}{k_{steel}} \quad VI.2$$

Where $d = 4\text{cm}$ is the thickness of the mould wall

$$h_{overall} \approx 900 \frac{\text{W}}{\text{m}^2 \text{ } ^\circ\text{K}}$$

McAdams (43) claims that the heat transfer coefficient due to metal/metal contact is approximately $1200 \text{ W/m}^2 \text{ } ^\circ\text{K}$. This fact makes the overall heat transfer coefficient from the ingot surface to the water in the passages of:

$$h_{overall} \approx 500 \text{ W/m}^2 \text{ } ^\circ\text{K}$$

Table V - Thermal Properties

Silica glass:	Thermal conductivity (k)	= 1.26 W/m ^{°C}
	Thickness (d)	= 0.006 m
50% lead-tin alloy*	Thermal conductivity (k)	= 46.4 W/m ^{°C}
	Density (ρ)	= 8890 kg/m ³
	Latent heat of fusion (H)	= 53560 J/kg
	Specific heat (c)	= 213 J/kg ^{°C}
	Liquidus temperature (θ_L)	= 216 ^{°C}
	Solidus temperature (θ_S)	= 183 ^{°C}

*(Source of data: ASTM handbook 1969).

Pure tin*	Thermal conductivity (k)	= 58.6 W/m ^{°C}
	Density (ρ)	= 5765 kg/m ³
	Latent heat of fusion (H)	= 60668 J/kg
	Specific heat (c)	= 259.5 J/kg ^{°C}
	Solidus temperature (θ_S)	= 231.9 ^{°C}

Steel properties used in the analysis of Vok and Wunnemberg data:

Thermal conductivity (k)	= 0.03 KW/m ^{°C}
Density (ρ)	= 7500 kg/m ³
Latent heat of fusion (H)	= 300 kJ/kg
Specific heat (c)	= 0.67 kJ/kg ^{°C}
Solidus temperature (θ_S)	= 1537 ^{°C}

Mould properties used in the analysis of Mackenzie and Donald data:

Thermal conductivity (k)	= 0.025 KW/m ^{°C}
Specific heat (a)	= 5900 J/kg ^{°C}
Density (ρ)	= 7500 kg/m ³
Initial temperature (θ_H)	= 1520 ^{°C}

Table V - Continued

Thermal properties of air**		at 20°C	at 120°C
Density (ρ)	=	1.22 kg/m ³	-
Specific heat (c)	=	1001.6 J/kg°C	-
Viscosity (μ)	=	0.0217 cp	-
Thermal conductivity (k)	=	0.026 W/m°C	0.034 W/m°C
Prandtl number (Pr)	=	0.709	0.690

** Source: Chemical Engineering handbook. (1972).

Thermal properties for water** at 20°C

Viscosity (μ)	=	1.01 cp (at 120°C	= 0.281 cp)
Thermal conductivity (k)	=	0.594 W/m°C	
Density (ρ)	=	1000 kg/m ³	
Specific heat	=	4184 J/kg°C	

VI.4 Estimation of Solidification times

An estimation was made of the solidification times of the ingots studies in this work using Hills' formalism. The following assumptions were made: the solidification was assumed to be uni-directional in all cases; perfect thermal contact between metal and mould walls was assumed; the thermal properties of the metal were considered to be independent of temperature and of phase changes, the heat transfer coefficients were assumed to remain constant during the solidification period.

Using the above assumptions, Hills⁴⁴ provides graphs of t^* (the dimensionless thickness) versus ξ (the dimensionless dwell time) for different values of h^* (the dimensionless latent heat). For any given thickness and heat transfer coefficient values of ξ could be obtained from these graphs and used to calculate solidification times.

Table VI shows estimated solidification times for the different cooling conditions at the front face of the mould for both cases: the 50%lead-tin alloy and pure tin.

The latent heat of the alloy was assumed to be liberated at the mean of its liquidus and solidus temperatures. Also, the solidification time was assumed to be the time that it took for the solidification front to reach the mid-plane of the ingot.

TABLE VI

Cooling Condition		$h [W/m^2 \text{ } ^\circ K]$ calculated in Section VI.3	$\tau_{(min)}$ experi- mental	$\tau_{(min)}$ estima- ted
50% lead- tin alloy	natural convection	9	45	70
	forced convection	21	17	27
	water cooling	204	4	3.5
pure tin	natural convection	9	not per- formed	-
	forced convection	21	not per- formed	-
	water cooling	204	3.5	2.5

The agreement between the solidification times measured experimentally and the estimated times is fairly good, especially when it is remembered that the theory assumes uni-directional heat flow whereas some heat is lost to the side walls of the mould in the experimental apparatus. That this heat loss is the principal cause of the differences between the experimental and the estimated values can be seen because the agreement is the poorest when the heat transfer coefficient governing the cooling has its lowest value. The value of the heat transfer coefficient through the side walls estimated in section VI.2.1 is about the same as the lowest value through the glass face when it is cooled by natural convection. This explains why the experimentally determined solidification time for this case is just a little over half the time estimated theoretically.

VI.5 Theoretical calculations for comparison with published heat flow data during solidification to ascertain the influence of the air gap on the heat transfer

VI.5.1 Comparison for metal moulds

Mackenzie and Donald⁽⁷⁾ experimentally determined the heat flow through the inner mould surface and its variation with time. Their work was summarised in section II.1.2.2 and their experimental results are shown in fig 1. In order to ascertain the influence of the air gap theoretical values of the heat removal rate are here determined for the ideal case of a semi-infinite liquid metal in the region $x > 0$, solidifying in perfect thermal contact with a semi-infinite solid in the region $x < 0$. For this case Carslaw and Jaeger⁽³³⁾ quote the solution introduced by Schwarzschild⁽³⁴⁾ for the solidification of metal cast in a mould. Assuming that the properties of the liquid and solid metal are the same, Schwarz's solution for temperatures in the mould

$$\theta_x = \frac{\theta_N}{1 + \operatorname{erf} \lambda} \left(1 + \operatorname{erf} \frac{x}{2\sqrt{\alpha t}} \right) \quad \text{VI.6}$$

where θ_N is the temperature of the liquid metal. The value of λ is fixed by a transcendental equation VI.7. For the case where the liquid is initially at its melting point, this equation is

$$\lambda e^{\lambda^2} (1 + \operatorname{erf} \lambda) = \frac{c \theta_M}{H \pi^{1/2}} \quad \text{VI.7}$$

For the steel used in Mackenzie and Donald's work

$$\frac{c \theta_M}{H \pi^{1/2}} = 2.2$$

Using this value, and the graphs of $\lambda e^{\lambda^2} (1 + \operatorname{erf} \lambda)$ vs $\frac{c \theta_M}{H \pi^{1/2}}$ provided by Carslaw and Jaeger a value of $\lambda = 0.68$ was found.

The heat flux through the interface is given by

$$\dot{q}''_{x=0} = -k \left. \frac{\partial \theta}{\partial x} \right|_{x=0} \quad \text{VI.8}$$

and can thus be determined from the equation for $\dot{q}''_{x=0}$ VI.6 to be

$$\dot{q}''_{x=0} = \frac{k}{1 + \operatorname{erf} \lambda} \frac{e^{-\lambda^2/4\alpha t}}{\sqrt{\pi \alpha t}} \bigg|_{x=0}$$

substituting relevant values gives:-

$$\dot{q}''_{x=0} = \frac{1312}{\sqrt{t/[\text{min}]}} \frac{\text{cal}}{\text{cm}^2 \text{ min}} \quad \text{VI.9}$$

The physical constants for the mould and steel used to make these calculations are given in table V. The relation VI.9 was evaluated for different values of t and plotted in fig 29 together with the experimental results obtained by

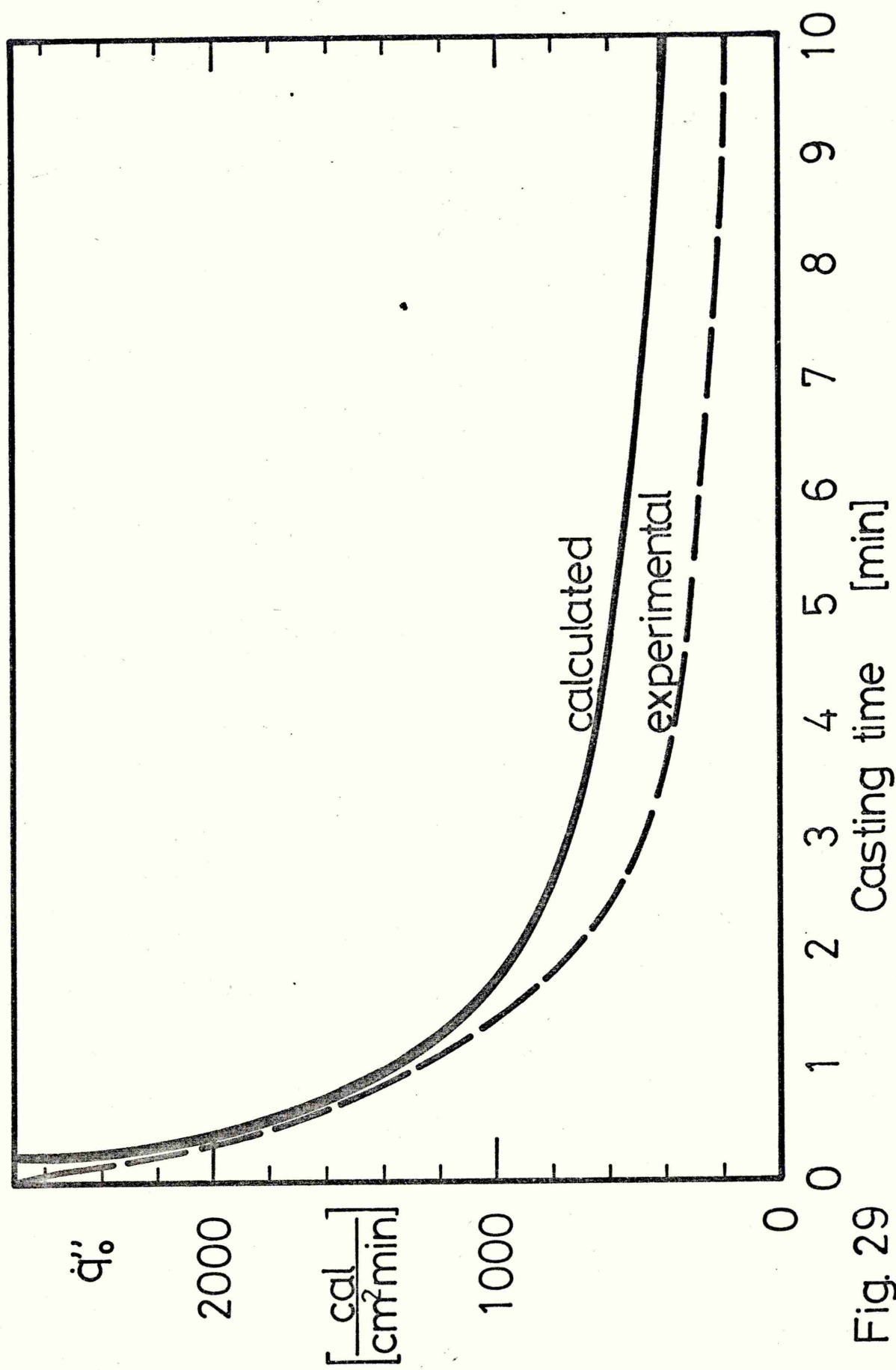


Fig. 29

Mackenzie and Donald. Fig 29 indicates a 40% difference between the two curves after the third minute. The calculated values are higher than the experimental, but, these curves are very similar. The sudden fall in the heat flow that they measured was interpreted by Mackenzie and Donald as evidence for the formation of an air gap. However, comparison of the two curves shown in fig 29 shows that much, if not all of the fall is due to the reduction in heat flow that occurs as the mould heats up. Indeed, in view of the uncertainties in the various parameters used in the calculations, the two curves in fig 29 suggest that the formation of an air gap may have a relatively minor effect on cooling rates in metal moulds.

VI.5.2 Comparison with continuous casting

A number of workers have determined the way in which the heat removal rate within the mould of a continuous casting machine decreases with distance below the liquid metal meniscus. The results obtained by Volk and Wunnenberg¹² will be analysed here to ascertain the extent to which this variation is due to the decreasing surface temperature or to the formation of an air gap.

Volk and Wunnenberg split the mould of their continuous casting machine into a series of separate sections arranged vertically below one another, and determined the rate at which the cooling water removed heat from each section.

The total rate of heat removal between the liquid meniscus and the bottom of any one section can be obtained by adding to the heat removal rate in all the preceding sections. Hills⁽⁴⁴⁾ has developed a theoretical technique by which this total heat removal rate can be used to determine the mean heat transfer coefficient between the billet surface and the cooling water that applies over the distance from the liquid metal meniscus to the bottom of the particular section in question.

If this distance is denoted as X_m , the total heat removal rate per unit of length of billet perimeter can be denoted as \dot{Q}'_{X_M} . This is related to the billet's surface temperature and to the local value of the heat transfer coefficient by the equation:

$$\dot{Q}'_{X_M} = \int_0^{X_M} \dot{q}''_x dx = \int_0^{X_M} h_x \theta_x dx \quad \text{VI.10}$$

We can now define a mean value of the heat transfer coefficient such that:

$$\dot{Q}'_{X_M} = \bar{h}_{X_M} \int_0^{X_M} \theta_x dx \quad \text{VI.11}$$

Hills defines a dimensionless heat removal rate as:

$$Q^*_{\xi_M} = \frac{\dot{Q}'_{X_M}}{\theta_s \sqrt{\text{upck} X_M}} = \frac{1}{\xi_M} \int_0^{\xi_M} \theta^* d\xi \quad \text{VI.12}$$

where ξ_M is a dimensionless length:

$$\xi_M = \frac{(h_{X_M})^2 X_M}{\text{upck}}$$

VI.13

and presents theoretically determined graphs of $Q_{\xi_M}^*$ against ξ_M for different parametric values of H^* , the dimensionless latent heat ($H^* = H/c\theta_s$).

The heat removal data obtained by Volk and Wunnenberg¹² can be used to determine values of Q_{X_M}' that correspond to a series of values of X_M . Corresponding values of $Q_{\xi_M}^*$ can thus be calculated and used with Hills' theoretical graphs to determine the value of ξ_M that corresponds to the bottom of each of the water cooling sections of their mould. These values can then be used to determine the value of \bar{h}_{X_M} that applies over the distance between the liquid meniscus and the bottom of that particular section.

Fig. 30 shows the values of \bar{h}_{X_M} determined in this way for a range of different casting speeds plotted against X_M , and fig 31 shows the mean values applying over the entire mould plotted against the dwell time in the mould.

The mean heat transfer coefficients shown in fig 30 can be seen to fit straight lines for all the casting speeds except that the data for the casting speed of 1m/m is somewhat scattered. The slopes of the lines vary and no relation can be drawn up between them. For the casting

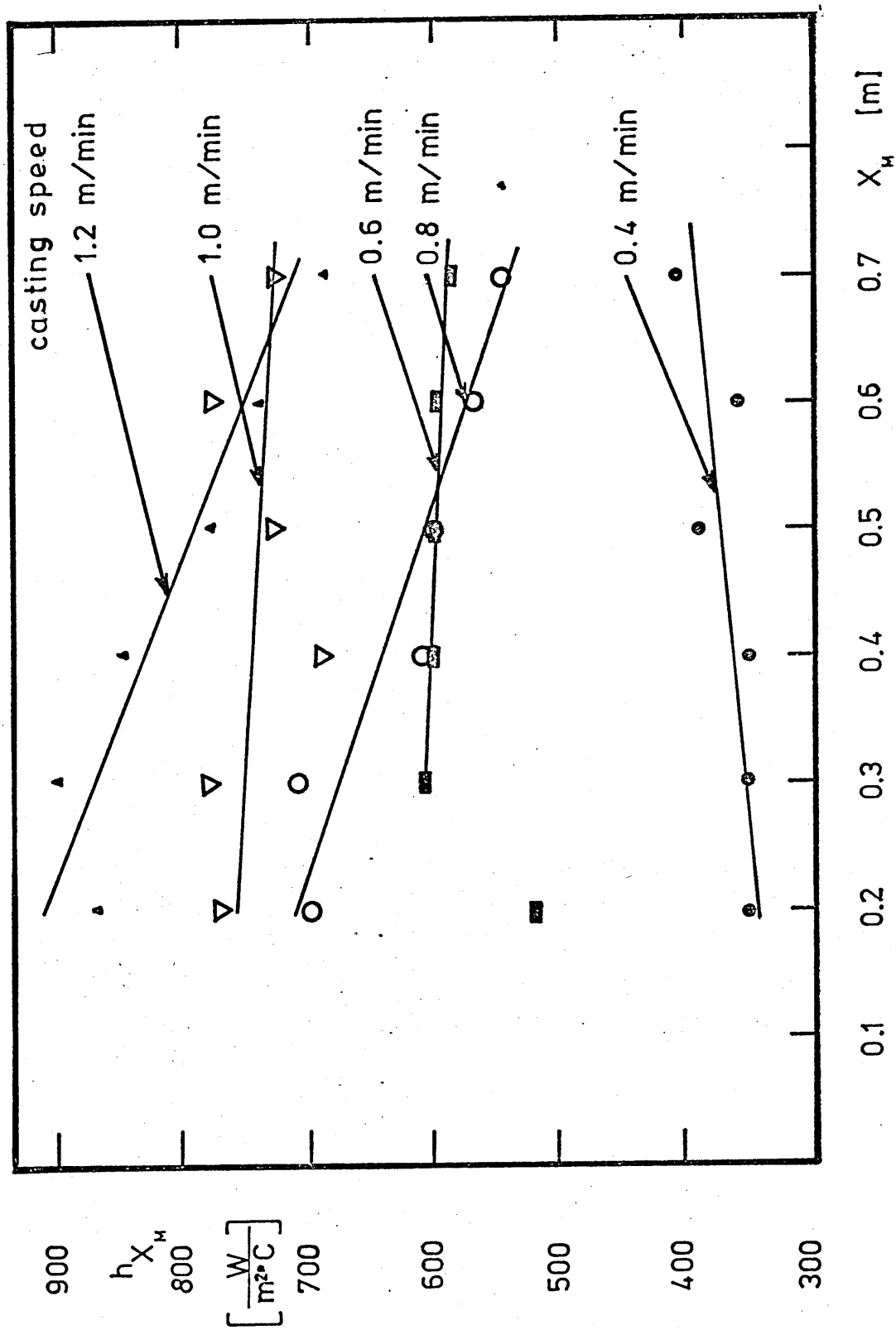


Fig.30. Calculated heat transfer coefficients vs. distance below metal meniscus.

speeds 1.2, 1.0 and 0.8m/min the heat transfer coefficients decrease with distance down the mould, whereas for the casting speeds of 0.6 and 0.4m/min they increase. This latter effect is probably caused by the 1%/m taper of the mould and the longer residence time of the billets in the mould.

Fig 31 shows the heat transfer coefficients for the entire mould at each casting speed plotted against the different dwell times. The slope of that line, if compared with the slopes of previous published data, subjected to the same treatment^(44, 45) does not show any precise functional relationship, except that both sets of data exhibit the same tendency for the overall heat transfer coefficient to increase as the dwell time decreases i.e. to increase with the casting speed.

Hills has presented a particular expression for the variation of surface temperature of a continuously cast steel ingot with distance down the mould. The value of H^* for steel is 0.3 and, for this value, Hills presents the following relationship:

$$\theta^* = \frac{\theta_o}{\theta_s} = 1 - 0.525 \xi^{0.74} \quad \text{VI.14}$$

Values of the surface temperature determined from this expression for the result of Volk and Wunnenberg are plotted in fig 32 against distance for each of the casting speeds that they investigated. The shape of these curves for 0.4

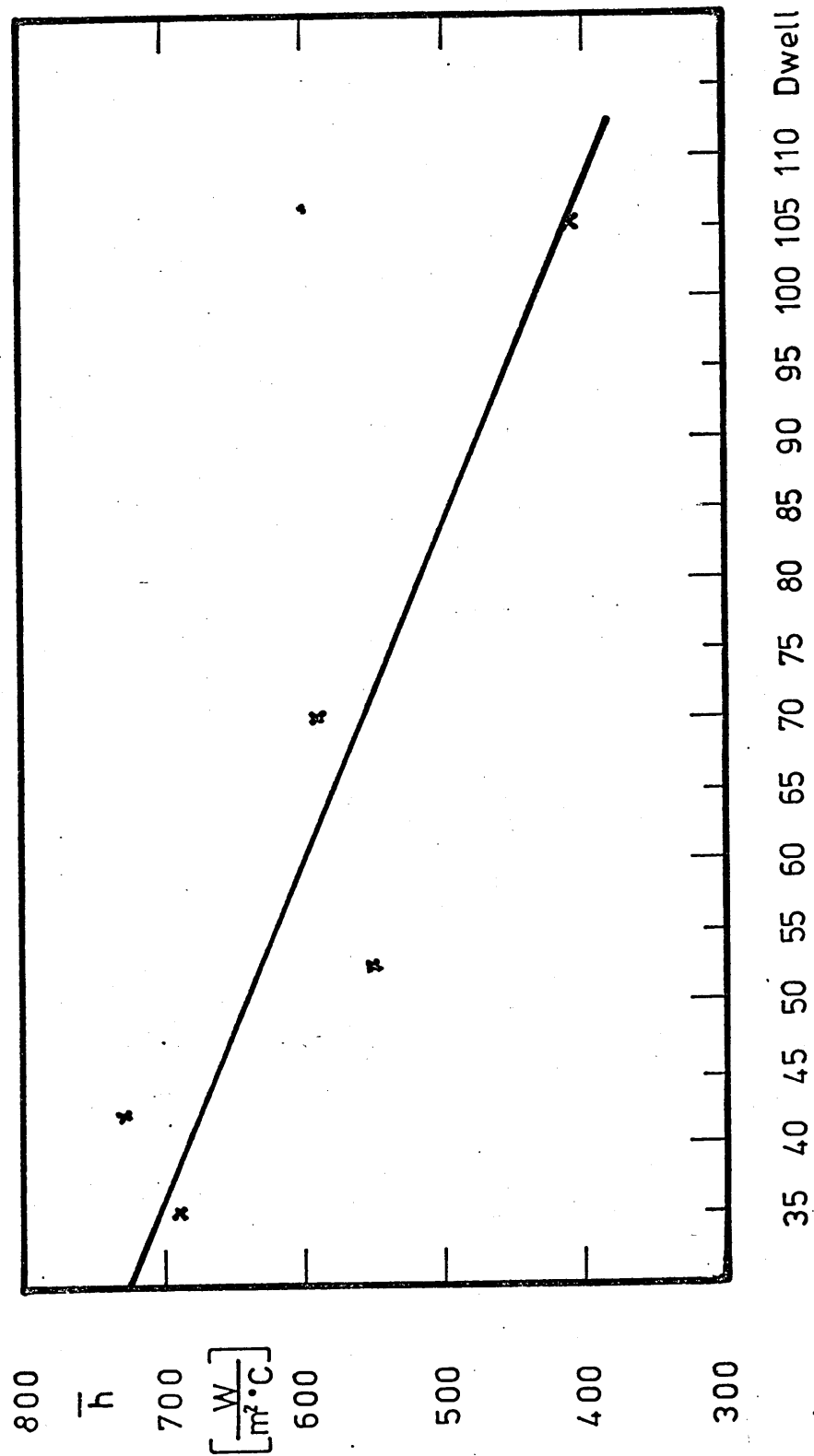


Fig. 31. Calculated overall heat transfer coefficients from Volk and Wunnenberg's data

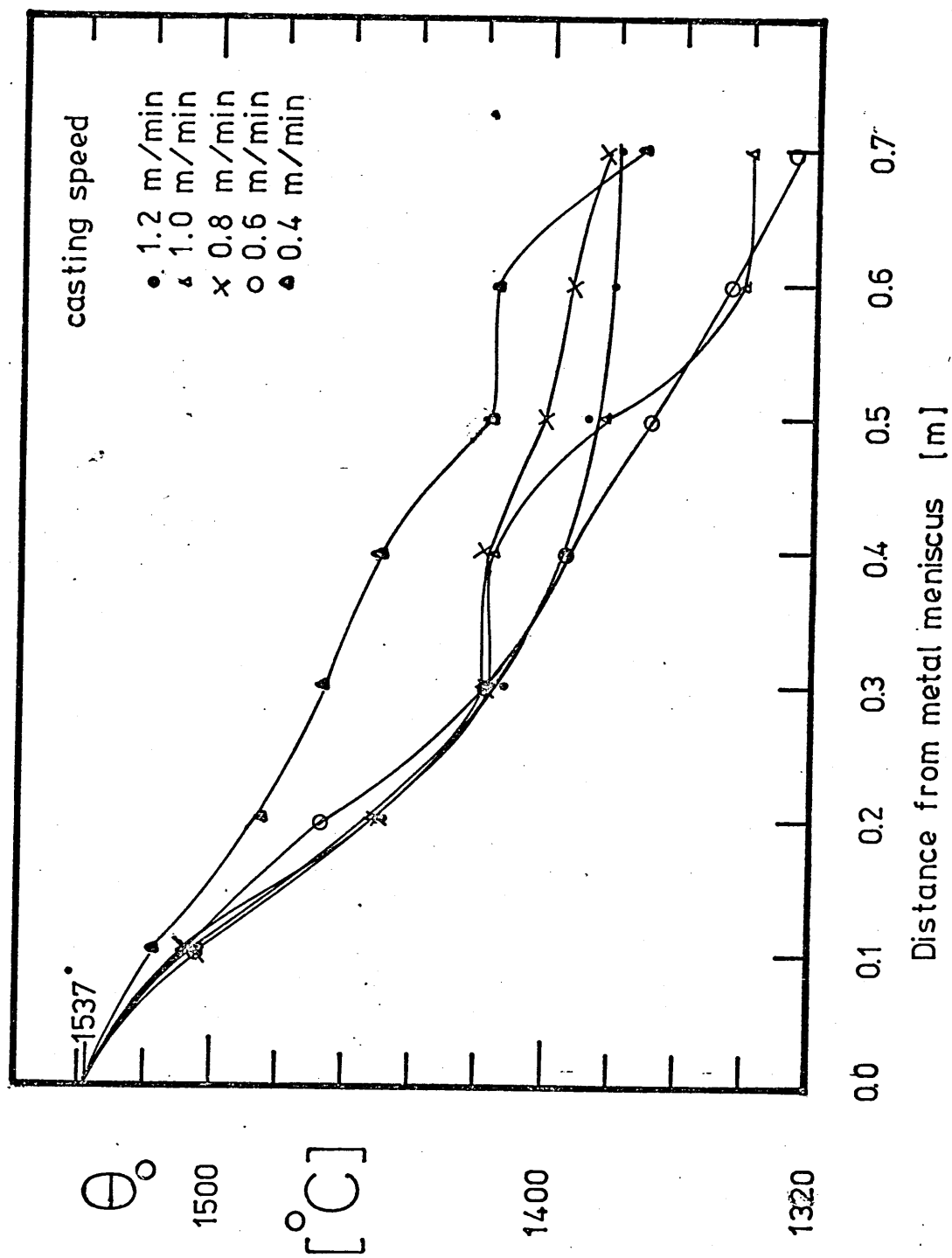


Fig. 32

0.8, 1.0 and 1.2 m/min indicates that the cooling rate is affected by the formation of the air gap as it must be for these speeds which show a decreasing heat transfer coefficient in fig 30.

However, in all cases, the effect is relatively small and, in some cases, the mean heat transfer coefficient does not decrease at all.

Thus this analysis shows that the formulation of an air gap has a relatively small effect on heat removal rates in the moulds of continuous casting machines and, in some cases, has no effect at all.

.6 Laser defocussing

In section IV.3.2 an attempt to measure air gap widths using a laser beam is described. It is reported that the spot produced on the observation screen by reflection, at the metal surface moved away from the other two spots and became diffuse immediately solidification commenced. An explanation of this defocusing phenomenon is to be found in the dendritic solidification characteristics of the alloy. This mode of solidification destroyed the mirror like surface of the metal causing it to become granular which in turn produced the scattering of the laser beam and the diffused spot on the screen.

VII CONCLUSIONS

1. The experimental results obtained in this work have shown that:

- (i) an air gap forms only when cooling rates on the various mould walls are approximately the same and relatively high;
- (ii) air gap formation starts at the corners of the solidifying ingot where there is the greatest intensity of heat extraction;
- (iii) subsequently as solidification continues air gap formation proceeds towards the middle of the face;
- (iv) at very low cooling rates there is a sudden formation of a contraction gap at the metal glass interface shortly after the point of completion of solidification.

2. It has been possible to correlate the solidification experiments with Hills' algorithm for solidification of pure metals and binary alloys to show the influence of the freezing range of an alloy on the conditions which lead to air gap formation.

3. Theoretical analyses made using the published results of other experimental work, has shown the maximum effect

that air gap formation has on heat extraction rates is to halve them, but in many cases the reduction is somewhat less.

4. The apparatus used here has allowed the development of the air gap to be observed during the solidification of prismatic ingots of metals and alloys.
5. A modification to the apparatus used in which better control could be exerted over cooling rates and in which the leakage of cooling water into the air gap cavity could be prevented, would allow precise measurements to be made of the progression of the air^{gap} and would allow a detailed comparison to be made between fairly precise experimental results^{and} the various published theories for air gap formation.

REFERENCES

1. E. R. Linacre; Iron and Steel 1952 25 3.
2. E. T. Mykura; Report SM/97/48 1948 BISRA.
3. B. Matuschka; Arch. Eisenhuttenwes 1930 2 405.
4. C. R. Taylor; Met. Trans B. 1975 6b 359.
5. L. S. Rudoi; Jzv. Vyssh Ucheb Zaved. Chem Met 1972
2 52 HB=5567.
6. M. S. Gordienko; Sb. Nauch Tr. 1965 11 109 HB=7220.
7. I. M. Mackenzie and A. Donald; T. Iron Steel Inst.
1950 166 19.
8. H. F. Bishop, F. A. Brandt and W. S. Pellini; Trans
American Inst. Min Met. 1952 194 44.
9. V. P. Druahinin and A. I. Mazun; Stal in English 1961
5 328.
10. A. I. Veinik; Thermodynamics for the Foundryman 1960
(MacLaren New York).
11. R. T. Fowler and J. Savage; J. Iron Steel Inst. 1952
171 277.
12. G. Volk and K. Wunnenberg; Kleipzig Fachber 1972,
80 491 HB=9010.
13. J. Savage; J. Iron Steel Inst. 1962 198 41.
14. R. H. Tien and V. Koump. J. Appl. Mech. 1960 36 763.
15. F. Oeters and K. Sandemann, Arch. Eisenhuttenwesen
1974 45 737.
16. J. H. Weiner and B. A. Boley; J. Mech. Phys. Solids
1963 11 145.
17. B. A. Boley and J. H. Weiner; Theory of Thermal Stresses
(Wiley, New York). 1958
18. N. M. H. Lightfoot, Iron and Steel, Special Report
1933 4 64.
19. C. H. Feltham; Nature 1950; 165, 25.
20. O. Richmond and R. H. Tien; J. Mech. Phys. Solids
1971 19 273.

21. A. Grill, K. Sorimachi, and J. K. Brimacombe; Met Trans B 1976 7B 1977.
22. D. M. Lewis and J. Savage Met Rev. 1956 1 65.
23. J. Savage and W. H. Prichard, J. Iron Steel Inst 1954 1978 269.
24. A. A. Skvortov; Izv.Vysssh Ucheb Zaved, Chem Met 1961 17 78 HB=5347.
25. V. Koump, R. H. Tien and W. J. Kim Trans TMS-AIME, 1967 239 1305.
26. R. H. Tien and V. Koump Trans TMS-AIME, 1968 242 283.
27. A. W. D. Hills, S. L. Malhotra and M. R. Moore, Met Trans B 1975 6B 131.
28. S. L. Malhotra Diploma Thesis, Imperial College, 1969, London.
29. J. D. Hunt and J. P. Chilton; J.Inst Metals 1967 95 21.
30. A. Moore and R. Elliott; J. Inst Metals 1967 95 369.
31. R. W. Ruddle, The Solidification of Castings; Institute of Metals, London 1950.
32. I. Doherty and Feest, Solidification of Castings, ISI publication, p.25 1968 London.
33. H. S. Carslaw and J. C. Jaeger; Conduction of heat in solids, Oxford 1959 2nd ed.
34. Schwarz; Arch Eisenhuttenw 1931 5 1939.
35. S. Ostrach; Nat. Advisory Comm. Aeronaut Tech Note (1952) 2635.
36. E. Z. Pohlhausen; Z. f. angew Math u Mech 1921 1 115.
37. G. H. Geiger and D. R. Poirier; Transport Phenomena in Metallurgy, Addison-Wesley P. Co. Reading, Massachusetts, 1973.
38. J. Gryzagoridis; Int. J. Heat Mass Transfer 1975 18 911.
39. R. L. Pigford; C.E.P. Symposium Series, 1955, 51 79.
40. R. B. Bird, W. E. Stewart, and E. N. Lightfoot; Transport phenomena; John Wiley and Sons Inc. 1960, New York.

41. E. N. Wieder and G. E. Tate; Ind. Eng Chem 1936
28 1429.
42. J. Szekely and N. J. Themelis; Rate Phenomena in
Process Metallurgy; Wiley-Interscience 1971, New
York.
43. H. W. Mc Adams; Heat transmission; 3rd Ed. McGraw-
Hill Book Co. New York. 1954.
44. A. W. D. Hills; J. Iron and Steel Inst. 1965 203 18.
45. J. K. Brimacombe and F. Weinberg; J. Iron and Steel
Inst. 1973, 211, 24.

LIST OF SYMBOLS

c	Specific heat
g	Gravity acceleration
h	Overall heat transfer coefficient from the inner mould wall to the cooling water or air $W/m^2 \text{ } ^\circ C$
H	Latent heat of a metal or alloy (J/kg)
k	Thermal conductivity ($W/m^\circ C$)
L	Plate height (m)
\dot{q}''	Heat flow from the surface, $hA (\theta_o - \theta_a)$ $[W/m^2]$
u	Casting speed (m/s).
v	Speed of air or water (m/s).
x	Distance co-ordinate along the heat flow direction (m)
x_M	Distance below the liquid metal meniscus

GREEK SYMBOLS

α	Thermal diffusivity (m^2/s)
β	Coefficient of thermal expansion ($^\circ C^{-1}$)
τ	Casting time (min)
ξ	Dimensionless time
ρ	Density (kg/m^3)
μ	Viscosity (cp)
ν	Dynamic viscosity
θ	Temperature ($^\circ C$)
θ_a	Ambient temperature ($^\circ C$)
θ_D	Temperature of the remote boundary ($^\circ C$)
θ_L	Liquidus temperature ($^\circ C$)
θ_M	Initial temperature ($^\circ C$)
θ_S	Solidus temperature ($^\circ C$)
θ_o	Temperature of the surface ($^\circ C$)

Variable defined by equation No VI - 4

$$\beta = \frac{\mu k}{\rho c g \delta}$$

Dimensionless variables and groups:

ξ

Dimensionless time

$$\xi = \frac{h^2 \tau}{\rho c k}$$

θ^*

Dimensionless surface temperature $\theta^* = \theta / \theta_s$

Q^*

Dimensionless heat flow from the surface

Nu

Nusselt number $Nu = hL/k$

Re

Reynolds number $Re = vL/\nu$

Gr_L

Grashof number $Gr = \frac{\beta g (\theta_0 - \theta_a) L^3}{\nu^2}$

Pr

Prandtl number $Pr = \frac{\mu c}{k}$

H^*

Dimensionless latent heat $H^* = H/c\theta_s$

SOLIDIFICATION MODES

Mode 1	The thermal layer growing alone.
Mode 1F	Entire liquid region cooling.
Mode 2	The solid and thermal layers growing together.
Mode 2F	The solid layer is growing after the thermal layer has reached the remote boundary.
Mode Z2	The partial layer is growing into the liquid at the liquidus temperature.
Mode ZF2	Partial layer occupies entire region.
Mode Z3	Partial layer is growing ahead of solid layer.
Mode Z3F	Partial layer is shrinking in front of growing solid layer.
Mode S1	Thermal layer growing.
Mode S1F	Entire liquid region cooling.
Mode S2	Partial layer and thermal layer are growing together.
Mode S2F	The partial layer is growing after the thermal layer has reached the remote boundary.
Mode S3	The solid, partial and thermal layers are growing together.
Mode S3F	The solid and partial layer has reached the remote boundary.

LIST OF FIGURES

Fig.No.

1. Rate of heat transfer from ingot to mould 107cm level.
(After Mackenzie and Donald (7)).
2. Heat transfer between ingot and mould (after Fowler and Savage (11)).
3. Effect of strand speed and distance from the mould top on heat flux (After Volk and Wunnenberg (12)).
4. Schematic diagram indicating regions of importance of different modes of inelastic behaviour. (After Boley and Winer (17)).
5. Estimated air gap widths between ingot and mould
(After Lewis and Savage (23)).
6. Cooling modes for a pure metal or an eutectic alloy
(After Hills et al (28)).
7. Algorithm showing the relationship between the cooling and solidification modes (After Hills et al (28)).
8. Mould B.
9. Thermocouple bridges.
10. E.M.F. versus θ curve.
11. Schematic representation of the Michelson's interferometer.
12. Laser experiment set up.
13. Typical cooling curves (run 18)
14. 50% lead-tin cooling curve.
- 14a to Cooling curves for 50% lead.
- 21b Tin alloy in mould B.
- 22a to
- 27 Cooling curves for pure tin in mould B.

- 28 Solidification algorithm for pure metals and binary alloys (after Hills et al (27,28).
- 29 Comparison of theoretical heat flow analysis with experimental results.
- 30 Calculated heat transfer coefficients versus distance below metal meniscus.
- 31 Calculated overall heat transfer coefficients from Volk and Wunnenberg's data versus dwell time.
- 32 Billet surface temperature versus distance from the metal meniscus downwards.

LIST OF PLATES

Plate No.

1	Mould A
2	Coils
3	Multiple Nozzle
4	Mould B and Final Apparatus
5 to 16	Air gap development: run 4C
17 to 25	Separation development run 3C

LIST OF TABLES

Table

I	Mikura results
II	Matckhusca results
III	Cooling conditions
IV	Cooling modes
V	Thermal data
VI	Comparison of estimated casting times with experimental results